Technische Universität München
Fakultät für Informatik
Lehrstuhl VII: Theoretische Informatik

Multi-Task and Transfer Learning with Recurrent Neural Networks

Sigurd Spieckermann

Vollständiger Abdruck der von der Fakultät für Informatik der Technischen Universität München zur Erlangung des akademischen Grades eines

Doktors der Naturwissenschaften (Dr. rer. nat.)

genehmigten Dissertation.

Die Dissertation wurde am 19.05.2015 bei der Technischen Universität München eingereicht und durch die Fakultät für Informatik am 28.09.2015 angenommen.

Abstract

Being able to obtain a model of a dynamical system is useful for a variety of purposes, e.g. condition monitoring and model-based control. The dynamics of complex technical systems such as gas or wind turbines can be approximated by data driven models, e.g. recurrent neural networks. Such methods have proven to be powerful alternatives to analytical models which are not always available or may be inaccurate. Optimizing the parameters of data-driven models generally requires large amounts of operational data. However, data is a scarce resource in many applications, hence, data-efficient procedures utilizing all available data are preferred.

In this thesis, recurrent neural networks are explored and developed which allow for data-efficient knowledge transfer from one or multiple source tasks to a related target task that lacks sufficient amounts of data. Multiple knowledge transfer scenarios are considered: dual-task learning, multi-task learning, and transfer learning. Dual-task learning is a particular case of multi-task learning in which multiple tasks are learned simultaneously, thus, allowing to share knowledge among the tasks. Transfer learning implies a sequential protocol in which the target task is learned subsequent to learning one or multiple source tasks. Knowledge transfer is explored and applied in the context of fully and partially observable system identification to improve the model of a little observed system by means of auxiliary data from one or multiple similar systems. Fully observable system identification assumes that the observed system state corresponds to the true state while partial observability implies the observation of either a subset of the state variables or proxy variables.

The primary contribution of this thesis comprises a novel recurrent neural network architecture for knowledge transfer which uses factored third-order tensors to encode cross-task and task-specific information within composite affine transformations. This model is investigated in a series of experiments on synthetic as well as real-world gas turbine data. Empirically, the proposed Factored Tensor Recurrent Neural Network architecture outperforms the other considered methods consistently in all experiments by transferring information from one or multiple well-observed source task(s) to a little observed target task. Without any transfer approach, the target task cannot be modeled successfully because of insufficient amounts of available data. Besides this empirically proven merit, the proposed Factored Tensor Recurrent Neural Network is appealing due to its principal approach of incorporating cross-task and task-specific information into the architecture, thereby, allowing for task-specific adaptation in a data-efficient way.

Acknowledgments

I would like to thank the “Learning Systems” research group at Siemens AG, Corporate Technology, in Munich, Germany, for supporting this work. In particular, I would like to thank my supervisors, Thomas Runkler and Steffen Udluft, for their guidance and support as well as proofreading the papers and this thesis. My gratitude extends to the head of “Learning Systems”, Volkmar Sterzing, who enabled my research in his group. I would also like to thank Alexander Hentschel for the many enlightening conversations, both technical and more general in nature, and his extraordinarily accurate proofreading of the papers that he co-authored as well as part of this thesis. Further thanks go to Siegmund Düll for his advice and support, particularly in familiarizing myself with the internal “Learning Systems” code base, which I used for generating data for the experiments. I am grateful to Andrew Ng whose machine learning course I took at Stanford University in 2011. His fascination for machine learning as well as his unique ability to teach the material in an outstandingly clear and concise way sparked my passion for machine learning motivating me to dive deeper into this field myself.

I particularly thank my parents, Helga and Rainer Spieckermann, who have constantly supported and encouraged me in my personal and academic development in many ways—morally, advisory, financially, etc. They laid the foundation for all that I have become and that enabled this thesis. Last but not least, I would like to express my gratitude to my fiancée, Caroline Roeger, who has been by my side unconditionally despite the difficult times when we were having a long-distance relationship during my studies in the U.S. and later when I moved to Munich to pursue my PhD.

Contents

CHAPTER 1

Introduction

Much technological progress has been made in the area of machine learning to automatically find structure in data. Especially in the field of deep learning, methods have been developed that are competitive with human judgment on difficult classification tasks (Taigman et al., 2014). However, many such methods make the assumption that the data-generating process is time-invariant. This assumption is strong and may not always hold in practice. The following examples describe real-world scenarios which motivated the research presented in this thesis and for which this assumption is likely invalid.

Example 1.1 *Consider an industrial plant that is subject to modifications over time. During normal operation, the system behavior is observed and a simulation model is trained from the collected data. As a consequence of the modifications, the plant's dynamical properties change thereby invalidating the available model. However, an accurate model is needed as soon as possible after recommissioning the plant. Given that the overall plant remains largely the same, no fundamental changes of the general structure and complexity of the dynamics are expected. Therefore, information collected prior to the plant modifications can be exploited to learn a new model with significantly fewer data from the modified plant, compared to learning a new model from scratch.*

Example 1.2 *Consider multiple similar industrial plants, e.g. plants of the same family, that have been operated and observed for sufficient time such that the recorded data are a representative sample of their dynamical properties. Then, a model of each plant can be derived from fitting its parameters to the data which may be utilized for e.g. condition monitoring or model based control (Schäfer et al., 2007b). Over time, new instances of this family may be deployed* *and commissioned. However, observing each new one sufficiently long in order to learn a good model is impractical because the plant would need to be operated using default methods until enough data have been gathered. Hence, the goal is to learn an accurate model of a new plant with as little data as possible, i.e. as soon as possible after commissioning. The fact that prior knowledge of similar plants is available lends itself to exploiting this knowledge and transferring it to the new plant.*

More abstractly, there may be a task for which only little data is available, but plenty of additional data from one or multiple related task(s) is accessible. Naïvely, only the data from the new task is used to learn a model which likely shows inferior performance because of lacking data. Alternatively, based on the assumption that the tasks are sufficiently related to each other it may be possible to exploit their relation and utilize the data from the related task(s) as prior knowledge about the global structure of the new task. Then, only particular aspects of the new task need to be inferred which is likely to require significantly less data.

This thesis addresses the question of how to make effective use of prior knowledge in the context of modeling dynamical systems. Multiple knowledge transfer scenarios are explored which are applied in the context of modeling the dynamics of fully observable dynamical systems and soft-sensor modeling under partial observability. Full observability assumes that the observed system state corresponds to the true state while partial observability is given when only observations of either a subset of the state variables or proxy variables are accessible. Many real-world systems are partially observable because their state is observed through sensors, but the set of sensor values at a given point in time does not fully determine the state of the system. A simple example is the task of quantifying the acceleration of a car by observing its speedometer. The speedometer displays the momentary speed of the car, but the reading at a single point in time does not give information about its acceleration. However, aggregated information from one or multiple preceding readings allows to reconstruct the missing information. While this example is rather simplistic, the dynamics of complex technical systems such as gas or wind turbines are typically much more complicated. Consequently, data-driven models such as recurrent neural networks (Bailer-Jones et al., 1998; Zimmermann & Neuneier,

2001) have proven to be powerful alternatives to analytical models which are not always available or may be inaccurate (Schäfer et al., 2007a). Optimizing the parameters of data-driven models generally requires large amounts of operational data. However, data is a scarce resource in many applications. Hence, data-efficient procedures utilizing all available data are preferred including data from other systems based on the prior knowledge of system similarity.

Two system identification problems are explored. The first problem deals with fully observable multi-system identification under the paradigms dual-task and transfer learning. Dual-task learning is a special case of multi-task learning where multiple tasks are learned simultaneously within a joint model, thus, enabling knowledge transfer among the tasks. Transfer learning implies a sequential protocol in which the target task is learned subsequent to learning multiple source task models. Experiments were conducted using the cart-pole and mountain car dynamics because they are well known benchmarks, intuitively configurable in order to obtain multiple similar systems, and convenient for generating arbitrary amounts of data. In the dual-task learning setting, a scarcely observed target system is modeled by exploiting plenty of auxiliary data from a related source system. Several model architectures are compared by plotting the respective model error against the data ratio between the source and target system data. In the transfer learning setting, a scarcely observed target system is modeled by exploiting auxiliary data from multiple related source systems according to the sequential protocol implied by the learning paradigm. Several model architectures are compared by plotting the respective model error against numerous target system configurations. The second problem deals with partially observable multi-system identification under the multi-task learning paradigm. Therein, a NO_x emission sensor of a real-world gas turbine is modeled based on a historical sequence of other environment and control sensor values. Since the emission sensor model of the target system is inaccurate when it is trained exclusively on the target system data, data from multiple related turbines are used to augment the training data set. Several model architectures are compared by plotting the respective model predictions as well as the ground truth for each instance in the test set.

1.1 Contributions

The field of knowledge transfer has received increased attention in recent years as an emerging field within the area of machine learning. However, much research has focused on classification problems with non-sequential inputs, e.g. with applications in computer vision or natural language processing, while knowledge transfer in the context of dynamical system modeling has mostly remained unstudied. The major contributions of this thesis are summarized as follows:

1. The importance of knowledge transfer among related dynamical systems is introduced and motivated through industrial use cases where system identification needs to be performed in the absence of sufficient data of a target system.

2. Related work on knowledge transfer and other relevant prior work in machine learning is identified and discussed such that the novel approaches presented in this thesis are associated with prior research.

3. Viable approaches for knowledge transfer among related systems are explored and proposed that enable effective utilization of data from the related systems to serve as prior knowledge of the target system in the model building process. In particular, a novel recurrent neural network architecture family is proposed for this purpose. In addition, a novel regularization technique is presented which strengthens the prior assumption of the systems' relatedness to increase data-efficiency with respect to the target system.

4. The learning tasks of fully and partially observable system identification are studied, and two learning paradigms—multi-task learning, and transfer learning—are explored, which relate to different application scenarios.

5. Empirical analyses of the proposed methods are conducted in the above-described learning problems and paradigms on data from simulations and real-world gas turbines.

Over the course of the doctoral research, several papers have been authored and published in peer-reviewed media which lay the foundation of this thesis. The publications are listed and summarized as follows:

- Spieckermann, S., Düll, S., Udluft, S., Hentschel, A., and Runkler, T. Exploiting similarity in system identification tasks with recurrent neural networks. In *Proceedings of the 22nd European Symposium on Artificial Neural Networks, Computational Intelligence and Machine Learning (ESANN)*, 2014a.
  The problem of fully observable system identification of a target system despite insufficient amounts of available data through effective utilization of additional data from a related system was addressed. The Factored Tensor Recurrent Neural Network architecture was proposed and empirically evaluated on synthetic simulation data.

- Spieckermann, S., Düll, S., Udluft, S., Hentschel, A., and Runkler, T. Exploiting similarity in system identification tasks with recurrent neural networks. *Neurocomputing*, (Special Issue ESANN 2014), 2015. Extended version. Invited paper.
  The preceding work was extended by analyzing the proposed Factored Tensor Recurrent Neural Network architecture in more in-depth and motivated based on theoretical grounds. Further, the empirical evaluation of the model was extended to a second simulation and additional analyses were conducted with regard to the weighting of each system in the optimization objective.

- Spieckermann, S., Düll, S., Udluft, S., and Runkler, T. Regularized recurrent neural networks for data efficient dual-task learning. In *Proceedings of the 24th International Conference on Artificial Neural Networks (ICANN)*, 2014c.
  A novel regularization technique was proposed which penalizes dissimilarity between the target system and the related system asymmetrically such that only the target system parameters are tied to those of the related system but not vice versa. Experiments were conducted on two synthetic simulations.

- Spieckermann, S., Düll, S., Udluft, S., and Runkler, T. Multi-system identification for efficient knowledge transfer with factored tensor recurrent neural networks. In *Proceedings of the European Conference on Machine Learning (ECML), Workshop on Generalization and Reuse of Machine*

Learning Models over Multiple Contexts, 2014b.
The problem of fully observable system identification of a target system by means of effective utilization of additional data from multiple related systems using the transfer learning paradigm was investigated. The afore proposed Factored Tensor Recurrent Neural Network architecture was evaluated in this learning paradigm on two synthetic simulations.

- Spieckermann, S., Udluft, S., and Runkler, T. Data-efficient temporal regression with multi-task recurrent neural networks. In *Advances in Neural Information Processing Systems (NIPS), Second Workshop on Transfer and Multi-Task Learning: Theory meets Practice*, 2014.
A real-world problem of partially observable system identification in the multi-task learning paradigm was studied. There, the afore proposed Factored Tensor Recurrent Neural Network was adapted and evaluated on data from six real-world gas turbines.

1.2 Overview of the Thesis

The thesis consists of three main parts: (i) the introduction, motivation, outline, and theoretical background in Chapters 1 and 2; (ii) an introduction to multi-task and transfer learning with recurrent neural networks on sequential data as well as the development of appropriate architectures including the proposed Factored Tensor Recurrent Neural Network in Chapter 3; (iii) the application of such methods to fully and partially observable multi-system identification using multiple learning paradigms in Chapters 4 and 5. Chapter 2 reviews the general concepts of machine learning and knowledge transfer, neural networks and relevant learning algorithms, hidden Markov models, tensor factorization, the system identification learning problem, relevant simulations of dynamical systems, and a software package that enables rapid prototyping of complex neural architectures. Chapter 3 introduces two learning paradigms—multi-task and transfer learning—and discusses their relatedness. Then, the space of recurrent neural network architectures capable of performing knowledge transfer among multiple tasks with sequential data is explored and suitable approaches are identified and developed. In particular, the Factored Tensor Recurrent Neural Network architecture is proposed and discussed. Chapter 4 addresses the problem of fully observable system identification under the constraint of few available data from the system of interest. The dual-task learning, regularized dual-task learning, and transfer learning scenarios are studied for exploiting the similarity of the system of interest with other related systems. Experiments were conducted to compare the effectiveness of the respective approaches. Chapter 5 investigates the problem of partially observable system identification again under the constraint of insufficient data of the system of interest. The multi-task learning paradigm is studied for exploiting the similarity of the system of interest with other related systems. Experiments were conducted on real-world gas turbine data. Chapter 6 concludes the work presented in this thesis and suggests future research directions.

CHAPTER 2

Theoretical Background

This chapter provides a theoretical background on the main concepts of machine learning, which form the basis of the research presented in this thesis. First, the field of machine learning is briefly introduced (Section 2.1). Therein, basic concepts such as the hypothesis space, parameter space, data distribution, empirical risk minimization, and the exponential family distribution are covered. Second, the problem of and motivation for knowledge transfer is discussed wherein various transfer settings and approaches are presented giving an overview of the field (Section 2.2). Third, a particular class of parametric models—neural networks—is revised (Section 2.3) ranging from the most basic type of neural network—the perceptron—to multi-layer perceptrons to recurrent neural networks. Fourth, learning and optimization algorithms are discussed (Section 2.4), covering the idea of backpropagation, the Hessian-Free optimization algorithm, and the problem of overfitting. Fifth, the hidden Markov model being a popular choice for sequence modeling tasks is introduced (Section 2.5). Sixth, the field of tensor factorization is presented (Section 2.6) by introducing relevant notation and concepts, a particular factorization technique called Parallel Factor Analysis, and typical applications. Seventh, the process of system identification is briefly outlined (Section 2.7) followed by a formal introduction of two simulations of dynamical systems (Section 2.8). Finally, the software library which was used to implement all models in this thesis is discussed (Section 2.9).

2.1 Machine Learning

Machine learning is a subject within computer science, with close relation to other fields such as statistics and mathematical optimization, that is concerned with computer software and algorithms enabling machines to learn autonomously from data. Several definitions have been proposed by researchers over more than half a century:

Definition 2.1 *Field of study that gives computers the ability to learn without being explicitly programmed. (Samuel, 1959)*

Definition 2.2 *A computer program is said to learn from experience E with respect to some class of tasks T and performance measure P, if its performance at tasks in T, as measured by P, improves with experience E. (Mitchell, 1997)*

Definition 2.3 *Machine Learning is the field of scientific study that concentrates on induction algorithms and on other algorithms that can be said to "learn". (Kohavi & Provost, 1998)*

More formally, the goal of machine learning is to find a hypothesis h within a hypothesis space H that approximates the structure or relationships described by a data distribution $\mathcal{D}$. A hypothesis h can be parametric, i.e. the hypothesis can be parameterized by a set of adaptive weights θ within a parameter space Θ, or non-parametric, i.e. the hypothesis relies on the data itself. In the scope of this thesis only the hypothesis subspace of parametric hypotheses is considered and further discussed in the following paragraphs.

Let X be an input space and Y be a target space with $x \in X$ and $y \in Y$. Further, let $\mathcal{D}$ denote an unknown probability distribution over the product space $X \times Y$, and $(x, y) \sim \mathcal{D}$ be a sample drawn from this distribution. A parametric hypothesis space $H = \{h_\theta \,|\, \theta \in \Theta\}$ consists of hypotheses $h_\theta \colon X \to Y$, that represent the mapping from the input space to the target space. The hypothesis space H determines the family of hypotheses that are assumed to be able to approximate the data generating process. The choice of H typically requires domain knowledge of an expert. The parametric members h_θ of the hypothesis space are particular instances within the space. The optimal parametric hypothesis h_θ^* within the predefined hypothesis space H is obtained by minimizing the generalization error ε with respect to the parameters θ over the data distribution $\mathcal{D}$. The generalization error uses an appropriate task-dependent loss $\mathcal{L} \colon Y \times Y \to \mathbb{R}$ to quantify the difference between the prediction $h_\theta(x)$ and the target y.

$$\begin{aligned} h^*_\theta &= \operatorname*{arg\,min}_{h_\theta \in H, \theta \in \Theta} \varepsilon(h_\theta) && (2.1a) \\ &= \operatorname*{arg\,min}_{h_\theta \in H, \theta \in \Theta} \int_{X \times Y} p(x,y) \mathcal{L}(h_\theta(x), y) dx dy && (2.1b) \\ &= \operatorname*{arg\,min}_{h_\theta \in H, \theta \in \Theta} \mathrm{E}_{(x,y) \sim \mathcal{D}} [\mathcal{L}(h_\theta(x), y)] && (2.1c) \end{aligned}$$

Unfortunately, ε is not available in practice. Instead, only a finite number $m \in \mathbb{N}$ samples $(x^{(i)}, y^{(i)})$, $i = 1, ..., m$, drawn from the distribution $\mathcal{D}$ is available, i.e. $D = \{(x^{(i)}, y^{(i)}) \sim \mathcal{D} \,|\, i = 1, ..., m\}$ with $|D| = m$. Thus, the empirically optimal hypothesis $\hat{h}_\theta$ is found by minimizing the empirical error $\hat{\varepsilon}$ on the data set D.

$$\begin{aligned} \hat{h}_\theta &= \operatorname*{arg\,min}_{h_\theta \in H, \theta \in \Theta} \hat{\varepsilon}_D(h_\theta) && (2.2a) \\ &= \operatorname*{arg\,min}_{h_\theta \in H, \theta \in \Theta} \frac{1}{|D|} \sum_{(x,y) \in D} \mathcal{L}(h_\theta(x), y) && (2.2b) \end{aligned}$$

Whether the empirical error $\hat{\varepsilon}$ is a suitable proxy for the expected error ε depends on the complexity of the mapping to be approximated, the complexity class of the hypothesis space, and on the number and quality of the samples.

The loss function $\mathcal{L}$ is often chosen according to the distribution of the target variable conditioned on the data, e.g. $y|x \sim \mathcal{N}(\mu, \sigma^2)$. Assuming $y|x$ is drawn from a member of the exponential family of distributions, maximum likelihood estimation yields a matching loss function. Let η denote the natural/canonical parameter of the distribution, $T(y)$ be the sufficient statistic, and $a(\eta)$ be the log partition function. Then, the exponential family of distributions is defined by the term

$$p(y; \eta) = b(y) \cdot e^{\eta^T T(y) - a(\eta)}. \qquad (2.3)$$

Many common distributions are part of the exponential family. To obtain the Gaussian distribution from the exponential family, which is a common assumption for the target variable in many regression problems, one must choose $\eta = \mu$, $T(y) = y$, $a(\eta) = \frac{\mu^2}{2} = \frac{\eta^2}{2}$, $b(y) = \frac{1}{\sqrt{2\pi}} e^{\frac{-y^2}{2}}$. The hypothesis shall predict $\mathrm{E}_{(x,y) \sim \mathcal{D}}[y|x]$, thus, it must satisfy $h_\theta(x) = \mathrm{E}_{(x,y) \sim \mathcal{D}}[y|x; \theta]$. Given a specific hypothesis the optimal choice of parameters is found by maximizing the likelihood.

$$\hat{\theta} = \arg\max_{\theta\in\Theta} \ell(\theta; D) \tag{2.4a}$$

$$= \arg\max_{\theta\in\Theta} \prod_{(x,y)\in D} \prod_{i=1}^{\dim(y)} \frac{1}{\sqrt{2\pi}\sigma_i} e^{-\frac{1}{2\sigma_i^2}(y_i - [h_\theta(x)]_i)^2} \tag{2.4b}$$

For mathematical convenience the log-likelihood instead of the likelihood is maximized which is an equivalent optimization objective because the logarithmic function is monotonic.

$$\hat{\theta} = \arg\max_{\theta\in\Theta} \ln \ell(\theta; D) \tag{2.5a}$$

$$= \arg\max_{\theta\in\Theta} \ln \prod_{(x,y)\in D} \prod_{i=1}^{\dim(y)} \frac{1}{\sqrt{2\pi}\sigma_i} e^{-\frac{1}{2\sigma_i^2}(y_i - [h_\theta(x)]_i)^2} \tag{2.5b}$$

$$= \arg\max_{\theta\in\Theta} \sum_{(x,y)\in D} \sum_{i=1}^{\dim(y)} \left(- \ln(\sqrt{2\pi}\sigma_i) - \frac{1}{2\sigma_i^2}(y_i - [h_\theta(x)]_i)^2 \right) \tag{2.5c}$$

$$= \arg\max_{\theta\in\Theta} \sum_{(x,y)\in D} \sum_{i=1}^{\dim(y)} -\frac{1}{2\sigma_i^2}(y_i - [h_\theta(x)]_i)^2 \tag{2.5d}$$

$$= \arg\max_{\theta\in\Theta} \sum_{(x,y)\in D} \sum_{i=1}^{\dim(y)} -(y_i - [h_\theta(x)]_i)^2 \tag{2.5e}$$

Then, maximizing the log-likelihood is equivalent to minimizing the negative log-likelihood which is equivalent to minimizing the mean squared error.

$$\hat{\theta} = \arg\min_{\theta\in\Theta} \{- \ln \ell(\theta; D)\} \tag{2.6a}$$

$$= \arg\min_{\theta\in\Theta} \sum_{(x,y)\in D} \sum_{i=1}^{\dim(y)} (y_i - [h_\theta(x)]_i)^2 \tag{2.6b}$$

$$= \arg\min_{\theta\in\Theta} \sum_{(x,y)\in D} \mathrm{MSE}(h_\theta(x), y) \tag{2.6c}$$

The mean squared error is a common loss function in many regression problems including the ones presented in this thesis. Other common loss functions include cross-entropy used for binomial and multinomial target variables as well as heuristics such as the $\ln\cosh$ function to reduce the importance of outliers, the hinge loss $\max(0, 1 - yh_\theta(x))$, and many more.

2.2 Knowledge Transfer

Knowledge transfer denotes the process of using previously gained knowledge from related tasks to improve the ability of learning a new task compared to learning the task in isolation. The question of how to share or transfer knowledge among multiple learning tasks dates back at least two decades.

Caruana (1993) suggested that learning multiple tasks simultaneously may yield better generalization compared to learning multiple individual tasks separately. He considered multiple related learning tasks to be sources of inductive bias with mutual benefit to each other. Caruana focused on neural networks which model multiple tasks by sharing the hidden layer in a three-layer network.

Thrun (1996) introduced the *lifelong learning framework* in which he derived inspiration from human learning behavior. While a classical perspective on learning theory is concerned with finding the optimal hypothesis that describes a set of observed data of a particular task within a given hypothesis space, humans follow a different learning paradigm where prior knowledge from a vast amount of experience of related learning tasks is utilized. Thrun illustrates this perspective with an intuitive example: "[...] when learning to drive a car, years of learning experience with basic motor skills, typical traffic patterns, logical reasoning, language and much more precede and influence this learning task. The transfer of knowledge across learning tasks seems to play an essential role for generalizing accurately, particularly when training data is scarce". Figure 2.1 illustrates the difference between classical machine learning and transfer learning.

Significant research has been conducted since to explore methods allowing to transfer knowledge in various ways across domains and tasks, typically to alleviate the lack of labeled data in a target domain by exploiting prior knowledge from one or multiple relevant source domain(s)/task(s). Three major survey papers have been published in recent years that provide excellent overviews of the field. Taylor & Stone (2009) and Torrey & Shavlik (2009) focus on transfer learning in the context of reinforcement learning. Reinforcement learning is concerned with training an agent to act optimally in a given environment with respect to a particular task. Each action, that the agent invokes, returns a reward to the agent. The agent's goal is to accumulate as much reward as possible over time which, in turn, implies a well-behaved agent with respect to the underlying task. While this thesis is not concerned with control tasks, some

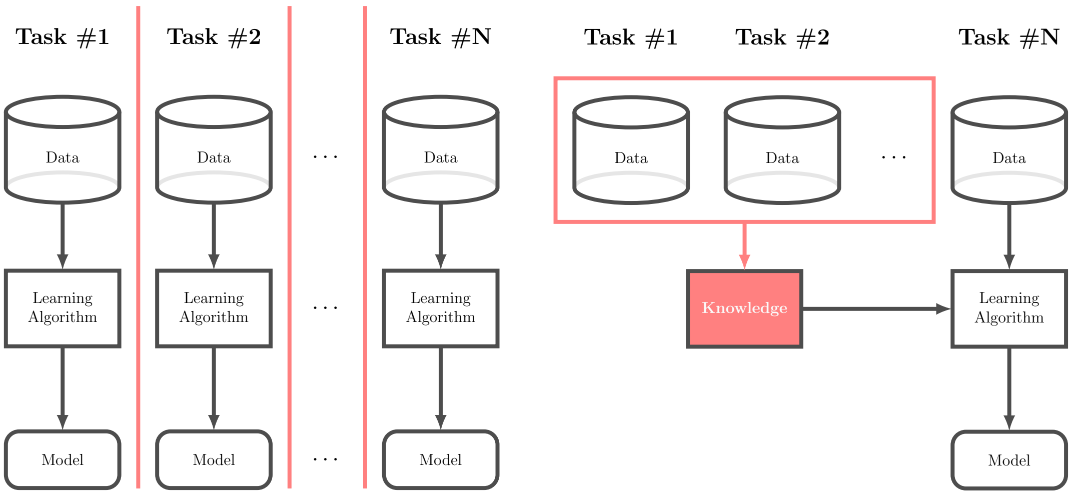

(a) Classical machine learning (b) Transfer learning

Figure 2.1: Comparison of classical machine learning vs. transfer learning. The illustration is adapted from Pan & Yang (2010).

of the aspects discussed in the papers are closely related to transfer learning in the context of modeling dynamical systems. Pan & Yang (2010) provide a more general perspective on the topic, formalize the problem of knowledge transfer across domains and tasks, identify various transfer learning settings, their applicability in different situations and under different constraints, as well as approaches how to achieve knowledge transfer, and depict which approach is viable or compatible with each learning setting.

2.2.1 Formal Definition

A learning problem consists of a domain $\mathbb{D} = (X, P)$, where X is an input space and P a probability measure which gives the marginal probability $P(x)$ of each example input $x \in X$, and a learning task $\mathbb{T} = (Y, h)$, where Y is a target space and $h\colon X \to Y$ is the hypothesis that models $P(y|x)$, $y \in Y$, which is learned from the training data $D = \{(x^{(i)}, y^{(i)}) \sim \mathcal{D} \,|\, i = 1, ..., m\}$. In a transfer learning scenario, there are source domains $\mathbb{D}_{S,i}$ and learning tasks $\mathbb{T}_{S,i}$, $i \in \mathbb{N}$, and there is a target domain $\mathbb{D}_T$ and a learning task $\mathbb{T}_T$. Given this scenario, a formal definition of transfer learning, which was adapted from Pan & Yang (2010), is provided as follows.

Definition 2.4 (Transfer learning (Pan & Yang, 2010)) *Given the source domains $\mathbb{D}_{S,i}$ and the learning tasks $\mathbb{T}_{S,i}$, a target domain $\mathbb{D}_T$ and a learning task $\mathbb{T}_T$, transfer learning aims to improve the learning of the target task hypothesis $h_T\colon X_T \to Y_T$ in the target domain $\mathbb{D}_T$ by utilizing the knowledge from $\mathbb{D}_{S,i}$ and $\mathbb{T}_{S,i}$ where $\mathbb{D}_{S,i} \neq \mathbb{D}_T$, i.e. $X_{S,i} \neq X_T$ and/or $P_{S,i} \neq P_T$, or $\mathbb{T}_{S,i} \neq \mathbb{T}_T$, i.e. $Y_{S,i} \neq Y_T$ and/or $h_{S,i} \neq h_T$, $\forall i \in \mathbb{N}$.*

2.2.2 Aspects of Transfer

Transfer learning requires the awareness and careful consideration of a variety of aspects concerning what kinds of knowledge shall be transferred, what sources of knowledge shall be selected, and how to proceed given certain constraints imposed by the nature of the tasks and the used learning algorithm. Taylor & Stone (2009) identify and formalize different aspects relevant for knowledge transfer in the context of reinforcement learning. They categorize transfer learning based on the following key aspects:

Allowed task differences. There may be numerous ways in which tasks can differ. Major task differences include non-identical state and/or action spaces, different observation functions, different reward functions as well as different dynamical properties, i.e. state transitions. Depending on the problem at hand, one or multiple differences may occur among the set of tasks. The task differences immediately affect the choice of viable approaches for successful knowledge transfer among the tasks.

Source task selection. There may be one or multiple tasks to exploit, but some subset of the tasks may not be suitable to improve the learning of the target task. Source task selection may be performed by humans based on domain knowledge or it may proceed automatically using an algorithm that estimates the relatedness and utility of the available source tasks with respect to the target task. Source tasks are not guaranteed to be useful and may even harm the learning process of the target task.

Transferred knowledge. There are multiple kinds knowledge that can be transferred among tasks ranging from low-level knowledge, such as raw data instances, to rather high-level knowledge, like task-specific or multi-task (sub)models that may serve as priors for the target task.

Task mappings. Tasks may have different state and/or action spaces and/or observation functions. For instance, the state variables may only be partially observable and different tasks may only be able to observe non-identical subsets of the state variables. It is also conceivable that multiple tasks observe the same subset of the state variables, but the variables are observed differently, e.g. sensors may be measuring the same quantities in different units. In such situations, it is desirable to map the available information to a unified representation which may be achievable either manually using domain knowledge or automatically from data.

Allowed learners. The choice of the learning algorithm may constrain the compatible scenarios. For instance, a partially observable system may require a method to reconstruct the full state while it is readily available given a fully observable system.

2.2.3 Settings

While traditional machine learning assumes identical source and target domains/tasks, the domains and/or tasks may differ in a transfer learning setting. Pan & Yang (2010) distinguish three transfer learning settings which account for different task relations between the source and target domains/tasks.

Inductive transfer learning. Inductive transfer learning utilizes few labeled data from the target domain to *induce* the target function of interest by transferring knowledge typically from labeled data in the source domain. When large amounts of labeled data are available in the source domain, inductive transfer learning is similar to multi-task learning except that it is only concerned with improving the target task performance by utilizing information from the source task.

Transductive transfer learning. Transductive transfer learning assumes identical source and target tasks but different domains. Further, while there are labeled data available in the source domain, only unlabeled data are available in the target domain. Transductive transfer can be divided into two cases where (i) the source and target domains are actually different, and (ii) the feature spaces of the source and target domains are equal, but the marginal probability distributions are different.

Unsupervised transfer learning. Unsupervised transfer learning assumes no labeled data in the source or target domain. It is, in principle, similar to the inductive transfer learning setting, however, it is concerned with unsupervised learning tasks such as clustering, dimensionality reduction, and density estimation in the target domain.

Each of these settings can be addressed by a (sub)set of the different approaches presented in the next subsection.

2.2.4 Approaches

Knowledge transfer can be achieved in multiple ways by transferring different kinds of information, e.g. a weighted subset of the training data from the source domain may be reused to improve learning in the target domain, a common feature representation may be sought which is useful for both the source and target domains, parameters may be shared within a joint model, or particular domain properties may be exploited. Pan & Yang (2010) distinguish different approaches to transfer learning which are listed as follows.

Instance transfer. Instance transfer assumes labeled data in the source domain which are re-weighted for the target domain in order to be useful.

Representation transfer. Representation transfer aims to learn representations of the input that are useful for the source and target tasks, thus, reducing domain divergence in the feature representation space.

Parameter transfer. Parameter transfer aims to learn parameters that are, at least in part, shared among multiple tasks. Many parameter transfer approaches use a regularization framework that ties the parameters of the tasks. Alternatively, models may be composed of cross-task and task-specific parameters (e.g. Caruana, 1993). Representation and parameter transfer methods may be related under some circumstances. For instance, a model may be composed of a task-dependent feature extraction layer, which maps the domain spaces to a common task-invariant feature space, followed by a shared classifier/regressor (e.g. Ajakan et al., 2014).

Relational knowledge transfer. Relational knowledge transfer assumes non-i.i.d. relational domains where relational knowledge is mapped from the source domain(s) to the target domain.

2.2.5 Discussion

According to Pan & Yang, some approaches have been applied in all transfer settings while others have not yet been explored in some settings. Table 2.1 provides an overview of the relations between approaches and settings. The work presented in this thesis uses a parameter transfer approach in the inductive transfer learning setting.

		Settings		
		Inductive	Transductive	Unsupervised
Approaches	Instance	✓	✓	
	Representation	✓	✓	✓
	Parameter	✓		
	Relational knowledge	✓		

Table 2.1: Comparison of the application of transfer learning approaches in different transfer settings (Pan & Yang, 2010).

Prominent applications of transfer learning, that have attracted much attention in recent years, are vision, acoustics or natural language which require learning good representations of the typically high-dimensional data for further processing. In supervised learning tasks only relatively few labels of a target task are available which motivated researchers to investigate into transfer learning approaches to share a common representation across multiple tasks using unsupervised methods (e.g. Glorot et al., 2011; Bengio, 2012). However, literature research indicates that multi-task and transfer learning approaches for system identification tasks using recurrent neural networks (RNN) have not been explored before. The problems investigated in this thesis exhibit data that is typically relatively low-dimensional and structured, e.g. a system is observed through sensors each measuring a particular aspect of the system. Hence, the kind of representation or feature learning tasks as they are common with natural data are uncommon in the considered scenarios.

2.3 Neural Networks

Neural networks (e.g. Kröse & van der Smagt, 1994) are biologically inspired nonlinear parametric models. They consist of neurons, which are represented as nodes in the network, and synapses, which are represented as connections or adaptive weights between nodes. The value of a weight determines the connection strength between two neurons. In order to identify the relationship between the presented inputs and targets the weights are adapted, or learned, such that the expected error of the model is minimized. Neural networks are highly configurable models which allows the designer to incorporate domain knowledge into the architecture. Among the vast space of possibilities several key architectures have emerged. The following subsections will introduce the perceptron, multi-layer perceptron, and the Elman recurrent neural network architecture.

2.3.1 Perceptron

The perceptron is the most basic type of neural network (Rosenblatt, 1958; Minsky & Papert, 1988). It implements a simple artificial neuron with a threshold function whose incoming weights are adaptive and learned from data. As opposed to the logistic regression model, whose output is a weighted linear combination of the inputs followed by a smooth nonlinear sigmoid function yielding values in the range $]0, 1[$, the perceptron's output is a weighted linear combination of the inputs forced to the binary values $\{0, 1\}$ by means of a threshold. Mathematically, the perceptron hypothesis is defined by the equation

$$h_\theta(x) = \begin{cases} 1 & \text{if } w^T x + b > 0 \\ 0 & \text{else} \end{cases} \tag{2.7}$$

where $x \in \mathbb{R}^n$ is the input vector, $w \in \mathbb{R}^n$ is the weights vector, and $b \in \mathbb{R}$ is a bias weight, thus, $\theta = \{w, b\}$. Figure 2.2 illustrates the perceptron model. After the weights are initialized randomly or with zero values they are adapted to minimize the empirical error between the predicted output $\hat{y} = h_\theta(x)$ and the target $y \in \{0, 1\}$ using the perceptron learning rule.

$$w \leftarrow w + \alpha(y - \hat{y}) \bullet x \tag{2.8a}$$

$$b \leftarrow b + \alpha(y - \hat{y}) \tag{2.8b}$$

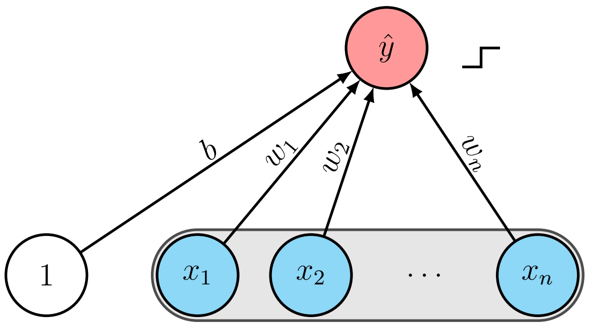

Figure 2.2: Perceptron

The bold bullet "•" denotes the pointwise vector product and $\alpha > 0$ is the learning rate. The perceptron learning rule is similar to the gradient descent learning rule, which is covered in Section 2.4.1.

2.3.2 Multi-Layer Perceptron

The multi-layer perceptron (MLP) is an extension of the perceptron consisting of multiple layers of artificial neurons equipped with nonlinear activation functions. In contrast to the perceptron model the MLP is able to extract increasingly abstract representations of the inputs by stacking multiple layers of hidden neurons on top of each other. It has been proven that the MLP is a universal function approximator, i.e. it can approximate any continuous function on a compact domain with arbitrary accuracy, provided it has at least a single hidden layer with a sufficient number of neurons (Cybenko, 1989; Hornik et al., 1989; Hornik, 1991; Haykin, 1998).

To formalize the model, let n_i denote the dimensionality of layer i in an MLP. Further, let $W^{(i)} \in \mathbb{R}^{n_i \times n_{i+1}}$ be the weight matrix from layer i to layer $i+1$, $b^{(i)} \in \mathbb{R}^{n_{i+1}}$ be the bias weight vector of layer $i+1$, and $\phi^{(i)} \colon \mathbb{R} \to \mathbb{R}$ be an elementwise nonlinear activation function applied to layer i. Typical activation functions are

$$\tanh(x) := \frac{e^x - e^{-x}}{e^x + e^{-x}} \tag{2.9}$$

$$\text{logistic}(x) := \frac{1}{1 + e^{-x}} \tag{2.10}$$

$$\text{relu}(x) := \begin{cases} x & \text{if } x > 0 \\ 0 & \text{else} \end{cases}. \tag{2.11}$$

Figure 2.3 depicts the activation functions. An MLP with l layers (including

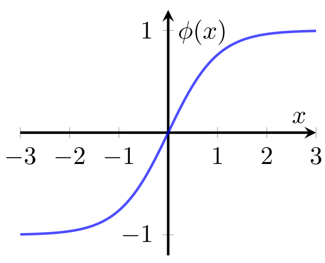

(a) $\phi(x) = \tanh(x)$

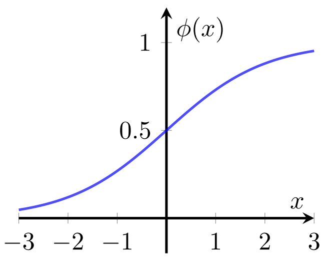

(b) $\phi(x) = \text{logistic}(x)$

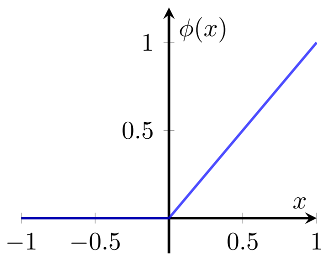

(c) $\phi(x) = \text{relu}(x)$

Figure 2.3: Activation functions

the input and output layer) is described by the following equations.

$$z^{(1)} = x \tag{2.12a}$$

$$a^{(2)} = W^{(1)} z^{(1)} + b^{(1)} \tag{2.12b}$$

$$z^{(2)} = \phi^{(2)}(a^{(2)}) \tag{2.12c}$$

$$\vdots$$

$$a^{(l)} = W^{(l-1)} z^{(l-1)} + b^{(l-1)} \tag{2.12d}$$

$$z^{(l)} = \phi^{(l)}(a^{(l)}) \tag{2.12e}$$

$$\hat{y} = z^{(l)} \tag{2.12f}$$

Figure 2.4 depicts the MLP architecture.

Let $\theta := \{W^{(1)}, b^{(1)}, ..., W^{(l-1)}, b^{(l-1)}\}$ be the parameters of the MLP of equations (2.12a) to (2.12f). Then, the optimal parameters θ^* of the model are found by minimizing the error between the model output and the data $(x, y) \in D$ given the inputs x and the targets y.

$$\theta^* = \arg\min_{\theta} \frac{1}{|D|} \sum_{(x,y) \in D} \mathcal{L}(\hat{y}, y) \tag{2.13}$$

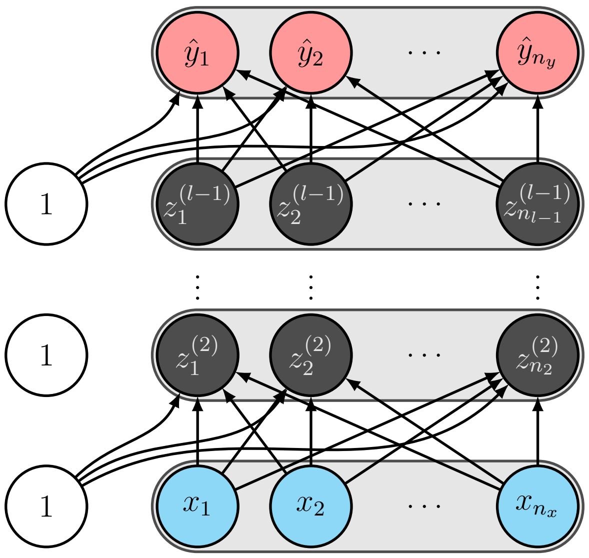

Figure 2.4: Multi-Layer perceptron with l layers including the input and output layer.

2.3.3 Recurrent Neural Networks

Recurrent neural networks (RNN) are powerful models for sequence modeling tasks (e.g. Rehkugler & Zimmermann, 1994; Mikolov et al., 2010; Socher, 2014). In contrast to multi-layer perceptrons (also known as feed-forward neural networks), RNNs are cyclic with temporal delays in the recurrent connections. Thus, they are able to naturally model sequential data and learn to build an internal temporal memory. A common recurrent architecture is known as the Elman network (Elman, 1990). Similar to MLPs, RNNs are universal approximators as well (Schäfer & Zimmermann, 2006; 2007). In addition, they possess the computational power of a Turing machine (Siegelmann & Sontag, 1991).

Let n_u and n_v denote the dimensionality of layer u and v in an RNN. Further, let $W_{vu} \in \mathbb{R}^{n_v \times n_u}$ be the weight matrix from layer u to layer v, $b_v \in \mathbb{R}^{n_v}$ be the bias vector of layer v, and $\phi\colon \mathbb{R} \to \mathbb{R}$ be an elementwise nonlinear function as described in Section 2.3.2. The input vectors $(x_{[1]}, ..., x_{[T]})$, $x_{[t]} \in \mathbb{R}^{n_x}$, of the Elman RNN are processed sequentially and mapped to a hidden state sequence $(h_{[1]}, ..., h_{[T]})$, $h_{[t]} \in \mathbb{R}^{n_h}$. Based on the hidden state sequence the output sequence $(\hat{y}_{[1]}, ..., \hat{y}_{[T]})$, $y_{[t]} \in \mathbb{R}^{n_y}$, is computed. The Elman RNN is defined recursively for $t = 1, ..., T$ by the following equations

$$h_{[0]} = h_{\text{init}} \tag{2.14a}$$

$$h_{[t]} = \phi_h(W_{hx}x_{[t]} + W_{hh}h_{[t-1]} + b_h) \tag{2.14b}$$

$$\hat{y}_{[t]} = \phi_y(W_{yh}h_{[t]} + b_y) \tag{2.14c}$$

with some initial state $h_{\text{init}} \in \mathbb{R}^{n_h}$. It is common to either set $h_{\text{init}} = 0$ or treat it as an additional parameter vector to be learned. Figure 2.5 illustrates the Elman RNN architecture using recurrent connections in the hidden layer. An

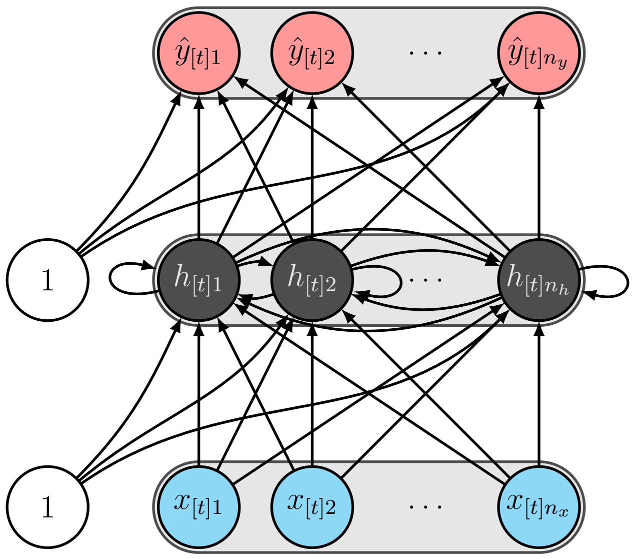

Figure 2.5: Elman RNN

alternative visualization of RNN architectures draws the network unfolded in time for a finite number of time steps. To improve readability only clusters of neurons are drawn instead of each individual one. An arrow then represents a full connection between two clusters of neurons, i.e. each neuron in the source cluster is connected with each neuron in the destination cluster. Figure 2.6 depicts the network architecture unfolded for three time steps.

Let $\theta := \{W_{hx}, W_{hh}, b_h, W_{yh}, b_y\}$ be the RNN parameters of equations (2.14a) to (2.14c). Then, the optimal parameters θ^* of the model are found by fitting the model to the data, given the inputs $x_{[t]}$ and the targets $y_{[t]}$, over a fixed number of T time steps.

$$\theta^* = \arg\min_{\theta} \frac{1}{|D| \cdot T} \sum_{(x_{[1]}, y_{[1]} \ldots, x_{[T]}, y_{[T]}) \in D} \sum_{t=1}^{T} \mathcal{L}(\hat{y}_{[t]}, y_{[t]}) \tag{2.15}$$

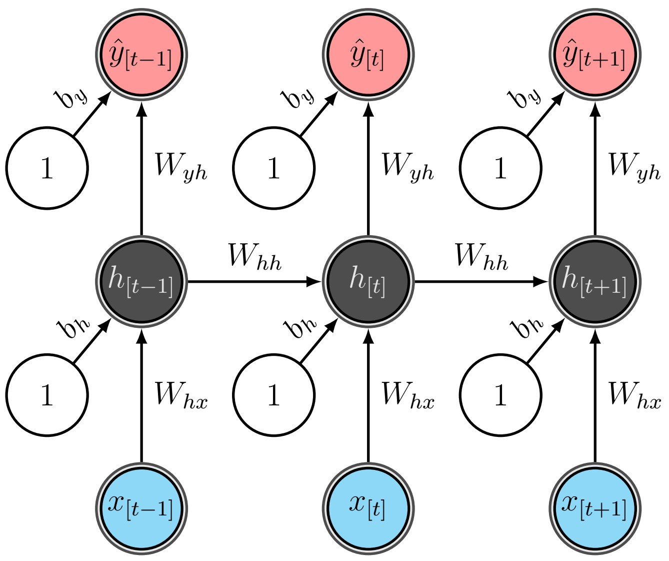

Figure 2.6: Elman RNN unfolded over time

Initialization. The parameter initialization of RNNs is more sensitive compared to feed-forward neural networks in order to achieve robust optimization (Jaeger & Haas, 2004; Sutskever et al., 2013). Special care should be taken to initialize the hidden-to-hidden matrix W_{hh} because it primarily affects the dynamics and memory of information propagated through time. According to Jaeger & Haas, when the spectral radius of W_{hh} is less than 1, the network "forgets" exponentially due to repeated multiplication of the hidden state with the matrix which can lead to vanishing gradients. On the other hand, when its spectral radius is larger than 1, the network dynamics may become chaotic and can lead to exploding gradients. Results by Sutskever et al. suggest to rescale the randomly initialized matrix W_{hh} to have a spectral radius around 1.1.

Block validation. In order to estimate the generalization performance of a model, a test set needs to be set aside before training whose examples are not used to optimize the model parameters. For non-sequential models, the data set simply needs to be split into two subsets. However, the procedure requires special care to be taken when dealing with sequential data. A sequential model requires examples that span multiple time steps which are usually created by the concatenation of examples obtained from a fixed-size sliding window moved along the time axis. When splitting the resulting data set into training and test subsets, some of the examples in both the training and test set contain the same observations. Figure 2.7 illustrates the issue. At the top of the figure, a

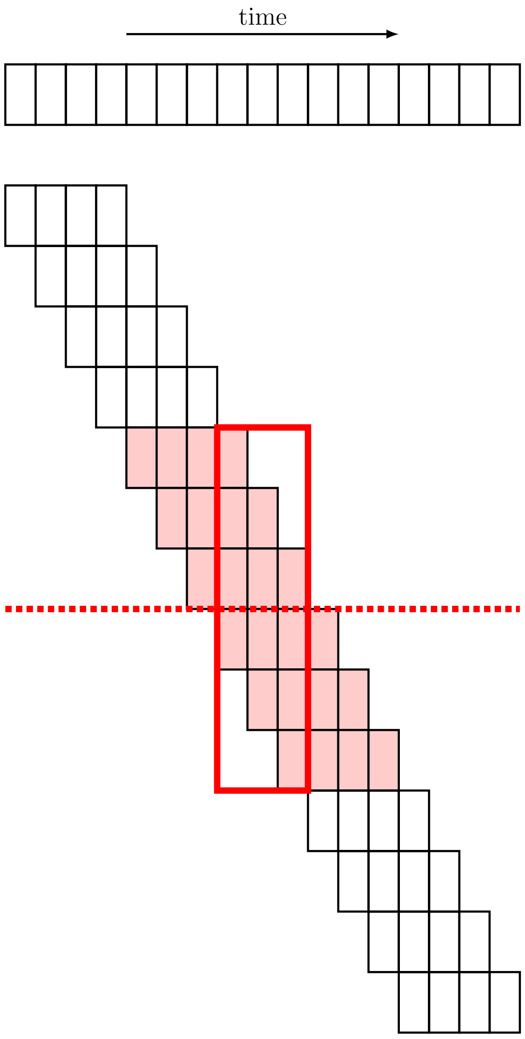

Figure 2.7: Creation of training and test examples with sequential data.

sequence of observations is shown from which windows of four time steps are extracted to create a data set suitable for training and evaluation. When the resulting data set is split into two subsets, six examples close to the splitting point contain observations that are also contained in the other subset. Thus, an observations seen during training is also part of the test set. However, it is important to have training and test sets that do not overlap in order to avoid misleading generalization performance estimates. Düll et al. (2012) propose a procedure called *block validation* which omits examples that have overlapping observations in the training and test set. Further, they suggest to select multiple blocks at random instead of splitting the data set into two contiguous chunks.

2.4 Learning & Optimization

Learning the parameters of a neural network is typically performed using first-order optimization techniques, such as gradient descent or variants thereof. To do so, it is necessary to compute the partial derivatives of the error function with respect to the parameters. While, in general, this simply requires multivariate calculus and, in particular, means applying the chain rule repeatedly, it is not immediately obvious that computing the partial derivatives naïvely results in redundant computations. However, combining the rules of calculus and dynamic programming yields an algorithm called *backpropagation* which is an efficient way of obtaining the partial derivatives.

The following subsections introduce the *backpropagation* algorithm and *Hessian-Free optimization*—a second-order optimization method that has been shown to be a powerful technique to learn the parameters of recurrent neural networks. Further, complex models, such as neural networks, are prone to overfitting, i.e. memorizing input patterns rather than inferring the underlying structure from examples. Several techniques to reduce this phenomenon have emerged some of which are revised in this section.

2.4.1 Backpropagation

The backpropagation algorithm (Rumelhart, 1986; Rumelhart et al., 1988) is an efficient method to compute the partial derivatives of an error function with respect to its parameters. In essence, it combines multivariate calculus with dynamic programming in order to reuse previously computed parts of the gradient. A three-layer feed-forward network as introduced in Section 2.3.2 will serve as an example to derive the algorithm and discuss its importance for efficient learning.

Let $\theta = \{W^{(1)}, b^{(1)}, W^{(2)}, b^{(2)}\}$ be the parameters of a three-layer perceptron described by (2.16a) to (2.16f).

$$z^{(1)} = x \tag{2.16a}$$
$$a^{(2)} = W^{(1)}z^{(1)} + b^{(1)} \tag{2.16b}$$
$$z^{(2)} = \phi(a^{(2)}) \tag{2.16c}$$
$$a^{(3)} = W^{(2)}z^{(2)} + b^{(2)} \tag{2.16d}$$
$$z^{(3)} = \phi(a^{(3)}) \tag{2.16e}$$
$$\hat{y} = z^{(3)} \tag{2.16f}$$

A single example x is propagated through the network and compared against the ground truth y using the squared error $E(\theta; x, y) = \frac{1}{2}\sum_{i=1}^{n_3}(y_i - \hat{y}_i)^2$. Let $\bullet$ denote the elementwise product, or Hadamard product, of two vectors. First, the partial derivative of the error with respect to $W^{(2)}$ is computed.

$$\begin{aligned}
\frac{\partial E}{\partial W_{kl}^{(2)}} &= \sum_{\alpha=1}^{n_3} \frac{\partial E}{\partial z_\alpha^{(3)}} \frac{\partial z_\alpha^{(3)}}{\partial W_{kl}^{(2)}} && (2.17a)\\
&= \sum_{\alpha=1}^{n_3} \frac{\partial \left(\frac{1}{2}\sum_{i=1}^{n_3}(y_i - z_i^{(3)})^2\right)}{\partial z_\alpha^{(3)}} \frac{\partial \phi(a_\alpha^{(3)})}{\partial W_{kl}^{(2)}} && (2.17b)\\
&= \sum_{\alpha=1}^{n_3} (z_\alpha^{(3)} - y_\alpha) \frac{\partial \phi(a_\alpha^{(3)})}{\partial a_\alpha^{(3)}} \frac{\partial a_\alpha^{(3)}}{\partial W_{kl}^{(2)}} && (2.17c)\\
&= \sum_{\alpha=1}^{n_3} (z_\alpha^{(3)} - y_\alpha) \phi'(a_\alpha^{(3)}) \frac{\partial \left(\sum_{\beta=1}^{n_2} W_{\alpha\beta}^{(2)} z_\beta^{(2)} + b_\alpha^{(2)}\right)}{\partial W_{kl}^{(2)}} && (2.17d)\\
&= \sum_{\alpha=1}^{n_3} (z_\alpha^{(3)} - y_\alpha) \phi'(a_\alpha^{(3)}) \sum_{\beta=1}^{n_2} \delta_{\alpha k}\delta_{\beta l} z_\beta^{(2)} && (2.17e)\\
&= \sum_{\alpha=1}^{n_3} (z_\alpha^{(3)} - y_\alpha) \phi'(a_\alpha^{(3)}) \delta_{\alpha k} \sum_{\beta=1}^{n_2} \delta_{\beta l} z_\beta^{(2)} && (2.17f)\\
&= (z_k^{(3)} - y_k)\phi'(a_k^{(3)}) z_l^{(2)} && (2.17g)\\
&= \left[((z^{(3)} - y) \bullet \phi'(a_i^{(3)}))(z^{(2)})^T\right]_{kl} && (2.17h)
\end{aligned}$$

$$\Rightarrow \frac{\partial E}{\partial W^{(2)}} = ((z^{(3)} - y) \bullet \phi'(a^{(3)}))(z^{(2)})^T \tag{2.17i}$$

The partial derivative with respect to $b^{(2)}$ is obtained similarly.

$$\frac{\partial E}{\partial b^{(2)}} = (z^{(3)} - y) \bullet \phi'(a^{(3)}). \tag{2.18}$$

Second, the partial derivative with respect to $W^{(1)}$ is computed as follows.

$$\begin{aligned}
\frac{\partial E}{\partial W^{(1)}_{kl}} &= \sum_{\alpha=1}^{n_3} \frac{\partial E}{\partial z^{(3)}_\alpha} \frac{\partial z^{(3)}_\alpha}{\partial W^{(1)}_{kl}} && \text{(2.19a)}\\
&= \sum_{\alpha=1}^{n_3} \frac{\partial \left(\frac{1}{2}\sum_{i=1}^{n_3}(y_i - z^{(3)}_i)^2\right)}{\partial z^{(3)}_\alpha} \frac{\partial \phi(a^{(3)}_\alpha)}{\partial W^{(1)}_{kl}} && \text{(2.19b)}\\
&= \sum_{\alpha=1}^{n_3} (z^{(3)}_\alpha - y_\alpha) \frac{\partial \phi(a^{(3)}_\alpha)}{\partial a^{(3)}_\alpha} \frac{\partial a^{(3)}_\alpha}{\partial W^{(1)}_{kl}} && \text{(2.19c)}\\
&= \sum_{\alpha=1}^{n_3} (z^{(3)}_\alpha - y_\alpha) \phi'(a^{(3)}_\alpha) \frac{\partial \left(\sum_{\beta=1}^{n_2} W^{(2)}_{\alpha\beta} z^{(2)}_\beta + b^{(2)}_\alpha\right)}{\partial W^{(1)}_{kl}} && \text{(2.19d)}\\
&= \sum_{\alpha=1}^{n_3} (z^{(3)}_\alpha - y_\alpha) \phi'(a^{(3)}_\alpha) \sum_{\beta=1}^{n_2} W^{(2)}_{\alpha\beta} \frac{\partial z^{(2)}_\beta}{\partial W^{(1)}_{kl}} && \text{(2.19e)}\\
&= \sum_{\alpha=1}^{n_3} (z^{(3)}_\alpha - y_\alpha) \phi'(a^{(3)}_\alpha) \sum_{\beta=1}^{n_2} W^{(2)}_{\alpha\beta} \frac{\partial z^{(2)}_\beta}{\partial a^{(1)}_\beta} \frac{\partial a^{(1)}_\beta}{\partial W^{(1)}_{kl}} && \text{(2.19f)}\\
&= \sum_{\alpha=1}^{n_3} (z^{(3)}_\alpha - y_\alpha) \phi'(a^{(3)}_\alpha) \sum_{\beta=1}^{n_2} W^{(2)}_{\alpha\beta} \frac{\partial \phi(a^{(2)}_\beta)}{\partial a^{(1)}_\beta} \frac{\partial \left(\sum_{\gamma=1}^{n_1} W^{(1)}_{\beta\gamma} x^{(1)}_\gamma + b^{(1)}_\beta\right)}{\partial W^{(1)}_{kl}} && \text{(2.19g)}\\
&= \sum_{\alpha=1}^{n_3} (z^{(3)}_\alpha - y_\alpha) \phi'(a^{(3)}_\alpha) \sum_{\beta=1}^{n_2} W^{(2)}_{\alpha\beta} \phi'(a^{(2)}_\beta) \sum_{\gamma=1}^{n_1} \delta_{\beta k}\delta_{\gamma l} x^{(1)}_\gamma && \text{(2.19h)}\\
&= \sum_{\alpha=1}^{n_3} (z^{(3)}_\alpha - y_\alpha) \phi'(a^{(3)}_\alpha) \sum_{\beta=1}^{n_2} W^{(2)}_{\alpha\beta} \phi'(a^{(2)}_\beta) \delta_{\beta k} \sum_{\gamma=1}^{n_1} \delta_{\gamma l} x^{(1)}_\gamma && \text{(2.19i)}\\
&= \sum_{\alpha=1}^{n_3} (z^{(3)}_\alpha - y_\alpha) \phi'(a^{(3)}_\alpha) W^{(2)}_{\alpha k} \phi'(a^{(2)}_k) x^{(1)}_l && \text{(2.19j)}\\
&= \left[(((W^{(2)})^T((z^{(3)} - y) \bullet \phi'(a^{(3)}))) \bullet \phi'(a^{(2)}))x^T\right]_{kl} && \text{(2.19k)}
\end{aligned}$$

$$\Rightarrow \frac{\partial E}{\partial W^{(1)}} = (((W^{(2)})^T((z^{(3)} - y) \bullet \phi'(a^{(3)}))) \bullet \phi'(a^{(2)}))x^T \qquad \text{(2.19l)}$$

The partial derivative with respect to $b^{(1)}$ is obtained similarly.

$$\frac{\partial E}{\partial b^{(2)}} = ((W^{(2)})^T((z^{(3)} - y) \bullet \phi'(a^{(3)}))) \bullet \phi'(a^{(2)}). \qquad \text{(2.20)}$$

After examining (2.17i) and (2.19l) more closely it becomes obvious that $\frac{\partial E}{\partial W^{(1)}}$ contains part of the computation of $\frac{\partial E}{\partial W^{(2)}}$. More precisely, the term $(z^{(3)} - y) \bullet \phi'(a^{(3)})$ is present in both expressions. The idea of backpropagation is to reuse parts of the derivative computed in higher layers, i.e. layers close to the output of the network, in order to compute the derivatives of lower layers. Therefore, parts of the derivatives of the higher layers are tabulated and looked up instead of recomputed by the lower layer derivatives. Then, computing the derivatives looks similar to the forward propagation shown in (2.16a) to (2.16f) but performed in reverse direction, hence, the term backpropagation. First, the errors are propagated backwards yielding the following local error message, or so-called *delta* messages.

$$\delta^{(3)} = (z^{(3)} - y) \bullet \phi(a^{(3)}) \tag{2.21a}$$

$$\delta^{(2)} = ((W^{(2)})^T \delta^{(2)}) \bullet \phi(a^{(2)}) \tag{2.21b}$$

Second, once the delta messages are computed the partial derivatives are easily obtained as follows.

$$\frac{\partial E}{\partial W^{(2)}} = \delta^{(2)} (z^{(2)})^T \tag{2.22a}$$

$$\frac{\partial E}{\partial b^{(2)}} = \delta^{(3)} \tag{2.22b}$$

$$\frac{\partial E}{\partial W^{(1)}} = \delta^{(2)} (z^{(1)})^T = \delta^{(2)} x^T \tag{2.22c}$$

$$\frac{\partial E}{\partial b^{(1)}} = \delta^{(2)} \tag{2.22d}$$

While this example demonstrates the backpropagation algorithm for a three-layer feed-forward network, it generalizes for an arbitrary number of layers as well as for recurrent architectures, whose extension is called *backpropagation through time (BPTT)*, and for arbitrary directed acyclic computation graphs, which is called *backpropagation through structure (BTS)*. Using the first derivatives computed by backpropagation, the model parameters are adapted to minimize the error function. Often, simple first-order optimization methods, such as (stochastic) gradient descent or variants thereof, are used. However, it has been observed that learning the parameters of recurrent neural networks with first-order optimization methods may be troublesome due to the so-called vanishing and exploding gradient problem (Hochreiter, 1991; Bengio et al., 1994; Hochreiter et al., 2001). The next subsection introduces a second-order optimization method that has been shown to overcome these difficulties and which is capable of handling even a large number of parameters—a common property of neural network models.

2.4.2 Hessian-Free Optimization

Hessian-Free optimization (Martens, 2010; Martens & Sutskever, 2011; 2012) is an approximate Newton method suitable for training models with a large number of parameters, e.g. neural networks. Especially in deep learning, where many layers of abstraction are used to extract complex features from the input data, slow and ineffective learning has been observed. Non-random initialization through layerwise pre-training using Restricted Boltzmann Machines (Hinton & Salakhutdinov, 2006) and shallow autoencoders (Bengio et al., 2007) has been found to give significant improvements. However, these approaches are designed for deep feed-forward neural networks which is a rather strong limitation given the flexibility entailed by general neural networks. Since Hessian-Free optimization is a general optimization method, it imposes fewer constraints on the model. Martens & Sutskever demonstrated that this approach is well suited for non-convex neural network objective functions that had been difficult to optimize including deep feedforward and recurrent neural networks.

In contrast to first-order optimization methods, Hessian-Free optimization constructs a local quadratic approximation of the objective function at the current location in the parameter space, thus, utilizing curvature information in addition to the gradient. Let $B(\theta^{(k-1)})$ be the curvature matrix, e.g. the Hessian $H(\theta^{(k-1)})$ of the objective $f(\theta) := \varepsilon(h_\theta)$ at $\theta^{(k-1)}$ where h_θ is the parameterized hypothesis as described in Section 2.1. Then, a local quadratic approximation $M^{(k-1)}$ of f at $\theta^{(k-1)}$ is formed using the Taylor expansion up to degree two.

$$M^{(k-1)}(\Delta\theta) = f(\theta^{(k-1)}) + \nabla f(\theta^{(k-1)})^T \Delta\theta + \frac{1}{2}(\Delta\theta)^T B(\theta^{(k-1)})\Delta\theta \tag{2.23}$$

Using $M^{(k-1)}$, the parameters are updated according to the following rule

$$\theta^{(k)} = \theta^{(k-1)} + \alpha^{(k)} \left(\operatorname*{arg\,min}_{\Delta\theta\in\Theta} M^{(k-1)}(\Delta\theta) \right), \tag{2.24}$$

provided that the minimizer exists, with the step length $\alpha^{(k)} \in [0, 1]$ typically chosen using line-search (Nocedal & Wright, 2006). Martens & Sutskever propose to use the backtracking line-search starting with $\alpha^{(k)} = 1$.

The minimizer of $M^{(k-1)}$ exists if $B(\theta^{(k-1)})$ is positive definite and is found by the Newton step $(\Delta\theta^{(k)})^* = \theta^{(k-1)} - B^{-1}(\theta^{(k-1)})\nabla f(\theta^{(k-1)})$. There are a number of problems with the standard Newton method when used to optimize neural network objective functions.

1. First, $B(\theta^{(k-1)})$, e.g. the Hessian matrix, is prohibitively large for models with many parameters such as neural networks. It requires computing and storing the number of parameters squared. Architectures nowadays may easily consist of millions of parameters yielding a matrix with 10^{12} or more entries.

2. Second, even if $B(\theta^{(k-1)})$ could be computed and stored, inverting it, or equivalently solving the system of equations $B(\theta^{(k-1)})\Delta\theta^{(k)} = -\nabla f(\theta^{(k-1)})$, is impractical.

3. Third, since most neural network objectives are non-convex its Hessian is not positive definite everywhere in the parameter space. Thus, $B(\theta^{(k-1)}) = H(\theta^{(k-1)})$ may not always be invertible.

Martens & Sutskever address these obstacles as follows. In order to guarantee semi positive definiteness of $B(\theta^{(k-1)})$ they use the generalized Gauss-Newton matrix instead of the Hessian, which is an approximation of the Hessian matrix. For details, see (Martens & Sutskever, 2012, Section 6). Since the generalized Gauss-Newton matrix is only semi-positive definite, but inverting a matrix requires strict positive definiteness, Tikhonov damping is added which raises all eigenvalues by a small positive number $\lambda > 0$, thus, making it strictly positive definite. Further, the generalized Gauss-Newton matrix is symmetric. Inversion of this matrix is performed by solving the above system of equations using the (preconditioned) conjugate gradient method (Golub & van Loan, 1996; Nocedal & Wright, 2006) which is an iterative algorithm with desirable convergence properties. In theory, and given infinite precision arithmetic, the conjugate gradient method is guaranteed to converge in at most $|\theta|$ iterations. However, in practice, and despite finite precision arithmetic, it typically reaches a small residual after many fewer than $|\theta|$ iterations. For details, please consult the above referenced literature. Finally, computing and storing the curvature matrix can be avoided due to the work of Pearlmutter (1994) and by observing that the conjugate gradient method merely requires the matrix-vector product of the system matrix (typically the generalized Gauss-Newton matrix) with an internal vector. Pearlmutter proposes a computationally efficient method called the *R-operator*, similar in notion to the backpropagation algorithm, which computes the product of the Hessian with a vector exactly without explicitly forming the matrix.

Algorithm 2.1 outlines the steps of the Hessian-Free optimization method. To achieve good performance, Martens & Sutskever summarize a bag of tricks

Algorithm 2.1 Hessian-Free optimization based on (Martens & Sutskever, 2012)

```
Require: $\theta^{(0)}$, $\lambda$
  $\Delta\theta^{(0)} \leftarrow 0$
  $k \leftarrow 1$
  while not converged do
      Select a data set $D' \subseteq D$ to compute the gradient
      Compute descent direction $d \leftarrow -\nabla_{\theta^{(k-1)}} f(\theta^{(k-1)})$ on $D'$
      Select a data set $D'' \subseteq D$ to compute the curvature
      Compute a preconditioning matrix $P$ at $\theta^{(k)}$
      Define $A(v) \equiv G(\theta^{(k-1)})v + \lambda I v$ on $D''$ using the R-operator
      Choose a decay constant $\zeta \in [0, 1]$
      $\Delta\theta^{(k)} \leftarrow \mathrm{PCG}(d, A, \zeta\Delta\theta^{(k-1)}, P)$
      Update $\lambda$ with the Levenberg-Marquardt method
      Choose step size $\alpha$, e.g. using backtracking line-search
      $\theta^{(k)} \leftarrow \theta^{(k-1)} + \alpha\Delta\theta^{(k)}$
      $k \leftarrow k + 1$
  end while
```

including advice to use large mini-batches, different data sets $D' \subseteq D$ to compute the gradient and $D'' \subseteq D$ to compute the curvature matrix where usually $|D'| > |D''|$, a typical choice of the decay constant $\zeta = 0.95$, which is similar in notion with momentum methods, a dynamic adaptation rule of the Tikhonov damping strength λ according to the Levenberg-Marquardt method, and the use of backtracking line-search as a fallback to ensure a descent step on the error surface. Learning the parameters of recurrent neural networks is further improved by adding a regularization term to the curvature estimate called *struc-*

tural damping (Martens & Sutskever, 2011). The intuition behind structural damping is as follows. Adjusting the parameters of a recurrent neural network, in particular the hidden-to-hidden matrix W_{hh}, causes large fluctuations in the hidden state sequence due to the recursive and highly nonlinear nature of this model. Thus, large parameter update steps may be untrustworthy and harmful to the optimization process. To avoid this issue, one could reduce the step size α, or, similarly, use a large Tikhonov damping coefficient λ, but this alleviates the advantage of utilizing curvature information to make larger update steps in the directions of low curvature. Instead, structural damping penalizes large changes in the hidden state sequence, thus, the parameters themselves are not regularized but rather the effect of their update with respect to the hidden dynamics.

2.4.3 Overfitting

Overfitting is a phenomenon commonly faced in statistics and machine learning when a model memorizes the presented data instead of identifying the underlying structure. It typically occurs when complex models, i.e. models with many degrees of freedom, are fitted to comparatively few examples. Consequently, such a model has poor generalization capabilities which become apparent when it is tested on an independent set of examples that was unseen during training. To avoid overfitting, several techniques have emerged such as regularization, early stopping, and ensemble learning, among others.

Regularization

Regularization is a method to reduce the effective model complexity by introducing additional information to the model typically by imposing (smoothness) constraints on its parameters (Girosi et al., 1995). The most common techniques in machine learning are known as L_1 and L_2 regularization which are added to the objective function to be minimized. They penalize the model parameters according to the L_p norm which, in the case of $p = 1$, yields sparse parameters or, in the case of $p = 2$, avoids large values. Especially in the neural networks community the L_2 regularization is also known as *weight decay*.

Another more recently introduced and popular approach is called *dropout* (e.g. Hinton et al., 2012; Srivastava et al., 2014; Bayer et al., 2014). It randomly sets incoming neurons to zero in each training example and, thus, prevents co-adaptation feature extractors. Alternatively, dropout can be considered a model averaging technique where an exponential number of submodels shares the same set of parameters.

Early Stopping

Early-stopping (e.g. Yao et al., 2007) is a different kind of regularization technique that does not rely on altering the model and/or the objective function. However, the underlying idea is similar to that of L_2 regularization which assumes that smaller parameter values are preferable. Early-stopping monitors an estimate of the generalization error on a validation set whose examples are not used to update the model parameters. As long as the error on the validation set improves sufficiently, training proceeds. Else, the training procedure is stopped following the assumption that the model is starting to memorize rather than generalize.

Ensemble Learning

Ensemble learning is a technique to utilize multiple models of a given learning task to improve predictive performance. There exist various approaches to form an ensemble of learners, e.g. bagging, boosting, mixture of experts, or stacked generalization are some of the most widely used methods. In the bagging approach (Breiman, 1996), each ensemble member learns the same task on a subset of the training data drawn at random with replacement. Boosting is similar to bagging except that the different ensemble members are trained on a subset of the data that are expected to be most informative with respect to the other members. In the mixture of experts ensemble (Jacobs et al., 1991; Jordan & Jacobs, 1994), multiple models are combined using a gating network which learns to select the most appropriate ensemble member given a particular input. Stacked generalization (Wolpert, 1992) is a technique similar to the mixture of experts except that the experts are combined using a meta-model that is trained subsequent to the training of the ensemble members.

2.5 Hidden Markov Models

This brief introduction to hidden Markov models is based on a tutorial by Rabiner (1989) and an introduction paper by Stamp (2004).

Hidden Markov models (HMM) are stochastic time-discrete generative models which assume a system to be a Markov process with the following property:

Definition 2.5 (Markov property #1) *Given a random variable $X_{[t]}$, which can assume the set of values $x = \{x_1, x_2, ..., x_N\}$, then the probability of the event $x_{[t]} \in x$ occurring at time $t \in \mathbb{N}$ depends only on the preceding event $x_{[t-1]} \in x$, i.e. $P(X_{[t]} = x_{[t]}|X_{[t-1]} = x_{[t-1]}, X_{[t-2]} = x_{[t-2]}, ..., X_{[1]} = x_{[1]}) = P(X_{[t]} = x_{[t]}|X_{[t-1]} = x_{[t-1]})$.*

In contrast to Markov models, the states of a hidden Markov model are invisible. Instead, a sequence of observations is assumed to be generated by a sequence of *hidden* states. The relationship between the hidden states and the observations gives the second assumption made in a hidden Markov model.

Definition 2.6 (Markov property #2) *Given a random variable $X_{[t]}$, which can assume the set of values $x = \{x_1, x_2, ..., x_N\}$, and a random variable $Y_{[t]}$, which can assume the set of values $y = \{y_1, y_2, ..., y_M\}$, then the probability of the observed event $y_{[t]} \in y$ occurring at time $t \in \mathbb{N}$ depends only on the hidden event $x_{[t]} \in x$ occurring at time $t \in \mathbb{N}$, i.e. $P(Y_{[t]} = y_{[t]}|X_{[t]} = x_{[t]}, X_{[t-1]} = x_{[t-1]}, ..., X_{[1]} = x_{[1]}) = P(Y_{[t]} = y_{[t]}|X_{[t]} = x_{[t]})$.*

Thus, the state transition probabilities as well as the probability distribution over the possible observations conditioned on the hidden state are parameters of the HMM. Prominent applications of HMMs are found in natural language processing, e.g. speech and handwriting recognition, DNA sequencing, and some other domains where temporal pattern recognition is required. Figure 2.8 depicts an illustration of a hidden Markov model.

A hidden Markov model is defined by a 5-tuple $\lambda = (S, V, A, B, \pi)$ where S denotes the set of possible hidden states, V denotes the set of possible observations, A denotes the state transition probability matrix, B denotes the emission probability matrix, and π is the initial state probability distribution. More specifically, the components are defined as follows:

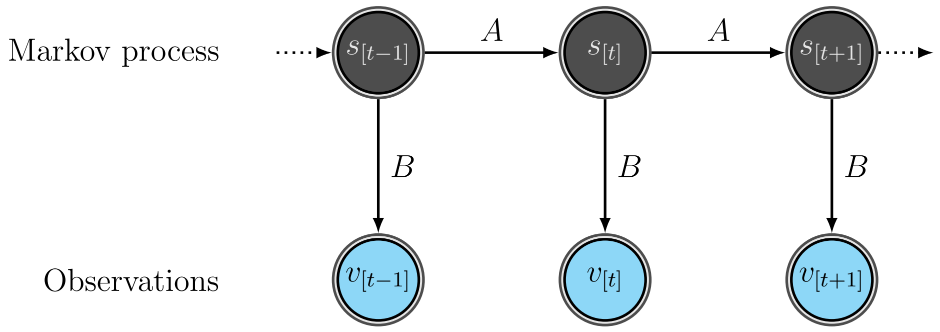

Figure 2.8: Hidden Markov model

- $S = \{s_1, s_2, ..., s_N\}$ is the set of unobserved states which are the possible values of the random variable $X_{[t]}$ at time $t \in \mathbb{N}$.
- $V = \{v_1, v_2, ..., v_M\}$ is the set of possible observations being the emissions of the random variable $Y_{[t]}$ at time $t \in \mathbb{N}$.
- $A \in [0,1]^{N \times N}$ is the state transition probability matrix modeling $P(X_{[t+1]} = s_j | X_{[t]} = s_i) = A_{ij}$ where $\sum_{j=1}^{N} A_{ij} = 1 \; \forall j \in \{1, 2, ..., N\}$.
- $B \in [0,1]^{n \times m}$ is the emission matrix where $b_i(v_j) = P(Y_{[t]} = v_j | X_{[t]} = s_i)$ is the probability of making the observation v_j given the unobserved state s_i.
- $\pi \in [0,1]^N$ is the initial probability distribution over the states S, i.e. $P(X_{[1]} = s_i) = \pi_i$ where $\sum_{i=1}^{N} \pi_i = 1$.

Thus, the parameters of the hidden Markov model are summarized as $\theta = \{A, B, \pi\}$. A common and natural assumption is to constrain the state transition probabilities A and the emission matrix B to be time-invariant, i.e. the probabilities do not change over time.

A hidden Markov model may be used in several inference scenarios.

Decoding/Filtering. Given the parameters θ of the model, the probability distribution π over the initial states, and a sequence of observations $(Y_{[1]}, Y_{[2]}, ..., Y_{[T]})$, the task is to determine the probability distribution over the hidden states $X_{[T]}$ after T time steps, i.e. $P(X_{[T]} | Y_{[1]}, X_{[2]}, ..., Y_{[T]})$. The hidden Markov model assumes that the underlying process moves through a sequence of states which emit the corresponding observations $(Y_{[1]}, Y_{[2]}, ..., Y_{[T]})$.

Smoothing. Given the parameters θ of the model, the probability distribution π over the initial states, and a sequence of observations $(Y_{[1]}, Y_{[2]}, ..., Y_{[T]})$, the task is to determine the probability distribution over the hidden states $X_{[T-\Delta t]}$ after $T - \Delta t$ time steps with $\Delta t \in \mathbb{N}$ and $1 < \Delta t < T$, i.e. $P(X_{[T-\Delta t]}|Y_{[1]}, X_{[2]}, ..., Y_{[T]})$. This task is similar to the decoding/filtering task, but instead of predicting the hidden state distribution at the end of the observed sequence, it shall be predicted somewhere in the middle of the sequence.

Prediction. Given the parameters θ of the model, the probability distribution π over the initial states, a sequence of observations $(Y_{[1]}, Y_{[2]}, ..., Y_{[T]})$, and a non-negative integer Δt, the task is to determine the probability distribution over the hidden states $X_{[T+\Delta t]}$ after $T + \Delta t \in \mathbb{N}$ time steps, i.e. $P(X_{[T+\Delta t]}|Y_{[1]}, X_{[2]}, ..., Y_{[T]})$. This task is similar to the decoding/filtering task, but instead of predicting the hidden state distribution at the end of the observed sequence, it shall be predicted after an additional Δt time steps without the availability of further observations from the Δt additional time steps.

Learning. Given a sequence of observations $Y = (Y_{[1]}, Y_{[2]}, ..., Y_{[T]})$, the task is to determine the parameters θ^* which maximize the probability of the observed sequence given a hidden state sequence $X = (X_{[1]}, X_{[2]}, ..., X_{[T]})$, i.e.

$$\theta^* = \arg\max_{\theta} P(Y) \tag{2.25a}$$

$$= \arg\max_{\theta} \sum_{X} P(Y, X) \tag{2.25b}$$

$$= \arg\max_{\theta} \sum_{X} P(Y|X)P(X) \tag{2.25c}$$

$$= \arg\max_{\theta} \sum_{X} \prod_{t=1}^{T} P(X_{[t]}|X_{[t-1]}, X_{[t-2]}, ..., X_{[1]})P(Y_{[t]}|X_{[t]}) \tag{2.25d}$$

$$= \arg\max_{\theta} \sum_{X} \prod_{t=1}^{T} P(X_{[t]}|X_{[t-1]})P(Y_{[t]}|X_{[t]}). \tag{2.25e}$$

Given the learned parameters θ^*, it is possible to determine the probability of a new observed sequence under the model.

2.6 Tensor Factorization

This section is largely based on a paper by Kolda & Bader (2009). Selected parts of the paper, that are relevant to this thesis, are summarized. The reader is referred to the paper for a detailed overview and introduction to tensor factorization and its applications.

2.6.1 Tensors

Tensors are multidimensional arrays. The number of dimensions is called *order* (or, alternatively, *ways* or *modes*). Tensors are a generalization of the more commonly known lower dimensional array types being vectors (first-order tensors) and matrices (second-order tensors). Tensors with more than two dimensions are called higher-order tensors.

Tensor slice. The slice of a tensor is a matrix-valued subtensor. It is obtained by fixing all but two indices. For third-order tensors the slices are distinguished as horizontal, lateral, and frontal slices. Figure 2.9 visualizes the different slice types of a third-order tensor.

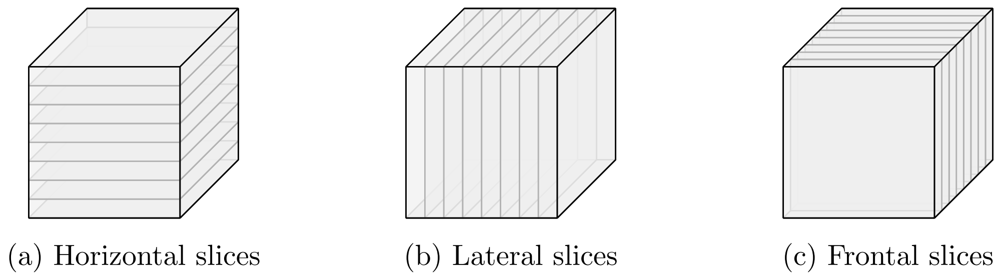
(a) Horizontal slices (b) Lateral slices (c) Frontal slices

Figure 2.9: Slice types of a third-order tensor.

Tensor rank. The rank of a tensor, i.e. rank$(\cdot)$, is defined as the minimum number of rank-one tensors that, when summed up, yield the original tensor (Hitchcock, 1927; Kruskal, 1977). An N-th order rank-one tensor X is defined as the outer product of N vectors $a_1, ..., a_N$, i.e.

$$X = a_1 \circ a_2 \circ ... \circ a_N, \tag{2.26}$$

where $\circ$ denotes the outer product of vectors. Figure 2.10 depicts a third-order rank-one tensor. Determining the rank of a higher-order tensor is more involved

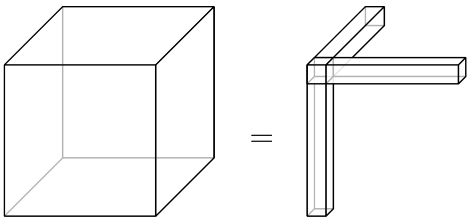

Figure 2.10: Third-order rank-one tensor.

than doing so for a matrix. The maximum rank of a general third-order tensor $X \in \mathbb{R}^{m \times n \times p}$ is weakly upper-bounded (Kruskal, 1977).

$$\operatorname{rank}(X) \leq \min\{mn, mp, np\} \tag{2.27}$$

Tighter upper bounds on the maximum rank are known for third-order tensors with two slices, i.e. $X \in \mathbb{R}^{m \times n \times 2}$, (JáJá, 1979; Kruskal, 1977).

$$\operatorname{rank}(X) = \min\{m, n\} + \min\left\{m, n, \left\lfloor \frac{\max\{m, n\}}{2} \right\rfloor\right\} \tag{2.28}$$

Results by Ten Berge (1991) show that the typical rank of a tensor $X \in \mathbb{R}^{n \times n \times 2}$ is n or $n + 1$.

2.6.2 Parallel Factor Analysis

Parallel Factor Analysis (Hitchcock, 1927; Harshman, 1970; Harshman & Lundy, 1994), or PARAFAC, is a tensor factorization method which decomposes an N-th order tensor into a sum of rank one tensors, i.e. the sum of outer products of N vectors. Figure 2.11 visualizes the PARAFAC decomposition applied to a third-order tensor. An alternative view on PARAFAC applied to third-order tensors shifts the focus to the decomposition of a particular slice. Let $A \in \mathbb{R}^{m \times n \times p}$ and Ae_i is the i-th frontal slice, then it may be decomposed into

$$Ae_i \approx U \operatorname{diag}(Se_i)V \tag{2.29}$$

with $U \in \mathbb{R}^{m \times r}$, $S \in \mathbb{R}^{r \times p}$, $V \in \mathbb{R}^{r \times n}$. Figure 2.12 illustrates PARAFAC according to the slice-based view. This perspective on the third-order PARAFAC may be understood as a weighted sum of rank one matrices where the weights are different for each slice. The slice-based perspective on PARAFAC is the preferred perspective in this thesis.

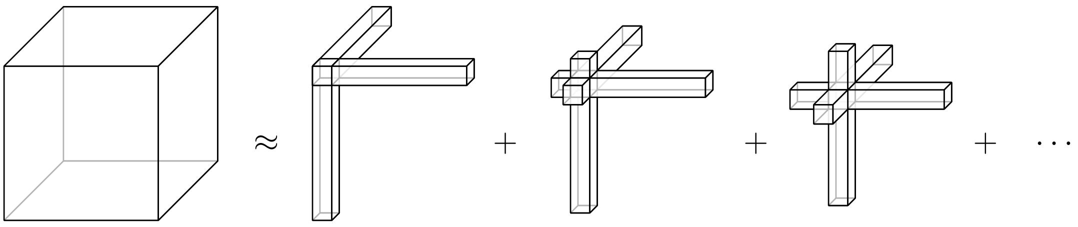

Figure 2.11: PARAFAC of a third-order tensor.

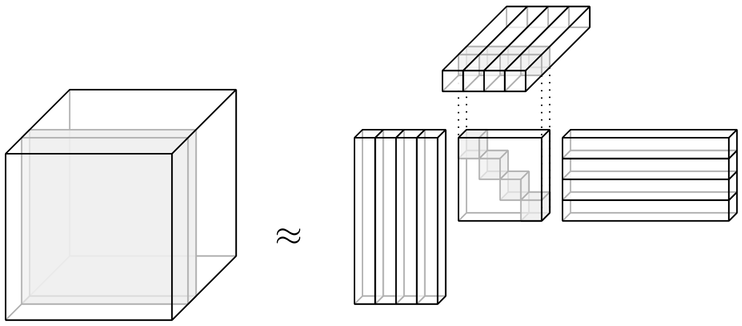

Figure 2.12: PARAFAC of a third-order tensor (alternative view).

2.6.3 Applications

Tensor factorization has had a wide a range of applications including psychometrics (e.g. Cattell, 1944; Carroll & Chang, 1970), chemometrics (e.g. Appellof & Davidson, 1981; Andersen & Bro, 2003), telecommunications (e.g. Sidiropoulos et al., 2000a;b; Sidiropoulos & Budampati, 2002; De Lathauwer & Castaing, 2007), and neuroscience (e.g. Mocks, 1988; Mitchell & Burdick, 1994; Andersen & Rayens, 2004; Martınez-Montes et al., 2004).

More recently, recommendation systems have become prominent applications of tensor factorization methods. A well known example of such is the “Netflix Prize”[1] which was a competition held by Netflix, Inc., a provider of DVD rental and on-demand video streaming. A brief outline of the Netflix Prize shall serve as an example to describe the idea behind tensor factorization approaches in this context.

The Netflix Prize was held to improve models that predict the rating of a movie given by a particular user based on previously recorded user-movie-ratings without any additional information about the user and movie. In order to sim-

[1]`http://www.netflixprize.com`

plify the illustration of tensor factorization, the date of the rating is ignored in this example. The set of triples (user, movie, rating), where the users and movies are encoded as nonnegative integers and the ratings are values in the set $\{1, 2, 3, 4, 5\}$, can be represented by a sparse matrix $X \in \{0, 1, ..., 5\}^{\#\text{users} \times \#\text{movies}}$ where a zero represents a missing rating of a particular movie given by a particular user. The matrix is sparse because most users have only rated a few movies. Figure 2.13 illustrates the user-movie-ratings matrix. Factorization of this rat-

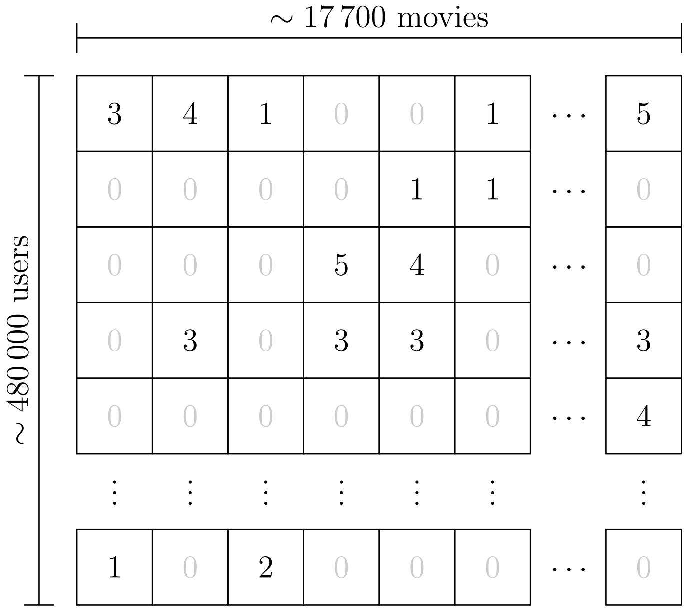

Figure 2.13: Example of the Netflix user-movie-ratings matrix.

ing matrix into low-rank components of the users and movies, i.e. PARAFAC in two dimensions, was a basic approach in the competition. Figure 2.14 depicts the low-rank factorization of the rating matrix. When fitted to the data matrix, latent representations of the users and movies are obtained whose pairwise inner products approximate the corresponding ratings in the rating matrix. The number of latent factors affects the rank of the approximated rating matrix. After learning the components, it turns out that they can be interpreted as properties of the users and movies, e.g.

- the movie may have a particular genre such as "action" and a user with this genre preference will be more likely to give a high rating;
- the movie may be serious in some sense and a user with a preference for

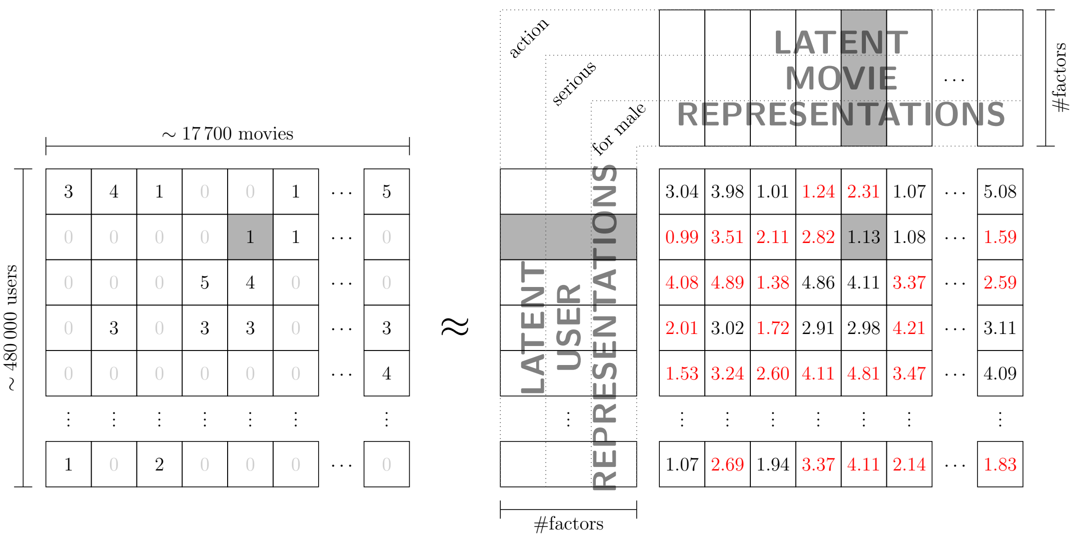

Figure 2.14: Low-rank decomposition of the Netflix user-movie-ratings matrix.

rather light content will be less likely to give a high rating;

- the movie may be targeted rather for the male audience and the rating will be affected by the user's gender.

Thus, matrix factorization of a data matrix aims to find a low-dimensional concept space that explains the observed data by computing the inner product of the entities in the given relation. While the presented approach is rather basic, much more sophisticated methods were being developed over the course of the competition (e.g. Koren, 2009; Töscher et al., 2009; Piotte & Chabbert, 2009). Since they are not the focus of this thesis the reader is referred to the respective literature for more information.

Tensors and factored representations are becoming increasingly popular as ingredients in neural architecture design (Sutskever et al., 2011; Yu et al., 2012; 2013; Socher et al., 2013a;b; İrsoy & Cardie, 2015) where they are used as learnable multi-linear operators rather than being an object that represents data.

2.7 System Identification

System identification denotes the process of building mathematical models of dynamical systems based on observed, or measured, data using statistical methods. Such models are typically distinguished as white, grey, and black box models. White box models are usually based on the fundamentals of physics, e.g. Newton's laws of motion, but they often become too complex or even impossible to derive in real-world applications. Grey box models are hybrids that rely on both a basic understanding of the system as well as on experimental data to estimate remaining unknown parameters. Grey box models are also known as semi-physical models (Forssell & Lindskog, 1997). Black box models rely entirely on observed measurements without utilizing any prior model. They are particularly common and useful when the system is poorly understood and/or very complex to describe using analytical methods. In this thesis black box models are investigated.

2.8 Artificial Benchmarks

This section introduces two artificial benchmarks which are well known in the reinforcement learning community. Their dynamics are described analytically and, thus, enable sampling data from varying configurations. Being able to easily generate data from similar dynamical systems is an important requirement in this thesis.

2.8.1 Cart-Pole

The cart-pole simulation (Michie & Chambers, 1968a;b; Barto et al., 1983; Sutton & Barto, 1998; Florian, 2007) consists of a cart, which moves on a one-dimensional track, and a pole hinged to the cart. Two control problems are commonly addressed in the context of this dynamical system: the pole swing-up task and the balancing task. In the swing-up task, the pole initially hangs downward and shall be swung up such that it is finally balanced in an upright position. The swing-up is achieved by applying an appropriate action sequence, i.e. a force applied to the cart, using as few steps as possible. The balancing task is a subtask of the swing-up task in which the pole starts in an upright position and shall remain balanced. Figure 2.15 depicts an illustration of the cart-pole environment. The state description consists of the tuple $(x, \dot{x}, \alpha, \dot{\alpha})$ being the position $x \in \mathbb{R}$ and velocity $\dot{x} \in \mathbb{R}$ of the cart as well as the angle $\alpha \in]-180°, 180°]$ and angular velocity $\dot{\alpha} \in \mathbb{R}$ of the pole. Contrary to settings

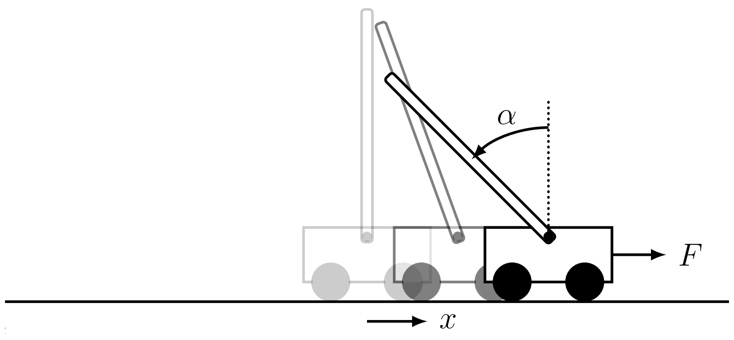

Figure 2.15: Cart-pole environment.

used in common reinforcement learning tasks, no constraints are enforced on the pole angle. In order to avoid discontinuities in the representation of the pole angle when the pole swings beyond 180°, its decomposition into the sine and cosine components is used. This transformation yields the new state space tuple $(x, \dot{x}, \cos(\alpha), \sin(\alpha), \dot{\alpha})$. The action space consists of the force $a \in [-1, 1]$ applied to the cart. The cart-pole simulation is observed every $\tau = 0.02\,\mathrm{s}$.

The cart-pole dynamics can be described by a set of differential equations. While first stated by Michie & Chambers (1968a;b), the simulation was popularized by Barto et al. (1983) and Sutton & Barto (1998), however, with incorrect equations as discovered by Florian (2007) who published a corrected set of equations as follows.

$$\ddot{\alpha} = \frac{g\sin(\alpha) + \cos(\alpha)\left(\frac{-F - m_p l \dot{\alpha}^2 \sin(\alpha)}{m_c + m_p}\right)}{l\left(\frac{4}{3} - \frac{m_p \cos^2(\alpha)}{m_c + m_p}\right)} \tag{2.30a}$$

$$\ddot{x} = \frac{F + m_p l(\dot{\alpha}^2 \sin(\alpha) - \ddot{\alpha}\cos(\alpha))}{m_c + m_p} \tag{2.30b}$$

The evolution of the dynamics can be approximated using the Euler method given a sufficiently high sampling frequency.

2.8.2 Mountain Car

The mountain car simulation (Sutton & Barto, 1998) consists of an underpowered car initially located in a valley. In control problems the learning objective is to drive the car up the hill. Since the car is underpowered, it must gain momentum in order to reach its goal position. Figure 2.16 depicts an illustration of

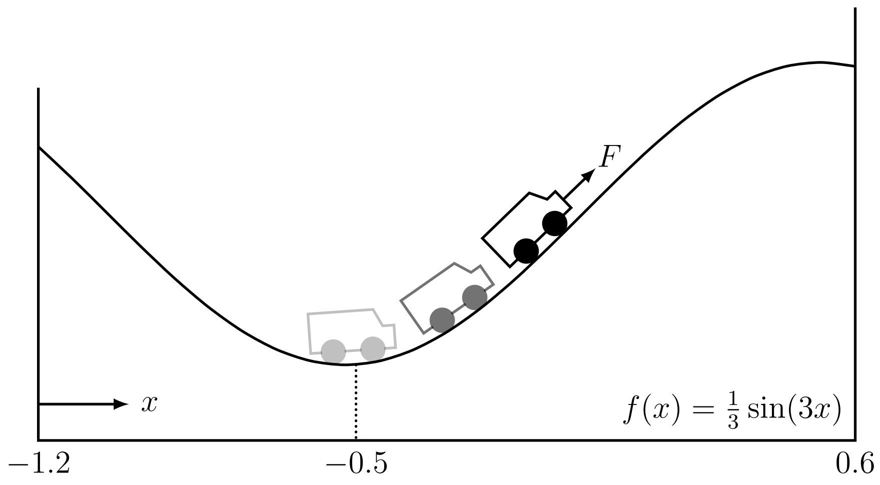

Figure 2.16: Mountain car environment.

the mountain car environment. The mountain shape follows the trigonometric function $f(x) = \frac{1}{3}\sin(3x)$. The state description consists of the tuple $(x, \dot{x})$, $x \in [-1.2, 0.6]$ and $\dot{x} \in [-0.07, 0.07]$, being the position and velocity of the car. The action space consists of the acceleration $a \in \{-1, 0, 1\}$ of the car which is altered to be continuous-valued in this thesis, i.e. $a \in [-1, 1]$, to make the simulation more realistic.

The mountain car dynamics can be described by the following update equations with typical values of the acceleration factor $\gamma = 0.001$ and the gravity $g = -0.0025$.

$$\dot{x}_{[t+1]} = \dot{x}_{[t]} + \gamma a + g\cos(3x) \tag{2.31a}$$

$$x_{[t+1]} = x_{[t]} + \dot{x}_{[t+1]} \tag{2.31b}$$

2.9 Implementation

All model implementations are based on *Theano* (Bergstra et al., 2010; Bastien et al., 2012). "Theano is a Python library that allows you to define, optimize, and evaluate mathematical expressions involving multi-dimensional arrays efficiently."[2] Theano allows to express a model, the objective to be optimized as well as the optimization algorithm through a symbolic graph of mathematical

[2]`http://deeplearning.net/software/theano`

symbolic types, e.g. scalar, vector, matrix, etc., and operations, e.g. matrix-{vector,matrix} multiplication, elementwise functions, slicing/indexing. Defining a computational graph follows NumPy's interface very closely making it convenient to use and easy to adopt. Defining computations symbolically implies several advantages over "direct" implementations. First and foremost, a symbolically defined optimization objective allows for automatic differentiation which is a core ingredient in many machine learning algorithms in order to fit the model parameters to data. Automatic differentiation is not only convenient it also accelerates the prototyping of new models as well as reduces errors in taking and implementing derivatives manually. Second, the availability of the computational graph in symbolical form allows for graph optimization that may replace expression patterns by equivalent but computationally faster and/or numerically more stable expressions. The graph optimization framework also enables substituting generic operations, that would eventually be executed on the CPU, by other implementations, that may be executed on a different device such as a GPU. Third, once a graph is optimized it gets compiled on-the-fly by automatically generating C/C++/CUDA/OpenCL code and executing the corresponding native compiler. A compiled function is transparently accessible from within Python.

Listing 1 depicts code of a logistic regression model that illustrates the usage of Theano.

Listing 1 Example of logistic regression implemented using Theano.

```
import numpy as np
import theano
import theano.tensor as T

floatX = theano.config.floatX

# define input and target
x = T.matrix('x')
t = T.vector('t')

# define and initialize parameters
w = theano.shared(np.zeros(100, dtype=floatX))
b = theano.shared(np.zeros(  1, dtype=floatX))

# compute logistic regression output
y = T.nnet.sigmoid(theano.dot(x, w) + b)

# define optimization objective
cost = T.nnet.binary_crossentropy(y, t).mean()

# compute gradients w.r.t. parameters
gw, gb = theano.grad(cost, [w, b])

# define SGD optimization
updates = [(w, w - 0.001 * gw), (b, b - 0.001 * gb)]

# compile Theano function which performs a single update step
f = theano.function([x, t], cost, updates=updates)
```

CHAPTER 3

Multi-Task and Transfer Learning with Recurrent Neural Networks

This chapter presents recurrent neural network architectures that are capable of transferring knowledge among related sequence learning tasks by means of parameter sharing. First the meaning, utility, and relatedness of multi-task and transfer learning is discussed (Section 3.1). Second, terminological differences and similarities between the learning paradigms multi-task and transfer learning are scrutinized in order to clearly distinguish the implications of both terms (Section 3.2). Third, three recurrent neural networks architectures suitable for multi-task and transfer learning on sequential data are introduced (Section 3.3). They form the conceptual bases of the models used in the subsequent chapters. Two simple approaches to learning joint models of multiple tasks are introduced and discussed. Thereafter, the Factored Tensor Recurrent Neural Network architecture is presented which is one of the main contributions of this thesis. Its natural way of incorporating task-specific as well as cross-task parameters is elaborated on by drawing the connection between recurrent neural language modeling and multi-task and transfer learning with factored tensor parameters on sequential data.

The subsequent sections are based on the following list of publications as part of the doctoral research:

- Spieckermann, S., Düll, S., Udluft, S., Hentschel, A., and Runkler, T. Exploiting similarity in system identification tasks with recurrent neural networks. In *Proceedings of the 22nd European Symposium on Artificial Neural Networks, Computational Intelligence and Machine Learning (ESANN)*, 2014a.

- Spieckermann, S., Düll, S., Udluft, S., Hentschel, A., and Runkler, T. Exploiting similarity in system identification tasks with recurrent neural networks. *Neurocomputing*, (Special Issue ESANN 2014), 2015. Extended version. Invited paper.

- Spieckermann, S., Düll, S., Udluft, S., and Runkler, T. Multi-system identification for efficient knowledge transfer with factored tensor recurrent neural networks. In *Proceedings of the European Conference on Machine Learning (ECML), Workshop on Generalization and Reuse of Machine Learning Models over Multiple Contexts*, 2014b.

3.1 Multi-Task Learning

Multi-task learning is a learning paradigm in machine learning that aims to reduce the model error of a target task by utilizing related auxiliary learning tasks. Thus, the model exploits commonalities among the provided tasks where the auxiliary tasks serve as an inductive bias. "Inductive bias is anything that causes an inductive learner to prefer some hypotheses over other hypotheses. Bias-free learning is impossible; much of the power of an inductive learner follows directly from the power of its inductive bias (Mitchell, 1980). [...] One does not usually think of training signals as a bias; *but when the training signals are for tasks other than the main task, it is easy to see that, from the point of view of the main task, the other tasks may serve as a bias.*" (Caruana, 1997) This approach often leads to improved generalization due to inductive transfer.

Multi-task learning can happen in multiple ways. Let (x, y) denote a training example consisting of an input vector x and a target y in a supervised learning problem. Instead of simply learning the mapping from x to y, it may be possible to come up with additional targets $(y', y'', ...)$ whose error signals help guide the learning process to discover more robust and generally useful patterns in the inputs across a variety of related tasks. The resulting model may share the parameters of its feature extraction component, e.g. the input-to-hidden weights of a feed-forward neural network, and predict the targets based on the cross-task hidden representation. Another common approach is to couple task-specific parameters by means of regularization to enforce information sharing. Alternatively, a training example (i, x, y) may originate from a specific task indexed i while all tasks share a common target y. The tasks then differ in terms of their mapping from x to y. The latter scenario will be investigated in this thesis.

3.2 Multi-Task vs. Transfer Learning

Multi-task and transfer learning are two related learning paradigms with similar goals but different angles of approach. The common goal of both paradigms is to reduce the model error of the target model by utilizing one or multiple related auxiliary task(s).

Caruana (1997) distinguishes between *parallel* and *sequential* transfer where parallel transfer is performed through multi-task learning and sequential transfer translates to transfer learning. Multi-task learning means to learn a joint model of all tasks, i.e. the target task and all auxiliary tasks, simultaneously. In contrast, transfer learning implies a sequence in which the models are learned. Typically, the target task is learned subsequent to the auxiliary tasks. Thus, the target task learning process cannot interact with the auxiliary tasks.

Another perspective was formulated by Pan & Yang (2010). They distinguish multi-task and transfer learning as follows: "[...] transfer learning aims to extract the knowledge from one or more source tasks and applies the knowledge to a target task. In contrast to multitask learning, rather than learning all of the source and target tasks simultaneously, transfer learning cares most about the target task. The roles of the source and target tasks are no longer symmetric in transfer learning."

3.3 Multi-Task Recurrent Neural Networks

This section identifies a number of neural network based models that enable multi-task learning of sequential data. While there are many ways to implement multi-task learning, this chapter focuses on parameter sharing approaches where data-efficiency is obtained by using many cross-task and few task-specific parameters. An RNN as introduced in Section 2.3.3 may allocate task-specific parameters in the input-to-hidden, hidden-to-hidden, and hidden-to-output transformations. Making one of those components task-specific has implications on the nature of the tasks, in what aspects they are similar and dissimilar, and how this knowledge can be incorporated into the joint model. For instance, in natural language processing a sequence of words may be subject to multiple simultaneous classification tasks such as sentiment classification of a sentence and named entity recognition of each word. A typical approach would be to have a cross-task recurrent feature extraction and task-specific classification layers following the assumption that features of the two tasks may be mutually beneficial because they reveal more information about the overall problem structure. Alternatively, multiple tasks may share the same learning problem, but the input data may originate from different domains. For instance, product reviews in an online shop may be available from different product categories and the task is to infer their sentiment. In this case, the feature extraction may be task-specific while the classification submodel is the same for both tasks.

The following subsections present variants of RNN models that are general in concept but selected with system identification tasks in mind. It is assumed that the different tasks have identical input and output spaces.

3.3.1 Naïve RNN

The most naïve approach of multi-task learning is to learn a joint model for all tasks. Figure 2.6 depicts a graphical representation of the model. The data of all tasks are concatenated prior to learning. Thus, the joint model needs to generalize over all tasks. Generalization is possible if the factors that distinguish the tasks can be quantified and are observable. Making them available to the model allows for task discrimination. Otherwise, the model can only learn the average task at best and should be inferior to simple ways of incorporating task-discriminating information. This model serves as a baseline to ensure that tasks are in fact non-identical or to indicate that task-discriminating information is not available.

3.3.2 RNN+ID

In absence of task-discriminating factors, a simple way to distinguish the tasks is to tag each task with a positive integer task identifier $i \in I$, i.e. the training examples of each task are tagged and concatenated to form a multi-task data set. This tag may be provided to the model at each sequential step as an extra input encoded as the i-th Euclidean standard basis vector e_i with $\dim(e_i) = |I|$ also known as "one-hot" encoding. The equations of the RNN+ID architecture are obtained by substituting (2.14b) with (3.1).

$$h_{[t]} = \phi_h(W_{hx}x_{[t]} + W_{hh}h_{[t-1]} + W_{hi}e_i + b_h) \tag{3.1}$$

Figure 3.1 depicts a graphical representation of the RNN+ID architecture. In

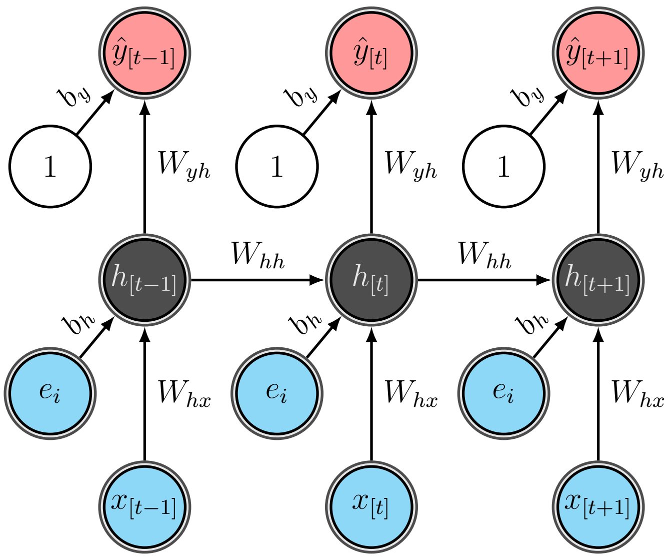

Figure 3.1: RNN+ID architecture for multi-task learning on sequential inputs.

fact, computing $W_{hi}e_i$ means selecting the i-th column of W_{hi} so the system identifier introduces a separate bias for each system. The cross-system bias b_h and the specific biases accessed through $W_{hi}e_i$ can be absorbed into a new system-specific bias $\widetilde{W}_{hi}e_i = b_h + W_{hi}e_i$. Thus, (3.1) can be rewritten as

$$h_{[t]} = \phi_h(W_{hx}x_{[t]} + W_{hh}h_{[t-1]} + \widetilde{W}_{hi}e_i). \tag{3.2}$$

3.3.3 Factored Tensor Recurrent Neural Network (FTRNN)

The previous subsection showed that providing the network with a "one-hot" encoded system identifier e_i is in fact equivalent to learning a different hidden layer bias $\widetilde{W}_{hi}e_i$ for each system. The bias of a particular neuron determines its activity threshold. Making the bias task-specific thus allows to learn a different threshold for each task. However, the main transformation from one layer is due to a parameter matrix $W_{vu} \in \mathbb{R}^{n_v \times n_u}$, so it is a natural choice to use a different parameter matrix W_{vu} for each task. Multiple such matrices can be viewed as frontal slices of a third-order tensor $W_{vui} \in \mathbb{R}^{n_v \times n_u \times |I|}$.

The primary source of the idea that yields the model of this subsection is a paper on character-level language modeling using recurrent neural networks (Sutskever et al., 2011). Language modeling is commonly defined as the task of assigning the probability of occurrences to a given sequence of words. That is, given a word vocabulary V and a sequence of words $(w_{[1]}, ..., w_{[k]})$, $w_{[i]} \in V$, the language model yields $P(w_{[1]}, ..., w_{[k]})$. By using the chain rule this joint probability can be decomposed into factors of conditional probabilities as follows.

$$P(w_{[1]}, ..., w_{[k]}) = P(w_{[k]}|w_{[1]}, ..., w_{[k-1]})P(w_{[k-1]}|w_{[1]}, ..., w_{[k-2]}) \cdots \tag{3.3a}$$

$$= P(w_{[1]}) \prod_{i=2}^{k} P(w_{[i]}|w_{[1]}, ..., w_{[i-1]}) \tag{3.3b}$$

Recurrent neural networks are a natural and effective choice to estimate the conditional probabilities (Mikolov et al., 2010). However, Sutskever et al. argue that a modified architecture with so-called "multiplicative" connections is superior to the standard architecture in the character-level language modeling task. Multiplicative interactions are derived as follows. In order to improve the expressiveness of the model the parameter matrix W_{hh} is conditioned on the current input character, thus, yielding a different state transition per character. Naïvely, the parameters would be stored in a third-order tensor where each slice represents the transition matrix of a particular character in the vocabulary. Although the vocabulary of characters is much smaller than the prohibitively large vocabulary of words the size of the three-way tensor is impractical nevertheless. Sutskever et al. propose to learn a factored representation as used by Taylor & Hinton (2009), who model multiple motion styles from images using Restricted Boltzmann Machines. While not explicitly stated in any of the papers the proposed factorization is known as Parallel Factor Analysis (PARAFAC, see Section 2.6.2 for details) for three-way tensors where the vectors of the third mode can be viewed as latent representations, or factors, of each character that adjust the state transition matrix.

This idea can be transferred to multi-task recurrent neural networks. In contrast to the language model, in which each frontal slice of the parameter tensor is associated with a character in the alphabet, the tensor holds a frontal slice per task. However, learning separate parameter matrices for each task has two major drawbacks.

1. Each additional system substantially increases the number of adaptive parameters which reduces data efficiency with respect to each task. This is of particular concern with regard to a little observed task.

2. The transformation, induced by each parameter matrix, is learned independently for each task, i.e. no information is shared among equivalent transformations across the tasks although it is most likely that they in fact do share structure.

Decomposing a three-way tensor W_{vui} according to PARAFAC yields a factored tensor of the form

$$W_{vui}e_i \approx W_{vf}\,\mathrm{diag}(W_{fi}e_i)W_{fu} \tag{3.4}$$

with $W_{vui} \in \mathbb{R}^{n_v \times n_u \times |I|}$, $W_{fu} \in \mathbb{R}^{n_f \times n_u}$, $W_{vf} \in \mathbb{R}^{n_v \times n_f}$, and $W_{fi} \in \mathbb{R}^{n_f \times |I|}$. Figure 3.2 depicts a visualization of the factorization. One perspective on the

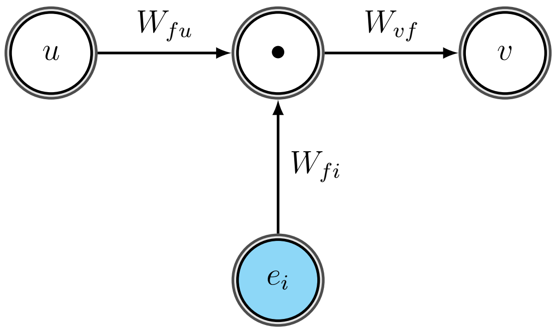

Figure 3.2: Third-order tensor decomposition using PARAFAC that, when expanded, approximates the i-th frontal slice. The node having the $\bullet$-symbol in its center is a "multiplication node", i.e. the input vectors of the node are multiplied component-wise. In contrast, the standard nodes imply the summation of all input vectors.

factored tensor representation as an approach to sharing structure among multiple tasks is the following. Let e_k denote the k-th Euclidean standard basis vector with an appropriate dimensionality, $e_k^T W_{fu}$ is the k-th row of W_{fu}, $W_{vf}e_k$ is the k-th column of W_{vf} and $e_k^T W_{fi} e_i$ is the k-th element of the diagonal matrix $\mathrm{diag}(W_{fi}e_i)$. Expanding the i-th slice of the factored tensor, i.e. the expanded parameter matrix for system $i \in I$, can be written as the weighted sum of rank-one matrices $(W_{vf}e_k)\left(e_k^T W_{fu}\right)$, i.e.

$$W_{vui}e_i \approx \sum_{k=1}^{n_f} (W_{vf}e_k)\left(e_k^T W_{fi} e_i\right)\left(e_k^T W_{fu}\right). \tag{3.5}$$

The equality of (3.4) and (3.5) can be shown as follows. Let $v \in \mathbb{R}^n$ be an n-dimensional column vector whose k-th element denotes $v_k = e_k^T v$. The $\mathrm{diag}(v)$ operator maps the vector v to a diagonal matrix in $\mathbb{R}^{n\times n}$ and is defined as follows.

$$\mathrm{diag}(v) := \sum_k e_k e_k^T v_k \tag{3.6}$$

In the following, let $[W]_{ab}$ denote the element of the matrix W at row a and column b. Using (3.6), the diagonal matrix $\mathrm{diag}(W_{fi}e_i)$ can be written as

$$\begin{aligned}
\mathrm{diag}(W_{fi}e_i) &= \mathrm{diag}\left(\left(\sum_{a,b}[W_{fi}]_{ab}e_a e_b^T\right)e_i\right) && \text{(3.7a)}\\
&= \mathrm{diag}\left(\sum_{a,b}[W_{fi}]_{ab}e_a(e_b^T e_i)\right) && \text{(3.7b)}\\
&= \mathrm{diag}\left(\sum_{a,b}[W_{fi}]_{ab}e_a\delta_{bi}\right) && \text{(3.7c)}\\
&= \mathrm{diag}\left(\sum_{a}[W_{fi}]_{ai}e_a\right) && \text{(3.7d)}\\
&= \sum_k e_k e_k^T\left(e_k^T\sum_a [W_{fi}]_{ai}e_a\right) && \text{(3.7e)}\\
&= \sum_{k,a} e_k e_k^T e_k^T e_a [W_{fi}]_{ai} && \text{(3.7f)}\\
&= \sum_{k,a} e_k e_k^T \delta_{ka}[W_{fi}]_{ai} && \text{(3.7g)}\\
&= \sum_k e_k e_k^T [W_{fi}]_{ki} && \text{(3.7h)}\\
&= \sum_k e_k [W_{fi}]_{ki} e_k^T. && \text{(3.7i)}
\end{aligned}$$

Substituting this result in (3.5) yields

$$\begin{aligned} W_{vui}e_i &\approx W_{vf}(\mathrm{diag}(W_{fi}e_i)W_{fu} && \text{(3.8a)} \\ &= W_{vf}\left(\sum_{k=1}^{n_f} e_k[W_{fi}]_{ki}e_k^T\right)W_{fu} && \text{(3.8b)} \\ &= \sum_{k=1}^{n_f}(W_{vf}e_k)[W_{fi}]_{ki}(e_k^T W_{fu}). && \text{(3.8c)} \end{aligned}$$

Since $[W_{fi}]_{ki}$ is the element in the k-th row and i-th column of W_{fi}, i.e. a scalar number, it is equivalently expressed as $e_k^T W_{fi} e_i$. Substitution of this term into (3.8c) yields (3.5).

$$\begin{aligned} W_{vui}e_i &\approx W_{vf}(\mathrm{diag}(W_{fi}e_i)W_{fu} && \text{(3.9a)} \\ &= \sum_{k=1}^{n_f}(W_{vf}e_k)(e_k^T W_{fi}e_i)(e_k^T W_{fu}) && \text{(3.9b)} \end{aligned}$$

The tasks's unique characteristics are encoded as the weights of the summed rank-one matrices and thus W_{vf} and W_{fu}, which are shared among the tasks, must learn appropriate column and row values such that the task-specific weighting of their sum of corresponding outer products best approximates the optimal task-specific transformation $W_{vui}e_i$. Due to the factored tensors, only n_f parameters are specific to each task compared to $n_u n_v$ parameters for independent parameter matrices W_{vui}. Their limited degree of freedom forces the model to identify common structure among the tasks. This way, every task has its own set of transformations that, however, are not independent.

A factored tensor recurrent neural network may replace some or all weight matrices by factored tensors. Figure 3.3 depicts a standard recurrent neural network where possible locations of factored tensor parameters are highlighted.

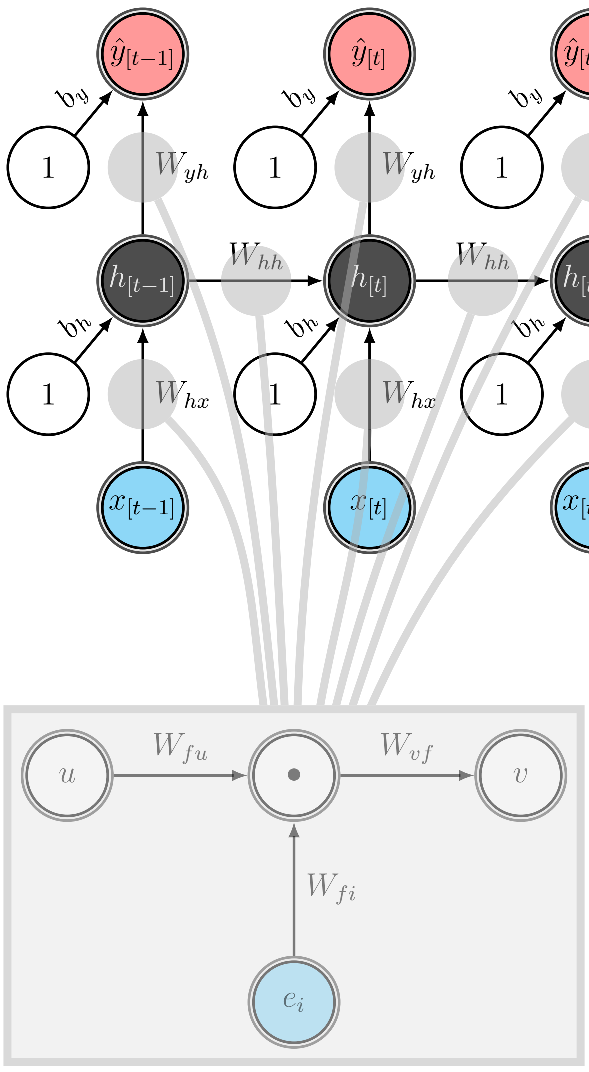

Figure 3.3: Factored Tensor Recurrent Neural Network for multi-task learning on sequential inputs. The node having the •-symbol in its center is a “multiplication node”, i.e. the input vectors of the node are multiplied component-wise. In contrast, the standard nodes imply the summation of all input vectors.

CHAPTER 4

Exploiting Similarity in Fully Observable System Identification Tasks

This chapter addresses the problem of fully observable system identification of a target system for which only an inaccurate model can be learned due to insufficient amounts of available data. To reduce the model error, multiple approaches along the lines of dual-task and transfer learning using recurrent neural networks are proposed and empirically evaluated.

The chapter is structured as follows. First, the problem of fully observable system identification is introduced and formalized (Section 4.1). Second, a recurrent neural network architecture suitable for fully observable system identification is presented (Section 4.2). Third, the original problem is extended to a multi-system identification task where only few observations are available from the target task while sufficient information from auxiliary systems can be utilized (Section 4.3). The recurrent neural network architectures developed in Section 3.3 are adapted to the fully observable multi-system identification problem. Two problem settings are investigated: a dual-task learning (Section 4.4) and a transfer learning (Section 4.6) scenario. Each problem is formalized and matching models are discussed. In addition, a new regularization technique is presented for the dual-task learning scenario which penalizes dissimilar system-specific parameters to further strengthen the prior assumption of the systems' similarity (Section 4.5). Experiments are conducted for each of the scenarios to compare the effectiveness of multiple recurrent neural network architectures in transferring information from the auxiliary system(s) to the target system. The results show that the proposed Factored Tensor Recurrent Neural Network, which is one of the main contributions of this thesis, outperforms the other approaches in all experiments.

The subsequent sections are based on the following list of publications as part of the doctoral research:

- Spieckermann, S., Düll, S., Udluft, S., Hentschel, A., and Runkler, T. Exploiting similarity in system identification tasks with recurrent neural networks. In *Proceedings of the 22nd European Symposium on Artificial Neural Networks, Computational Intelligence and Machine Learning (ESANN)*, 2014a.
- Spieckermann, S., Düll, S., Udluft, S., Hentschel, A., and Runkler, T. Exploiting similarity in system identification tasks with recurrent neural networks. *Neurocomputing*, (Special Issue ESANN 2014), 2015. Extended version. Invited paper.
- Spieckermann, S., Düll, S., Udluft, S., and Runkler, T. Multi-system identification for efficient knowledge transfer with factored tensor recurrent neural networks. In *Proceedings of the European Conference on Machine Learning (ECML), Workshop on Generalization and Reuse of Machine Learning Models over Multiple Contexts*, 2014b.
- Spieckermann, S., Düll, S., Udluft, S., and Runkler, T. Regularized recurrent neural networks for data efficient dual-task learning. In *Proceedings of the 24th International Conference on Artificial Neural Networks (ICANN)*, 2014c.

4.1 Fully Observable System Identification

4.1.1 Introduction

The task discussed in this chapter is to learn the state transition function of a fully observable deterministic dynamical system by observing its current state $s_{[t]}$, an action $a_{[t]}$, and the resulting successor state $s_{[t+1]}$. In general, the state transition function of such a system is described by some function $s_{[t+1]} = f(s_{[t]}, a_{[t]})$. However, in practice the learning process of this function often benefits from predicting the sequence of successor states $(s_{[t+1]}, ..., s_{[t+T]})$ given a trajectory of T actions $(a_{[t]}, ..., a_{[t+T-1]})$ for $T \in \mathbb{N} \setminus \{1\}$ time steps instead of predicting only a single step. For instance, if a system is observed at a high frequency, two subsequently observed states are typically very similar and a single step model would achieve low error by simply learning the identity function of the input state. In contrast, predicting a T-step trajectory will yield a large error for such a degenerate model thus forcing the learning process to find a better solution.

4.1.2 Formal Problem Definition

A system, observed in fixed time intervals τ, is defined by the tuple (S, A, f) with a state space S, an action space A, and an unknown state transition function $f\colon S \times A \to S$ describing the temporal evolution of the state.

Let D be a set of state transition observations $(s, a, s') \in D$ where each observation describes a single state transition from state $s \in S$ to state $s' \in S$ caused by action $a \in A$. Further, let D denote a data set of size $|D|$ drawn from a probability distribution $\mathcal{D}$.

Let $H \subseteq \{h \,|\, h\colon S \times A \to S\}$ denote a hypothesis space, i.e. a set of functions that are assumed to approximate the state transition function f. Further, let $\mathcal{L}\colon S \times S \to \mathbb{R}$ denote an error measure between a predicted successor state $\hat{s}'$ and the true successor state s'. The optimal hypothesis h^*, i.e. the best approximation of f within the considered space of hypotheses, minimizes the expected error $\varepsilon(h) := \mathrm{E}_{(s,a,s')\sim\mathcal{D}}[\mathcal{L}(h(s,a), s')]$ where E denotes the expectation operator, hence, $h^* = \arg\min_{h\in H} \varepsilon(h)$. Since $\mathcal{D}$ is generally unknown, an approximately optimal hypothesis is determined by minimizing the empirical error $\hat{\varepsilon}_D(h) := \frac{1}{|D|} \sum_{(s,a,s')\in D} \mathcal{L}(h(s,a), s')$ induced by a hypothesis h on a data set D, hence, $\hat{h} = \arg\min_{h\in H} \hat{\varepsilon}_D(h)$.

4.2 Fully Observable System Identification with Recurrent Neural Networks

In order to model the state transition function of an open fully observable dynamical system, a recurrent neural network may be defined which receives the initial state vector $s_{[1]}$ and a sequence of T actions $(a_{[1]}, ..., a_{[T]})$ yielding the predicted successor state sequence $(\hat{s}_{[2]}, ..., \hat{s}_{[T+1]})$. The network is defined by the following equations.

$$h_{[1]} = \phi_h(W_{hs}s_{[1]} + b_1) \tag{4.1a}$$
$$h_{[t+1]} = \phi_h(W_{ha}a_{[t]} + W_{hh}h_{[t]} + b_h) \tag{4.1b}$$
$$\hat{s}_{[t+1]} = \phi_s(W_{sh}h_{[t+1]} + b_s). \tag{4.1c}$$

More specifically, the initial state $s_{[1]}$ is mapped to the hidden state $h_{[1]}$ of the RNN by a linear transformation followed by the nonlinear function $\phi_h(\cdot)$, applied pointwise, which is typically chosen as $\tanh(\cdot)$. From there, the hidden state $h_{[t]}$ and the action $a_{[t]}$ are mapped to form the predicted hidden successor state $h_{[t+1]}$. The hidden successor state $h_{[t+1]}$ is then mapped back to the observed state space yielding the predicted successor state $\hat{s}_{[t+1]}$. The state space of a dynamical system is often real-valued and unbounded, hence, $\phi_s(\cdot)$ becomes the identity function. Figure 4.1 depicts a graphical representation of the RNN architecture.

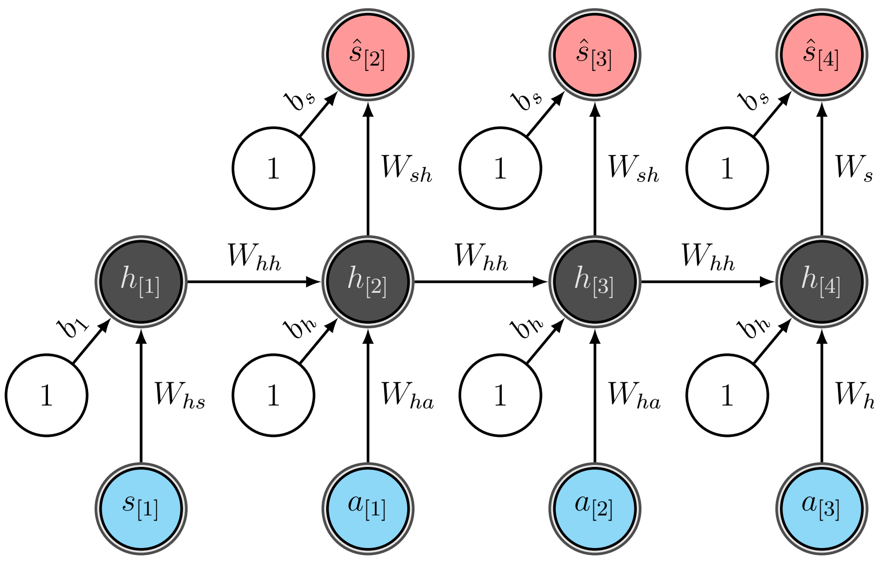

Figure 4.1: Recurrent neural network architecture for fully observable system identification.

4.3 Fully Observable Multi-System Identification with Recurrent Neural Networks

4.3.1 Naïve RNN

The most naïve approach to exploit information from one dynamical system and share it with another one is to concatenate the data of both systems and learn a joint model. This way, the model is forced to generalize over the different properties of the systems. However, since the training examples of both systems are not distinguished, the model can only learn the average dynamics which may be vastly suboptimal for rather different systems. This fact makes the Naïve RNN a good baseline model to ensure that the tasks are non-identical and cannot be explained by observed inputs.

The following subsections discuss two recurrent neural architectures that are able to distinguish the systems through an integer identifier. For both models, the hidden state $h_{[t]}$ is considered an internal representation of the equivalent real state representation of the systems. It is assumed that the state spaces and the corresponding semantics are identical for both systems, i.e. if the observed states of the two systems are identical, they describe identical system states.

4.3.2 RNN+ID

One way to incorporate information that allows the model to distinguish between the systems is to tag each training example with an identifier $i \in I$, which corresponds to the system that generated the data. This tag may be provided to the model at each time step as an extra input encoded as the i-th Euclidean standard basis vector e_i with $\dim(e_i) = |I|$. The equations of the RNN+ID architecture are obtained by substituting (4.1b) with (4.2).

$$h_{[t+1]} = \phi_h(W_{ha}a_{[t]} + W_{hh}h_{[t]} + W_{hi}e_i + b_h) \tag{4.2}$$

Figure 4.2 depicts a graphical representation of the RNN+ID architecture. In fact, computing $W_{hi}e_i$ means selecting the i-th column of W_{hi} so the system identifier introduces a separate bias for each system. The cross-system bias

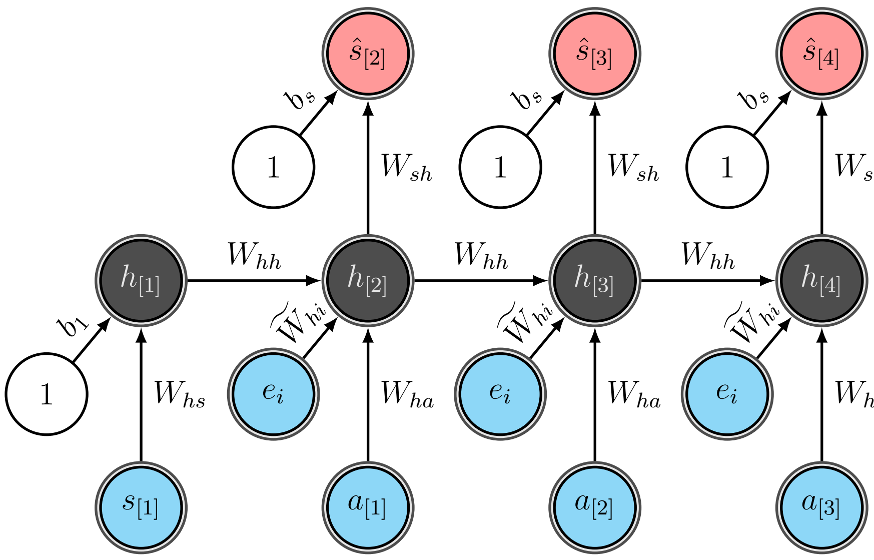

Figure 4.2: RNN+ID architecture for fully observable multi-system identification.

b_h and the specific biases accessed through $W_{hi}e_i$ can be absorbed into a new system-specific bias $\widetilde{W}_{hi}e_i = b_h + W_{hi}e_i$. Thus, (4.2) can be rewritten as

$$h_{[t+1]} = \phi_h(W_{ha}a_{[t]} + W_{hh}h_{[t]} + \widetilde{W}_{hi}e_i). \tag{4.3}$$

4.3.3 FTRNN

The previous subsection showed that providing the network with a "one-hot" encoded system identifier e_i is in fact equivalent to learning a different hidden layer bias $\widetilde{W}_{hi}e_i$ for each system. The bias of a particular neuron determines its activity threshold. Making the bias system-specific thus allows to learn a different threshold for each system. However, the state evolution of a system is predominantly determined by the matrix W_{hh}, which models the state evolution without external forces, and by the matrix W_{ha}, which models the effect of an external force applied to the system. Given that all systems share identical state and action spaces, these two matrices should be made system-specific.

The idea of introducing third-order tensors as parameter matrices conditioned on a categorical input, as described in Section 3.3.3, can be applied to the multi-system identification problem. Following the arguments made above an immediate approach is to learn separate parameter matrices $W_{hhi}e_i$ and $W_{hai}e_i$ for each system where $W_{hhi} \in \mathbb{R}^{n_h \times n_h \times |I|}$ and $W_{hai} \in \mathbb{R}^{n_h \times n_a \times |I|}$ are third-order tensors. As argued in Section 3.3.3 learning separate parameter matrices for each system has two major drawbacks regarding the number of parameters harming data efficiency and regarding the independence of each parameter matrix which prevents information sharing within the transformation. Decomposing the three-way tensors W_{hhi} and W_{hai} according to PARAFAC yields the factored tensors of the form

$$W_{hhi} e_i \approx W_{hf_h} \operatorname{diag}(W_{f_h i} e_i) W_{f_h h} \tag{4.4a}$$

$$W_{hai} e_i \approx W_{hf_a} \operatorname{diag}(W_{f_a i} e_i) W_{f_a a} \tag{4.4b}$$

Substituting the matrices W_{hh} and W_{ha} by their corresponding factored tensors yields the equations of the FTRNN by substituting (4.1b) with (4.5).

$$\begin{aligned} h_{[t+1]} = \phi_h(& W_{hf_a} \operatorname{diag}(W_{f_a i} e_i) W_{f_a a} a_{[t]} + \\ & W_{hf_h} \operatorname{diag}(W_{f_h i} e_i) W_{f_h h} h_{[t]} + b_h) \end{aligned} \tag{4.5}$$

Figure 4.3 depicts a graphical representation of the FTRNN architecture. Due to the factored tensors, only n_f parameters are specific to each system compared to $n_u n_v$ parameters for independent parameter matrices W_{vui}. Their limited degree of freedom forces the model to identify common structure among the systems. This way, every system has its own set of transformations describing the contributions of the previous hidden state and the current external force to yield the current hidden state. However, these transformations are not independent for each system since they are composed of two cross-system components and one system-specific component.

4.4 The Fully Observable Dual-Task Learning Problem

The fully observable dual-task learning problem addresses the task of learning the state transition function of a little observed fully observable dynamical system by utilizing data from a well-observed similar system. In order to achieve this goal, the data of both systems are used to learn a joint model thereof such that information is shared among the two systems. Typical applications of this

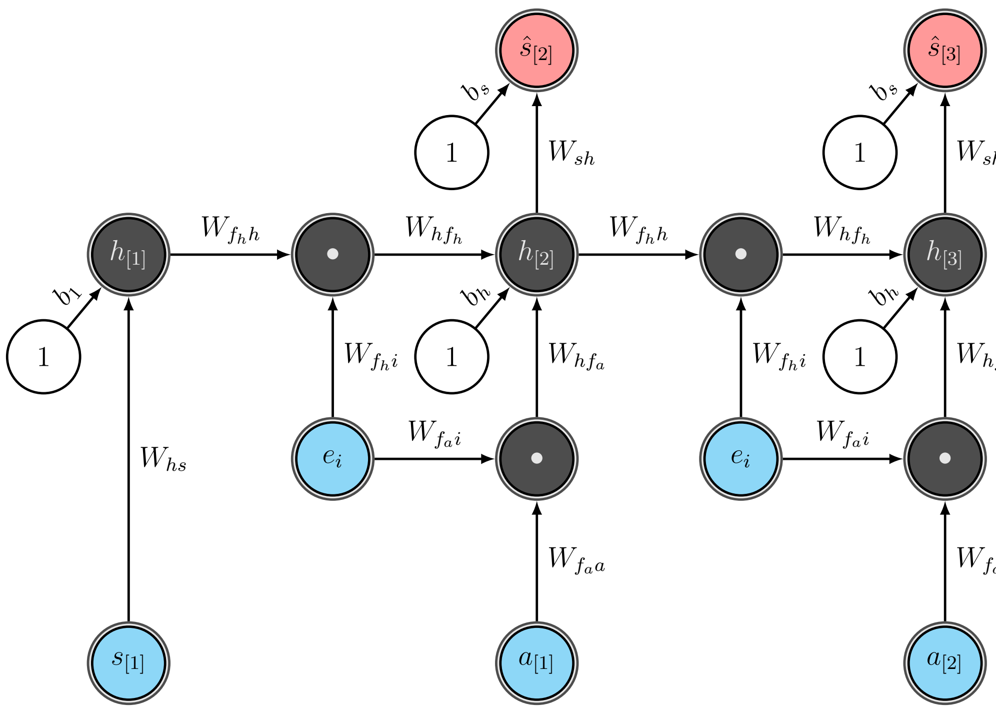

Figure 4.3: FTRNN architecture for fully observable multi-system identification. The nodes having the •-symbol in their centers are "multiplication nodes", i.e. the input vectors of the nodes are multiplied component-wise. In contrast, the standard nodes imply the summation of all input vectors.

scenario are situations where a technical system undergoes maintenance procedures after a sufficiently long period of operation that cause the system to change, or the deployment of a new instance whose data of observations are augmented by those of a related system.

4.4.1 Problem Definition

Let $I := \{1, 2\}$ denote a set of identifiers for fully observable deterministic systems, which are observed in fixed time intervals τ and show similar dynamics. A system is defined by the tuple (S, A, f_i) with a state space S, an action space A, and an unknown state transition function $f_i \colon S \times A \to S$ describing the temporal evolution of the state.

Let D_i be a set of state transition observations $(i, s, a, s') \in D_i$ of the i-th system where each observation describes a single state transition from state $s \in S$ to state $s' \in S$ caused by action $a \in A$. Further, let $D = \bigcup_{i \in I} D_i$ denote a data set of size $|D|$ drawn from a probability distribution $\mathcal{D}$.

Let $H \subseteq \{h \,|\, h \colon S \times A \to S\}$ denote a hypothesis space, i.e. a set of functions that are assumed to approximate the state transition function f_i. Further, let $\mathcal{L} \colon S \times S \to \mathbb{R}$ denote an error measure between a predicted successor state $\hat{s}'$ and the true successor state s'. The optimal hypothesis h_i^*, i.e. the best approximation of f_i within the considered space of hypotheses, minimizes the conditional expected error $\varepsilon_i(h) := \mathrm{E}_{(j,s,a,s') \sim \mathcal{D}}[\mathcal{L}(h(s, a), s') \,|\, j = i]$ where E denotes the expectation operator, hence, $h_i^* = \arg\min_{h \in H} \varepsilon_i(h)$. Since $\mathcal{D}$ is generally unknown, an approximately optimal hypothesis is determined by minimizing the empirical error $\hat{\varepsilon}_D(h) := \frac{1}{|D|} \sum_{(\cdot,s,a,s') \in D} \mathcal{L}(h(s, a), s')$ induced by a hypothesis h on a data set D, hence, $\hat{h}_i = \arg\min_{h \in H} \hat{\varepsilon}_{D_i}(h)$.

Given sufficient data D_1, it is expected that $|\varepsilon_1(\hat{h}_1) - \varepsilon_1(h_1^*)| \leq \epsilon$ for some small positive ϵ. In contrast, assuming the amount of data D_2 is insufficient, $|\varepsilon_2(\hat{h}_2) - \varepsilon_2(h_2^*)| \gg \epsilon$ and $\hat{h}_2$ may be useless. The problem addressed in this section is to develop and assess methods that yield a better hypothesis of the insufficiently observed system through dual-task learning in order to utilize auxiliary information from D_1 as prior knowledge of the transition function f_2.

Therefore, the hypothesis space and the empirical error are redefined as follows. Let $H' \subseteq \{h \,|\, h \colon I \times S \times A \to S\}$ denote an extended hypothesis space, which includes the system identifier into the product space of arguments and thus approximates both transition functions by a single function. Further, let $\hat{\varepsilon}'_D(h) := \frac{1}{|D|}\sum_{(i,s,a,s')\in D} w_i \mathcal{L}(h(i,s,a),s')$ denote the empirical error of a hypothesis $h \in H'$ with the system-specific error weight w_i. If the the empirically optimal hypothesis $\hat{h}' = \arg\min_{h\in H'} \hat{\varepsilon}'_D(h)$ $(D = \bigcup_{i\in I} D_i)$ yields a smaller expected error than $\hat{h}_2$, i.e. $\varepsilon_2(\hat{h}'_2) < \varepsilon_2(\hat{h}_2)$ with $\hat{h}'_2(s,a) := \hat{h}'(2,s,a)$, information from the well observed system is successfully utilized in the hypothesis search to find a better hypothesis of f_2 despite few data.

4.4.2 Experiments

In order to assess the effectiveness of the FTRNN model in comparison with the competing models, experiments were conducted using the frictionless cart-pole (see Section 2.8.1) and mountain car (see Section 2.8.2) simulations. For each simulation, two instances with non-identical but similar state transition functions were configured. The data sets D_1 and D_2 were obtained by observing the state transitions (i,s,a,s') along a trajectory of 500 actions $(a_{[1]},...,a_{[500]})$ defined by the equations

$$a_{[0]} = 0 \tag{4.6a}$$

$$\tilde{a}_{[t]} \sim \mathcal{U}(-1,1) \tag{4.6b}$$

$$a_{[t]} = \max(-1, \min(1, a_{[t-1]} + \tilde{a}_{[t]})). \tag{4.6c}$$

with $\mathcal{U}$ being the uniform distribution. These equations describe a random walk of actions clipped to the domain of the action space. After every 500 steps, the simulation was reset to its initial state. The examples used to train and evaluate the models were generated by extracting T-step windows of the sequences of observations. In order to decorrelate examples of the training, validation, and generalization data sets, the block validation method discussed in Section 2.3.3 was used. D_1 consisted of 15 000 examples $(i = 1, s_{[1]}, a_{[1]}, ..., s_{[T]}, a_{[T]}, s_{[T+1]})$ and was split into a training set $D_{1,\mathrm{T}}$ containing 10 000 examples and a validation set $D_{1,\mathrm{V}}$ sized 5000. The data set D_2 was obtained the same way, however, training and validation set sizes were reduced to $\{10000, 5000, ..., 156\}$ and $\{5000, 2500, ..., 78\}$ respectively throughout the experiments. Experiments were conducted on two simulations in order to (i) compare the model error as a function of $D_{2,\mathrm{T}}$ and $D_{2,\mathrm{V}}$, and (ii) assess whether $D_{2,\mathrm{T}}$ and $D_{2,\mathrm{V}}$ should be upsampled to match the sizes of $D_{1,\mathrm{T}}$ and $D_{1,\mathrm{V}}$ or not. The loss function for training was chosen to be the mean squared error (MSE) between the predicted and the true successor state sequence, i.e. $\mathcal{L}(\hat{s}_{[2]}, ..., \hat{s}_{[T+1]}, s_{[2]}, ..., s_{[T+1]}) = \frac{1}{2}\sum_{t=1}^{T} \|s_{[t+1]} - \hat{s}_{[t+1]}\|_2^2$. An alternative choice is the "ln cosh" loss function in case outliers are a concern (Neuneier & Zimmermann, 1998). To evaluate the model performances, the average MSE per time step per output component was used, i.e. $\mathcal{L}_{\text{test}} = \frac{1}{T \dim(s)}\mathcal{L}$.

Learning the state transition function of the differently configured systems cannot be solved through mere generalization because the quantities that invoke the different dynamical behavior are hidden. The only information that allows to distinguish the systems is a categorical system identifier. Thus, the hidden quantities need to be inferred from observations making the problem a dual-task learning problem rather than a problem of generalization.

Cart-Pole

Two cart-pole instances (CP1 and CP2) were configured to have the pole lengths 0.5 and 1.0, and the pole masses 0.05 and 0.1, respectively. Figure 4.4 depicts the performance of the best-of-five model (determined by the lowest error on $D_{1,\text{V}} \cup D_{2,\text{V}}$ with $|D_{1,\text{V}}| = 5000$ and $|D_{2,\text{V}}| = \frac{1}{2}|D_{2,\text{T}}|$) with $T = 10$ evaluated on $D_{2,\text{G}}$ with $|D_{2,\text{G}}| = 100\,000$. In each run, the initial model parameters were sampled at random. For all networks, the hidden state dimension was set to $n_h = 10$. The hyperparameters of the FTRNN were set to $n_{f_h} = n_h$ and $n_{f_a} = 1$. The simple RNN model was only trained on data from CP2. The other models, i.e. the Naïve RNN, RNN+ID and FTRNN, were trained on the concatenated data set $D_1 \cup D_2$. The model parameters were optimized using Hessian-Free optimization with the structural damping coefficient (see Section 2.4.2) set to $\mu_{\text{sd}} = 0.1$, a maximum number of 10 000 updates, at most 150 conjugate gradient (CG) iterations using all training examples to compute the gradient, and a random subset of the training data set sized 5000 to estimate the local curvature of the error surface. In addition, an early stopping procedure with a patience of 50 updates was used to reduce overfitting.

The first set of experiments, whose results are depicted in Figure 4.4a, compared the errors of the different models provided that $D_{2,\text{T}}$ and $D_{2,\text{V}}$ were upsampled such that $|D_{2,\text{T}}| = |D_{1,\text{T}}|$ and $|D_{2,\text{V}}| = |D_{1,\text{V}}|$. As a result, the simple RNN performed well for $|D_{2,\text{T}}| \in \{1250, 2500, 5000, 10\,000\}$ but degraded rapidly

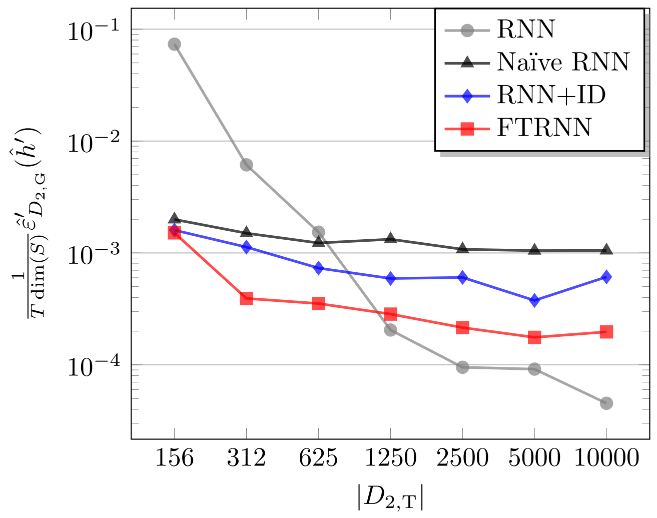

(a) Model errors with upsampled data from CP2 plotted on a logarithmic scale.

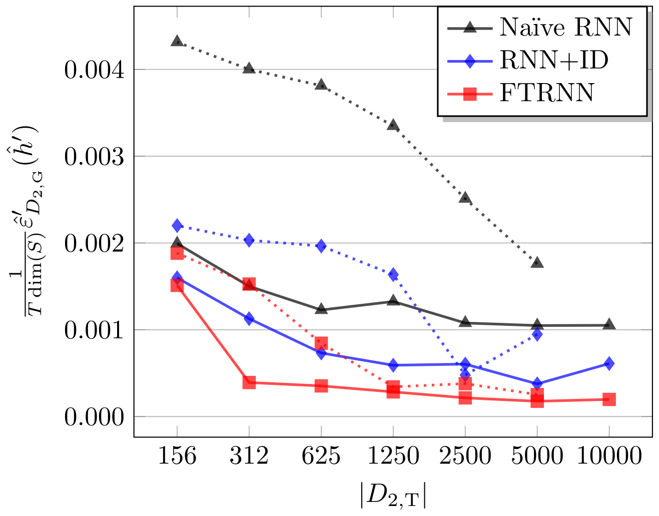

(b) Model errors with (solid lines) and without (dotted lines) upsampled data from CP2.

Figure 4.4: Experimental results using the cart-pole simulation. The plots show the error of the best-of-five model determined by the validation set error. The error is the MSE per state component per time step between the predicted and the true successor state sequence plotted against the varying training set sizes of CP2 for a fixed number of $|D_{1,\mathrm{T}}| = 10\,000$ training examples of CP1.

given fewer training examples. A considerable improvement was achieved by the Naïve RNN given $|D_{1,\mathrm{T}}| = 10\,000$ and $|D_{2,\mathrm{T}}| \in \{156, 312, 625\}$ despite its disability to distinguish between the two cart-poles. The RNN+ID model yielded an expected improvement over the Naïve RNN since it was provided information to tell examples of the two cart-poles apart. Thus, it was able to actually encode differences between the state transition functions of the two cart-poles. However, as shown in Section 4.3.2, the additional feature vector e_i merely acts as a system-specific bias in the hidden state of the RNN which limits its ability to properly account for the similar but non-identical state transition function of the two cart-poles. The FTRNN outperformed the Naïve RNN and the RNN+ID models consistently. Only for a data ratio of $\frac{|D_{1,\mathrm{T}}|}{|D_{2,\mathrm{T}}|} = \frac{10\,000}{156}$ the error increased notably and got close to the error of the RNN+ID model.

The second set of experiments, whose results are illustrated in Figure 4.4b, compared the effect of upsampling $D_{2,\mathrm{T}}$ and $D_{2,\mathrm{V}}$ versus keeping their original sizes during training. It turned out that upsampling the data sets was consistently superior, especially for increasing data ratios $\frac{|D_{1,\mathrm{T}}|}{|D_{2,\mathrm{T}}|}$. In particular, the error of the Naïve RNN increased significantly when no upsampling was used, but also the RNN+ID and FTRNN models performed worse without upsampling.

Mountain Car

Two mountain car instances (MC1 and MC2) were configured with gravity values 0.001 and 0.003. Figure 4.5 depicts the performance of the best-of-five model (determined by the lowest error on $D_{1,\mathrm{V}} \cup D_{2,\mathrm{V}}$ with $|D_{1,\mathrm{V}}| = 5000$ and $|D_{2,\mathrm{V}}| = \frac{1}{2}|D_{2,\mathrm{T}}|$) with $T = 10$ evaluated on $D_{2,\mathrm{G}}$ with $|D_{2,\mathrm{G}}| = 100\,000$. In each run, the initial model parameters were sampled at random. For all networks, the hidden state dimension was set to $n_h = 5$. The hyperparameters of the FTRNN were set to $n_{f_h} = n_h$ and $n_{f_a} = 1$. The simple RNN model was only trained on data from MC2. The other models, i.e. the Naïve RNN, RNN+ID and FTRNN, were trained on the concatenated data set $D_1 \cup D_2$. The model parameters were optimized using Hessian-Free optimization with the structural damping coefficient (see Section 2.4.2) set to $\mu_{\mathrm{sd}} = 0.1$, a maximum number of 10 000 updates, at most 50 conjugate gradient (CG) iterations using all training examples to compute the gradient, and a random subset of the training data

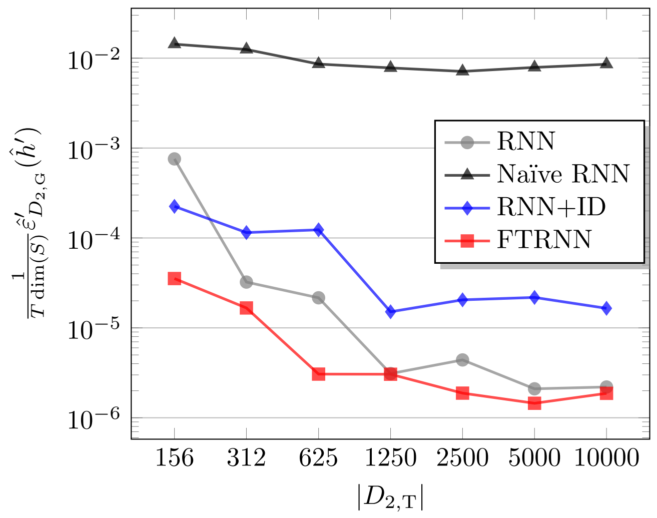

(a) Model errors with upsampled data from MC2 plotted on a logarithmic scale.

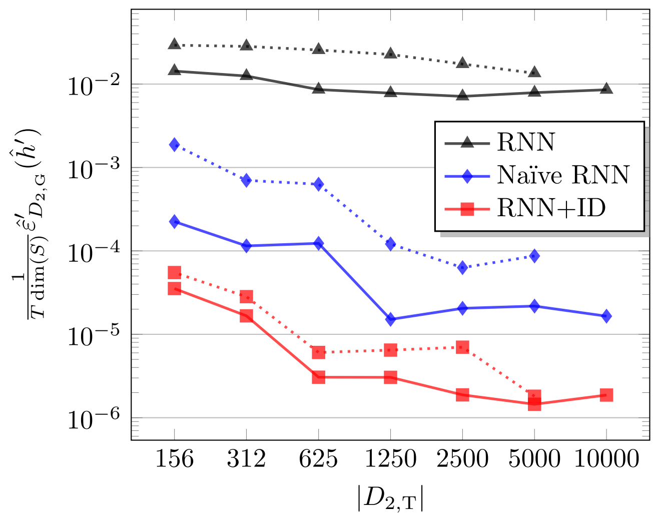

(b) Model errors with (solid lines) and without (dotted lines) upsampled data from MC2 plotted on a logarithmic scale.

Figure 4.5: Experimental results using the mountain car simulation. The plots show the error of the best-of-five model determined by the validation set error. The error is the MSE per state component per time step between the predicted and the true successor state sequence plotted against the varying training set sizes of MC2 for a fixed number of $|D_{1,\mathrm{T}}| = 10\,000$ training examples of MC1.

set sized 5000 to estimate the local curvature of the error surface. In addition, an early stopping procedure with a patience of 50 updates was used to reduce overfitting.

The first set of experiments, whose results are depicted in Figure 4.5a, compared the errors of the different models provided that $D_{2,\mathrm{T}}$ and $D_{2,\mathrm{V}}$ were upsampled such that $|D_{2,\mathrm{T}}| = |D_{1,\mathrm{T}}|$ and $|D_{2,\mathrm{V}}| = |D_{1,\mathrm{V}}|$. As a result, the simple RNN performed well in general, but its error increased for an increasing data ratio $\frac{|D_{1,\mathrm{T}}|}{|D_{2,\mathrm{T}}|}$. In contrast to the cart-pole experiments, the Naïve RNN performed orders of magnitude worse than all other models. The RNN+ID modeled the state transition function of MC2 considerably more accurately than the Naïve RNN, but it was almost consistently worse than the simple RNN. It only outperformed the simple RNN for $|D_{2,\mathrm{T}}| = 156$. The FTRNN again performed consistently best by a significant margin in comparison with the other models. Surprisingly, it even achieved a smaller error than the simple RNN for small data ratios $\frac{|D_{1,\mathrm{T}}|}{|D_{2,\mathrm{T}}|}$. For $|D_{2,\mathrm{T}}| = 156$ its error was more than an order of magnitude smaller than the error of the simple RNN. Upon further investigation, the RNN turned out to be slightly underfitting given many training examples.

The second set of experiments, whose results are illustrated in Figure 4.5b, compared the effect of upsampling $D_{2,\mathrm{T}}$ and $D_{2,\mathrm{V}}$ versus keeping their original sizes during training. The observations made during the mountain car experiments were qualitatively consistent with those of the cart-pole experiments. For all models, upsampling the data yielded smaller model errors.

4.4.3 Discussion

The problem class of modeling the state transition function of a dynamical system from few observations by utilizing auxiliary data from a similar system was introduced, motivated and formalized. For this purpose, the Factored Tensor Recurrent Neural Network (FTRNN) architecture was presented, discussed, and its effectiveness was assessed in a series of experiments using the cart-pole and mountain car simulations. The FTRNN was compared with two variants of recurrent neural networks which implement different approaches of information sharing in a dual-task learning setting. In addition, it was also investigated whether the few data of the target system should be upsampled to match the amount of data of the source system, thus, giving equal weight to the source and target systems in the training objective. As a result, the FTRNN turned out consistently and significantly superior to the compared methods on both simulations across the range of considered data ratios. Further, the experiments showed that matching the data set sizes of the two system by means of upsampling yielded a smaller error for all models.

4.5 The Fully Observable Dual-Task Learning Problem with Regularization

Given only few training examples from the target system the parameters of its corresponding model may converge to unfavorable values as the available information is insufficient. To address this problem, a regularization term, which extends the optimization objective of the FTRNN model, is presented preventing the model of the target system from diverging from the model of the source system. The latter is assumed to be trustworthy because its parameters are fitted to sufficiently many and rich data. Given the prior assumption of the systems' similarity the regularization acts as a similarity enforcing constraint applied to the model parameters.

4.5.1 Problem Definition

The problem definition of this section extends the problem definition of Section 4.4.1. The empirical error $\hat{\varepsilon}'_D(h) := \frac{1}{|D|}\sum_{(i,s,a,s')\in D} w_i \mathcal{L}(h(i,s,a),s')$ of a hypothesis $h \in H'$ is extended by a regularization term that constrains the choice of hypotheses in a way that the prior assumption of the two system being similar is further strengthened. The regularized empirical error $\hat{\varepsilon}'_{D,\lambda}(h) := \frac{1}{|D|}\sum_{(i,s,a,s')\in D} w_i \mathcal{L}(h(i,s,a),s') + \lambda||h||$ is obtained through an additional additive term. If the empirically optimal hypothesis $\hat{h}'_\lambda = \arg\min_{h\in H'} \hat{\varepsilon}'_{D,\lambda}(h)$ ($D = \bigcup_{i\in I} D_i$) yields a smaller expected error than $\hat{h}'$ and $\hat{h}_2$, i.e. $\varepsilon_2(\hat{h}'_{2,\lambda}) < \varepsilon_2(\hat{h}'_2) < \varepsilon_2(\hat{h}_2)$ with $\hat{h}'_2(\cdot,\cdot) := \hat{h}'(2,\cdot,\cdot)$, the regularization method improves the utilization of information from the well observed system in the hypothesis search to find a better hypothesis of f_2 despite few data.

4.5.2 Regularization

Let $\Omega\colon \mathbb{R}^{n_f \times |I|} \to \mathbb{R}^+$ be a regularization function that maps a matrix, whose columns hold the system-specific parameters of each system, to a non-negative real-valued regularization cost. The function asymmetrically penalizes the Euclidean distance between two columns of the parameter matrix, i.e. the system-specific parameters of the target system are tied to those of the source system but not vice versa. In the limit of a strong regularization coefficient, the regularized FTRNN objective makes the FTRNN and Naïve RNN equivalent because the system-specific parameters are forced to be equal. The regularization function is defined as

$$\Omega(W_{fi}) = \|\mathrm{const}(W_{fi})e_1 - W_{fi}e_2\|_2^2 \tag{4.7}$$

where const$(\cdot)$ is a function whose argument is made constant with respect to differentiation, i.e. $\frac{\partial \mathrm{const}(W_{fi})}{\partial W_{fi}} = 0$. The error function, minimized with respect to $\theta = \theta_{\mathrm{cross}} \cup \theta_{\mathrm{specific}}$ with $\theta_{\mathrm{cross}} = \{W_{hs}, b_1, W_{f_a a}, W_{hf_a}, W_{f_h h}, W_{hf_h}, b_h, W_{sh}, b_s\}$ and $\theta_{\mathrm{specific}} = \{W_{f_a i}, W_{f_h i}\}$, is given by

$$E(\theta; \lambda_a, \lambda_h) = \hat{\varepsilon}_D(h_{\mathrm{FTRNN},\theta}) + \lambda_a \Omega(W_{f_a i}) + \lambda_h \Omega(W_{f_h i}). \tag{4.8}$$

Thus, the optimal parameters θ^* are found as follows:

$$\theta^* = \arg\min_{\theta} E(\theta, \lambda_a, \lambda_h) \tag{4.9}$$

The hyperparameters $\lambda_a \geq 0$ and $\lambda_h \geq 0$ are determined via cross-validation.

There are two reasons for constraining the effect of the regularization to the target system. First, the system-specific parameters of the source system are assumed to be well determined by the data. Hence, there is no need to exploit information from the target system. In fact, the little and possibly incomplete information about the target system might even corrupt the parameters of the source system. Second, the cross-system parameters adjust according to the dual-task learning objective which is the minimization of (4.8). Since the data of the target system are considered insufficient and likely incomplete, minimizing the prediction error on the training data is likely to generalize poorly for this system. Thus, not only the system-specific parameters of the target system but also the cross-system parameters may adjust unfavorably. By constraining the system-specific parameters of the target system to remain similar to those of the source system, the cross-system parameters are less likely to be affected by incomplete information about the target system. Note, however, that the regularization nevertheless affects the system-specific parameters of the source system implicitly via the cross-system parameters, but the effect should be much more lenient.

4.5.3 Experiments

Experiments were conducted on the cart-pole (see Section 2.8.1) and mountain car (see Section 2.8.2) simulations. For each simulation two different instances of the respective systems were instantiated. One of the two systems was designated the source system from which sufficient data were available while the other system was designated the target system which had only been observed insufficiently in order to learn an accurate model thereof. The experiments especially focused on large data ratios between the source and target systems assessing the effectiveness of the regularization technique in such situations. Regularization coefficients in an appropriate range were compared across a range of data ratios. The training, validation, and test data sets were created using the block validation method (see Section 2.3.3).

Cart-Pole

Sequences of 1000 actions $a_{[t]} \sim \mathcal{U}(-1, 1)$ were applied to the cart-pole every $\tau = 0.02\,\mathrm{s}$ for which the resulting state transitions were observed. After completing a sequence, the simulation was reset to its initial state. Two different cart-poles, whose configurations varied in terms of the pole length l_{pole} and pole mass m_{pole}, were observed. The two cart-poles were configured by setting $l_{\text{pole}} \in \{0.5, 1.0\}$ and $m_{\text{pole}} = 0.1 l_{\text{pole}}$. For cart-pole 1 (CP1), a training data set with 10 000 and a validation data set with 5000 examples were created. For cart-pole 2 (CP2), various training data sets sized $\{10\,000, 5000, ..., 625\}$ and validation data sets sized $\{5000, 2500, ..., 312\}$ were created. During training, the two training and validation data sets were concatenated and the data of CP2 were upsampled to be equal in size with those of CP1. To test the performance of the models, a generalization data set for CP2 sized 30 000 was created. The FTRNN was configured using $n_h = n_{f_h} = 10$, $n_{f_a} = 2$ and $T = 10$. The regularization strength was set to $\lambda = \lambda_a = \lambda_h \in \{10^{-4}, 10^{-3}, 10^{-2}\}$. The maximum number of parameter updates was set to 10 000. The number of conjugate gradient (CG) iterations per update was limited to 150. The gradient was computed using the full training set and the curvature was estimated using 5000 examples.

Figure 4.6 depicts the performance of the FTRNN with and without regularization. The performance metric is the median of five runs of the average MSE

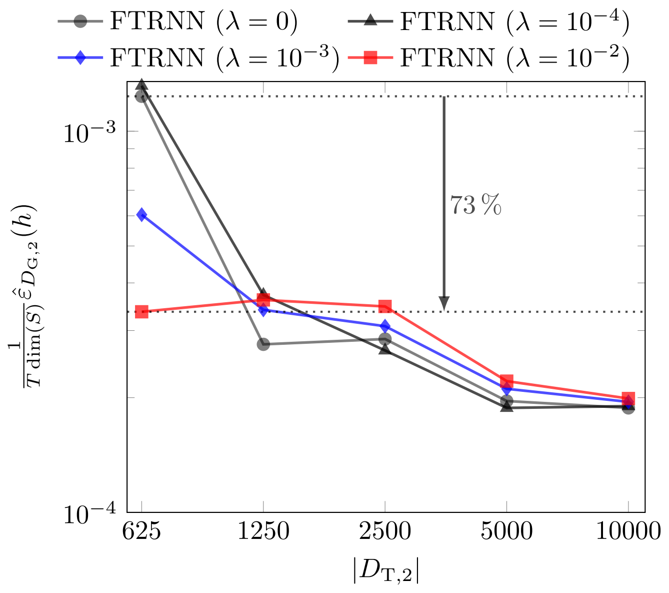

Figure 4.6: Experimental results of the cart-pole simulation. The average MSE per state component per time step of the predicted and the true successor state sequence is plotted against the varying training set size of CP2 for $|D_{1,T}| = 10\,000$ training examples of CP1.

per state component per predicted time step. At the beginning of each run, a new parameter initialization was sampled at random.

The experiments on the cart-pole simulation revealed superior performance of the regularized FTRNN over the plain FTRNN for $|D_{2,T}| = 625$. The smallest error was obtained by setting $\lambda = 10^{-2}$. A large coefficient reduced the error for $|D_{2,T}| = 625$ but increased it for $|D_{2,T}| \in \{1250, 2500, 5000, 10\,000\}$ compared to the plain FTRNN was observed. This observation is plausible because the regularization constrains the parameters of CP2 to be close to those of CP1. When enough data of CP2 were available, this heuristic was likely invalid and harmful to the model performance. However, given only few data of CP2, it guided the parameters towards a better optimum.

Mountain Car

Sequences of 500 actions $(a_{[1]}, ..., a_{[500]})$, computed by the equations

$$a_{[0]} = 0 \tag{4.10a}$$

$$\tilde{a}_{[t]} \sim \mathcal{U}(-1, 1) \tag{4.10b}$$

$$a_{[t]} = \max(-1, \min(1, a_{[t-1]} + \tilde{a}_{[t]})), \tag{4.10c}$$

were applied to the mountain car. After completing a sequence, the simulation was reset to its initial state. Two mountain cars, whose configurations differed in terms of the gravity $g \in \{0.0005, 0.0009\}$, were observed. For mountain car 1 (MC1), a training data set with 10 000 and a validation data set with 5000 examples were created. For mountain car 2 (MC2), various training data sets sized $\{10\,000, 5000, ..., 156\}$ and validation data sets sized $\{5000, 2500, ..., 78\}$ were created. During training, the two training and validation data sets were concatenated and the data of MC2 were upsampled to be equal in size with those of MC1. To test the performance of the models, a generalization data set for MC2 sized 100 000 was created. The FTRNN was configured using $n_h = n_{f_h} = 10$, $n_{f_a} = 2$ and $T = 10$. The regularization strength was set to $\lambda = \lambda_a = \lambda_h \in \{10^{-3}, 10^{-2}, 10^{-1}\}$. The maximum number of parameter updates was set to 5000. The number of conjugate gradient (CG) iterations per update was limited to 100. The gradient was computed using the full training set and the curvature was estimated using 10 000 examples.

Figure 4.7 depicts the performance of the FTRNN with and without regularization. The performance metric is the average MSE per state component per predicted time step of the best model among five runs, determined by the validation set error. At the beginning of each run, a new parameter initialization was sampled at random.

The experiments on the mountain car simulation revealed superior performance of the regularized FTRNN over the plain FTRNN for $|D_{\mathrm{T},2}| \in \{312, 156\}$. Given $|D_{\mathrm{T},2}| = 312$ and for $\lambda = 10^{-3}$, a relative error reduction of approximately 76 % compared to the plain FTRNN. For $|D_{2,\mathrm{T}}| = 156$ and $\lambda = 10^{-2}$, the regularization yielded a relative improvement of approximately 83 %. Similar to the observations made in the cart-pole experiments, the regularization reduced the error for $|D_{2,\mathrm{T}}| \in \{312, 156\}$ but tended to increase it for $|D_{2,\mathrm{T}}| \in \{625, 1250, ..., 10\,000\}$.

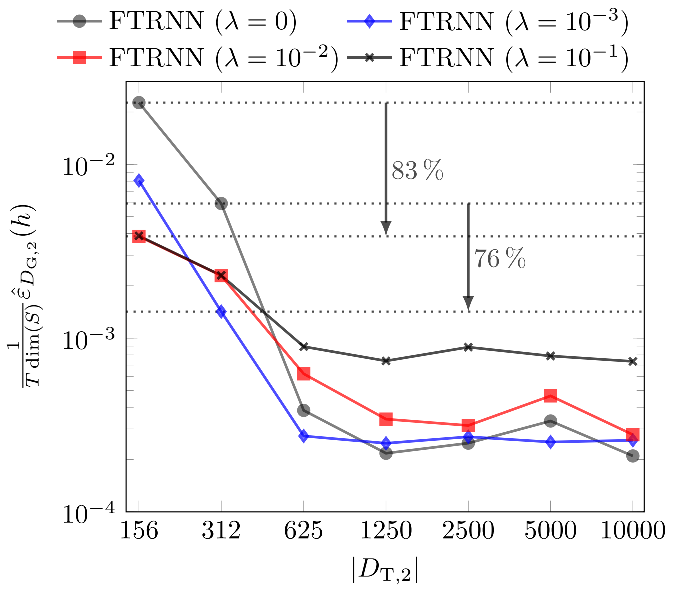

Figure 4.7: Experimental results of the mountain car simulation. The average MSE per state component per time step of the predicted and the true successor state sequence is plotted against the varying training set size of MC2 for $|D_{1,T}| = 10\,000$ training examples of MC1.

4.5.4 Discussion

A regularization technique for the Factored Tensor Recurrent Neural Network (FTRNN) to learn the dynamics of an insufficiently observed target system by exploiting its similarity with a well observed source system in a dual-task learning approach was presented. The FTRNN disentangles cross-system properties from peculiarities allowing to share knowledge efficiently among the systems. When information from the target system was insufficient in order to learn an accurate FTRNN model, it was discovered that especially the system-specific parameters converged to unfavorable values. This section addressed the problem through regularization which penalizes dissimilarities between the system-specific parameters of the source and target system asymmetrically such that the system-specific parameters of the target system were penalized for diverging from those of the source system but not vice versa. The effectiveness of this approach was demonstrated on the cart-pole and mountain car simulations achieving significantly lower errors using the regularized FTRNN compared to the plain FTRNN.

4.6 The Fully Observable Transfer Learning Problem

In this section, an efficient transfer learning approach based on recurrent neural networks with factored tensor components is introduced. The goal is to identify a target system based on few observations by exploiting its similarity with multiple well observed source systems. First, a joint model of the source systems is trained which encodes cross-system properties and system-specific characteristics into disjoint subsets of the model parameters. Second, a model of the target system is obtained by merely fitting the system-specific parameters to the few data of the target system while the cross-system parameters remain fixed. The benefits of this approach are manifold. First, once a joint model of the source systems is learned, knowledge transfer to a target system is fast, i.e. parameter optimization converges within seconds, whereas learning the parameters of an RNN from scratch can take many hours or even days. Second, this approach is data-efficient with respect to the number of required target system observations because the general dynamics of the source systems were identified based on plenty of observations. Third, this method alleviates tedious hyperparameter tuning, especially for the case of few available target system observations, since the number of system-specific parameters is small and their effect on the overall model is highly constrained. Fourth, the model complexity of the approach with respect to a single system is identical to the complexity of the corresponding simple RNN. Therefore, its evaluation time for a new system is the same.

The following subsections formalize the fully observable transfer learning problem and present experimental results of the proposed neural architecture with alternative approaches on data obtained from the cart-pole and mountain car simulations. The empirical results are discussed and conclusions are drawn.

4.6.1 Formal Problem Definition

Let $I := \{1, 2, 3, ...\}$ denote the set of identifiers for fully observable deterministic systems, which are observed in fixed time intervals τ and show similar dynamics. A system is defined by the tuple (S, A, f_i) with a state space S, an action space A, and an unknown state transition function $f_i \colon S \times A \to S$ describing the temporal evolution of the state.

Let D_i be a set of state transition observations $(i, s, a, s') \in D_i$ of the i-th system where each observation describes a single state transition from state $s \in S$ to state $s' \in S$ caused by action $a \in A$. Further, let $D = \bigcup_{i \in I} D_i$ denote a data set of size $|D|$ drawn from a probability distribution $\mathcal{D}$.

Let $H \subseteq \{h \mid h \colon S \times A \to S\}$ denote a hypothesis space, i.e. a set of functions that are assumed to approximate the state transition function f_i. Further, let $\mathcal{L} \colon S \times S \to \mathbb{R}$ denote an error measure between a predicted successor state $\hat{s}'$ and the true successor state s'. The optimal hypothesis h_i^*, i.e. the best approximation of f_i within the considered space of hypotheses, minimizes the conditional expected error $\varepsilon_i(h) := \mathrm{E}_{(j,s,a,s') \sim \mathcal{D}}[\mathcal{L}(h(s, a), s') \mid j = i]$ where E denotes the expectation operator, hence, $h_i^* = \arg\min_{h \in H} \varepsilon_i(h)$. Since $\mathcal{D}$ is generally unknown, an approximately optimal hypothesis is determined by minimizing the empirical error $\hat{\varepsilon}_D(h) := \frac{1}{|D|} \sum_{(\cdot,s,a,s') \in D} \mathcal{L}(h(s, a), s')$ induced by a hypothesis h on a data set D, hence, $\hat{h}_i = \arg\min_{h \in H} \hat{\varepsilon}_{D_i}(h)$.

Let the set of system identifiers I refer to $|I| - 1$ source systems with plenty of available data and one target system with only few data, i.e. $|D_{|I|}| \ll |D_i|$ for all $i \in I \setminus \{|I|\}$. Given the sufficient amount of data from the source systems $i \in I \setminus \{|I|\}$, $|\varepsilon_i(\hat{h}_i) - \varepsilon_i(h_i^*)| \leq \epsilon$ for some small positive ϵ. In contrast, given only few data $D_{|I|}$ from the target system, $|\varepsilon_{|I|}(\hat{h}_{|I|}) - \varepsilon_{|I|}(h_{|I|}^*)| \gg \epsilon$ and $\hat{h}_{|I|}$ may be useless. The problem addressed in this section is to develop and assess methods that yield a better hypothesis of the insufficiently observed system through transfer learning in order to utilize auxiliary information from $\bigcup_{i \in I \setminus \{|I|\}} D_i$ as prior knowledge of the transition function $f_{|I|}$.

Therefore, the hypothesis space and the empirical error are redefined as follows. Let $H' \subseteq \{h \,|\, h\colon I \times S \times A \to S\}$ denote an extended hypothesis space, which includes the system identifier into the product space of arguments and thus approximates both transition functions by a single function. Further, let $\hat{\varepsilon}'_D(h) := \frac{1}{|D|} \sum_{(i,s,a,s') \in D} w_i \mathcal{L}(h(i, s, a), s')$ denote the empirical error of a hypothesis $h \in H'$ with the system-specific error weight w_i. If the empirically optimal hypothesis $\hat{h}' = \arg\min_{h \in H'} \hat{\varepsilon}'_D(h)$ $(D = \bigcup_{i \in I} D_i)$ yields a smaller expected error than $\hat{h}_{|I|}$, i.e. $\varepsilon_{|I|}(\hat{h}'_{|I|}) < \varepsilon_{|I|}(\hat{h}_{|I|})$ with $\hat{h}'_{|I|}(s, a) := \hat{h}'(|I|, s, a)$, information from the well observed system was successfully utilized in the hypothesis search to find a better hypothesis of $f_{|I|}$ despite few data.

4.6.2 Experiments

Experiments were conducted using two standard simulations: the frictionless cart-pole (see Section 2.8.1) and mountain car (see Section 2.8.2) simulations both modified from their originals to support continuous actions. For each simulation, five different source system instances were labeled $\{1, ..., 5\}$ and various other instances were labeled $\{6\}$. The properties of the target systems were configured at random according to some distribution. Each system was observed under a random policy to obtain data for training and evaluation. In order to decorrelate the examples of the training, validation and generalization data sets, the block validation method discussed in Section 2.3.3 was applied.

Let $D_{i,\mathrm{T}}$ denote the set of training examples, let $D_{i,\mathrm{V}}$ be the validation set and $D_{i,\mathrm{G}}$ be the generalization set for system $i \in \{1, ..., 6\}$. The data set sizes of the target system were assumed to be much smaller than those of the source systems, i.e. $D_{6,\mathrm{T}} \ll D_{i,\mathrm{T}}$ and $D_{6,\mathrm{V}} \ll D_{i,\mathrm{V}}$ for $i \in \{1, ..., 5\}$. Each example was represented as a tuple $(i, s_{[1]}, ..., s_{[T+1]}, a_{[1]}, ..., a_{[T]})$.

The following protocol was used for all experiments:

1. Simple RNN models were trained for all source systems with different data set sizes to roughly determine the amount of training examples needed to learn good and poor models of the state transition function.

2. Data set sizes were chosen according to the results of step 1. The Naïve RNN, RNN+ID, and FTRNN models were trained on the concatenated training sets of all source systems (plenty of data) until the validation error, evaluated on the concatenated validation sets, stopped improving for at least 50 parameter updates. In addition, simple RNN models were trained for all target systems (few data) using their corresponding data sets until the validation error stopped improving for at least 50 parameter updates. This process was repeated five times, each time with a fresh random initialization of the model parameters. Among the five runs, the best set of parameters was picked according to the validation set error.

3. For the RNN+ID and FTRNN architecture, the cross-system parameters were transferred to the target system model by initializing its cross-system parameters with the parameters of the source systems' model. The system-specific parameters of the target system model were initialized as the average of the system-specific parameters of the source systems' model. When training the target system model, only the system-specific parameters were fitted to the training data of the target system until the validation set error stopped improving for at least 50 parameter updates. The cross-system parameters were considered constant with respect to the optimization objective. This process was repeated for all target systems.

4. Finally, the errors of the RNN, Naïve RNN, RNN+ID, and FTRNN models were evaluated on the generalization data sets of the target systems. For the RNN+ID and FTRNN models, the system-specific parameters of the respective target system model, which had been obtained in the previous step, were used.

Cart-Pole

A cart-pole was observed every $\tau = 0.02\,\mathrm{s}$ for sequences of 500 actions $(a_{[1]}, ..., a_{[500]})$ computed by the equations

$$a_{[0]} = 0 \tag{4.11a}$$

$$\tilde{a}_{[t]} \sim \mathcal{U}(-1, 1) \tag{4.11b}$$

$$a_{[t]} = \max(-1, \min(1, a_{[t-1]} + \tilde{a}_{[t]})). \tag{4.11c}$$

After every 500 steps, the simulation was reset to its initial state. Different cart-poles, whose configurations varied in terms of the pole length l_{pole} and pole mass m_{pole}, were observed. Each cart-pole $i \in I \setminus \{|I|\}$ was configured by setting $l_{\text{pole}} \in \{0.5, 0.6, 0.7, 0.8, 0.9\}$ and $m_{\text{pole}} = 0.1 l_{\text{pole}}$, and data sets of size $|D_{i,\text{T}}| = 10\,000$, $|D_{i,\text{V}}| = 5000$, and $|D_{i,\text{G}}| = 100\,000$ were created. Further, various other cart-pole configurations were created by sampling $l_{\text{pole}} \sim \mathcal{U}(0.3, 1.1)$. The corresponding data sets were sized $|D_{6,\text{T}}| = 156$, $|D_{6,\text{V}}| = 78$ and $|D_{6,\text{G}}| = 100\,000$. The RNNs were configured as follows: $n_h = n_{f_h} = 20$, $n_{f_a} = 1$, $T = 10$. The parameters were fitted to the data using Hessian-Free optimization with structural damping (see Section 2.4.2 for details) with the structural damping coefficient $\mu_{\text{sd}} = 0.1$ and the initial Levenberg-Marquardt coefficient $\lambda_{\text{LM}} = 1.0$. The gradient of the optimization objective with respect to the parameters was computed using 10 000 examples selected at random without replacement from the training data set. During the conjugate gradient (CG) iterations, 5000 examples from the training data set were selected at random without replacement. The CG method ran for at most 150 iterations per update. Further, at most 10 000 parameter updates were allowed. These hyperparameters were not exhaustively cross-validated, but they were found to work well based on testing several different settings.

Figure 4.8 depicts the results of the experiments conducted using the cart-pole simulation.

Figure 4.8a shows the similarity of the cart-poles labeled $\{1, ..., 5\}$ by evaluating every RNN model on every cart-pole configuration. Clearly, the models were accurate when trained and evaluated on the same configuration, but the accuracy decreased notably when a model was trained on a data from a particular cart-pole configuration and evaluated on data from another one. Further, increasing the difference between the pole lengths and pole masses of two cart-

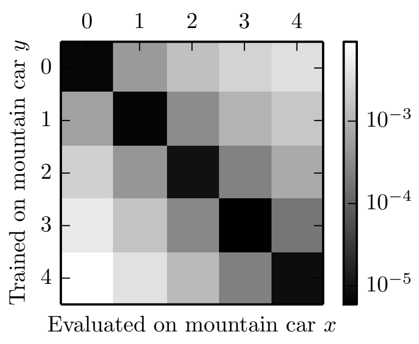

(a) Similarity of the source systems

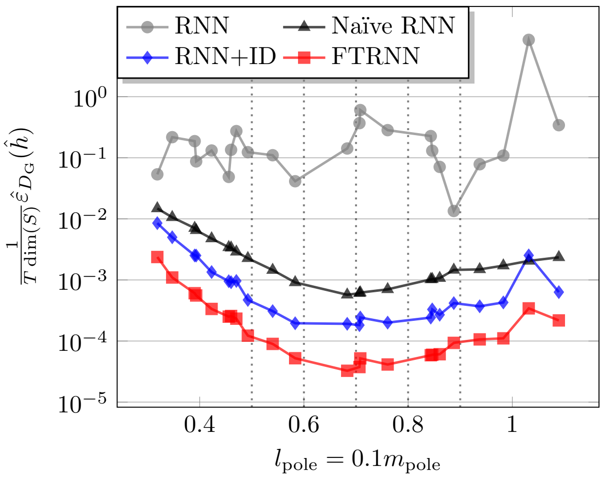

(b) Error of the target system models

Figure 4.8: Experimental results of the cart-pole simulation. The plots show the mean squared error, evaluated on the generalization data sets sized 100 000, divided by the number of state components and the number of predicted time steps. (a) compares the similarity of the source systems by evaluating an RNN model learned from 10 000 training examples of cart-pole x and evaluates the model on cart-pole y using the corresponding generalization data set. (b) compares the error of the different models for various target systems using 156 training examples to learn the system-specific parameters of the FTRNN and RNN+ID and all parameters of the RNN. The dotted vertical lines indicate the source system configurations used to learn the cross-system parameters of the FTRNN and RNN+ID as well as the parameters of the Naïve RNN.

poles made the respective models less accurate when evaluated on the other cart-pole. Thus, adjusting the pole length and mass of the cart-poles yields non-identical but nevertheless similar dynamical systems.

Figure 4.8b depicts the MSE divided by the number of state components and the number of predicted time steps against the different cart-pole configurations for the considered models.

The experiments show that the FTRNN was able to successfully learn a joint model of the five different cart-pole configurations labeled $\{1, ..., 5\}$ such that an accurate target system model could be learned from only 156 training examples by transferring the cross-system parameters of the source systems' model to the target system model. In comparison with the Naïve RNN and RNN+ID model, the FTRNN performed best by a significant margin followed by the RNN+ID and the Naïve RNN. This order of the model performances was consistent in the interpolation range $l_{\text{pole}} \in [0.5, 0.9]$ as well as the tested extrapolation range $l_{\text{pole}} \in [0.3, 0.5[\cup]0.9, 1.1]$. Learning an RNN model from only 156 training examples of a single target system was insufficient in order to learn the parameters of a system-specific model.

Mountain Car

A mountain car was observed for sequences of 500 actions $(a_{[1]}, ..., a_{[500]})$ computed by the equations

$$a_{[0]} = 0 \tag{4.12a}$$

$$\tilde{a}_{[t]} \sim \mathcal{U}(-1, 1) \tag{4.12b}$$

$$a_{[t]} = \max(-1, \min(1, a_{[t-1]} + \tilde{a}_{[t]})). \tag{4.12c}$$

After every 500 steps, the simulation was reset to its initial state. Different mountain cars, whose configurations varied in terms of the gravity g, were observed. Each mountain car $i \in I \setminus \{|I|\}$ was configured by setting $g \in \{0.0010, 0.0015, 0.0020, 0.0025, 0.0030\}$, and data sets of size $|D_{i,\text{T}}| = 10\,000$, $|D_{i,\text{V}}| = 5000$ and $|D_{i,\text{G}}| = 100\,000$ were created. Further, various other mountain car configurations were created by sampling $g \sim \mathcal{U}(0.0005, 0.005)$. The corresponding data sets were sized $|D_{6,\text{T}}| = 156$, $|D_{6,\text{V}}| = 78$ and $|D_{6,\text{G}}| = 100\,000$. The RNNs were configured as follows: $n_h = 10$, $n_{f_h} = n_{f_a} = 3$, $T = 10$. The parameters were fitted to the data using Hessian-Free optimization with structural damping (see Section 2.4.2 for details) with the structural damping coefficient $\mu_{\text{sd}} = 0.1$ and the initial Levenberg-Marquardt coefficient $\lambda_{\text{LM}} = 1.0$. The gradient of the optimization objective with respect to the parameters was computed using 10 000 examples selected at random without replacement from the training data set. During the conjugate gradient (CG) iterations, 5000 examples from the training data set were selected at random without replacement. The CG method ran for at most 50 iterations per update. Further, at most 10 000 parameter updates were allowed. These hyperparameters were not exhaustively cross-validated, but they were found to work well based on testing several different settings.

Figure 4.9 depicts the results of the experiments conducted using the mountain car simulation.

Figure 4.9a shows the similarity of all pairs of the five mountain cars labeled $\{1, ..., 5\}$ by evaluating every RNN model on every mountain car configuration. Similar to the cart-pole experiments, varying the gravity of the the mountain car simulation yielded non-identical but similar dynamical systems since a model trained on a particular mountain car configuration was a less accurate model of another configuration. The accuracy decreased as the difference of the two gravity settings increased.

Figure 4.9b depicts the performance of our considered models plotting the MSE divided by the number of state components and the number of predicted time steps against the different mountain car configurations.

The mountain car experiments support the results of the cart-pole experiments. Again, the FTRNN performed best by a significant margin followed by the RNN+ID. The Naïve RNN yielded the largest error among the considered models. This order of the model performances is consistent in the interpolation range $g \in [0.001, 0.003]$ as well as the tested extrapolation range $g \in [0.0005, 0.001) \cup (0.003, 0.005]$. The error of a simple target system RNN model using 156 training examples was large and erratic across the set of target systems. This suggests that it does not suffice to use few training examples of each target system to learn an accurate model.

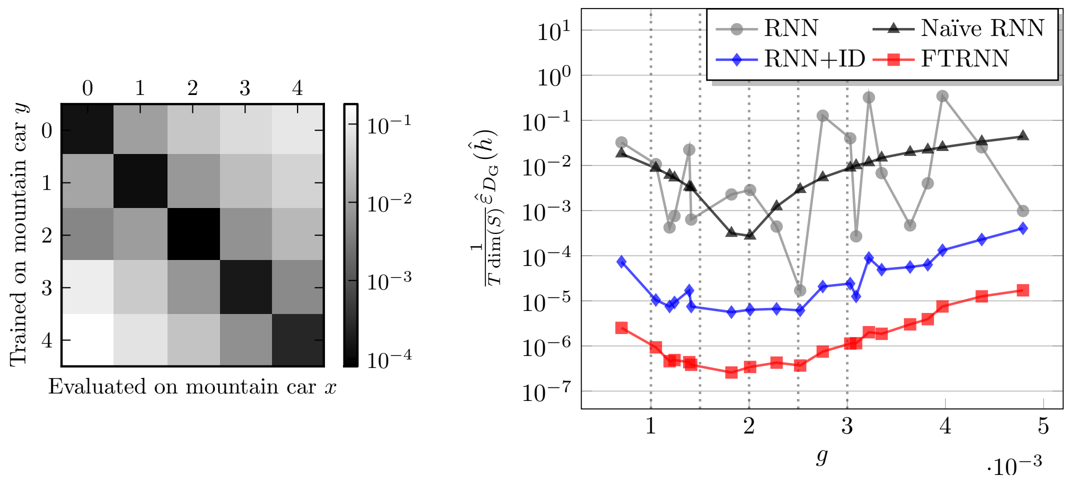

(a) Similarity of the source systems (b) Error of the target system models

Figure 4.9: Experimental results of the mountain car simulation. The plots show the mean squared error, evaluated on the generalization data set sized 100 000, divided by the number of state components and the number of predicted time steps. (a) compares the similarity of the source systems by evaluating an RNN model learned from 10 000 training examples of mountain car x and evaluates the model on mountain car y using the corresponding generalization data set. (b) compares the error of the different models for various target systems using 156 training examples to learn the system-specific parameters of the FTRNN and RNN+ID and all parameters of the RNN. The dotted vertical lines indicate the source system configurations used to learn the cross-system parameters of the FTRNN and RNN+ID as well as the parameters of the Naïve RNN.

4.6.3 Training Time

Besides the ability to exploit prior knowledge in order to decrease the model error despite only few available observations of a target system, the proposed transfer learning approach speeded up the training process dramatically. To demonstrate this additional benefit, the training time of a simple RNN model given sufficient data was compared with the time it took to train the system-specific parameters of the FTRNN model given few data. Figure 4.10 visualizes the training times for the cart-pole and mountain car simulations. As a result,

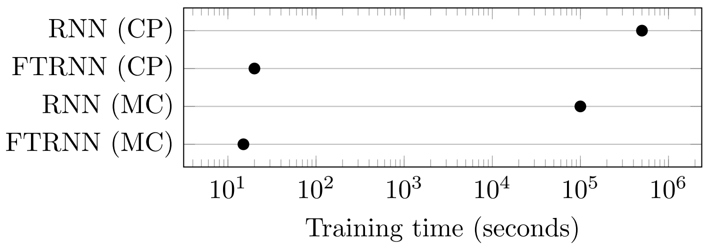

Figure 4.10: Training times of the RNN and the FTRNN for the cart-pole and mountain car simulations. The RNN was trained with 10 000 training examples from a random parameter initialization. In contrast, the FTRNN was pre-trained on the source systems and only the system-specific parameters, initialized as the average of the system-specific parameters of the source systems' model, were learned from the training data set of a target system.

the FTRNN was not only able to successfully transfer knowledge from a set of relevant source systems to an insufficiently observed target system, but it was also able to achieve high model accuracy within a small fraction of the time needed to train a comparable RNN model given sufficient training data. The speed-up for the cart-pole simulation was approximately 25 000× and more than 5000× for the mountain car simulation. Thus, after a joint model of a set of source systems had been learned, it was possible to adapt the model to a target system virtually instantaneously.

4.6.4 Discussion

The Factored Tensor Recurrent Neural Network (FTRNN) model was presented which enables efficient knowledge transfer in system identification tasks to learn the state transition function of a target system from few available observations given multiple well observed similar source systems. Besides the advantage of obtaining an accurate model despite few data, learning a target system model converged within seconds whereas, in contrast, learning an independent model from scratch, given enough data, often took many hours or even days. In addition, hyperparameter tuning was significantly reduced despite few data because the ratio between the amount of training data and the number of adaptive parameters was reasonable. Last, evaluation of the FTRNN and a standard RNN have identical complexity because the factored weight matrix per system can be expanded prior to evaluation.

To demonstrate the effectiveness of the proposed method, experiments were conducted using the well known cart-pole and mountain car simulations. The FTRNN model was compared with two more plain approaches to this problem—the Naïve RNN and the RNN+ID model. The first one was a simple RNN which learned the state transition function of multiple systems from a concatenated data set. The second one was a simple RNN with an extra "one-hot" input vector disclosing the system that generated the example to the model. The FTRNN performed consistently better than the RNN+ID and the Naïve RNN using both simulations.

CHAPTER 5

Exploiting Similarity in Partially Observable System Identification Tasks

This chapter addresses the problem of partially observable system identification of a target system despite only few available data. Standard modeling approaches, that learn a model only from the target system data, are inapplicable in this setting because the amount of data is insufficient. However, additional data from related but probably non-identical systems may provide prior knowledge about the target system and should be utilized in the model building process. Therefore, several multi-task recurrent neural network architectures, which are able to utilize information from related tasks as prior knowledge of the target task, are proposed and empirically evaluated.

The chapter is structured as follows. First, the problem of partially observable system identification in the context of soft-sensor modeling is introduced and formalized (Section 5.1). Second, a recurrent neural networks architecture suitable for partially observable system identification is presented (Section 4.2). Third, the original problem is extended to a multi-system identification task where only few observations are available from the target system while sufficient information from auxiliary systems can be utilized (Section 5.3). The recurrent neural network architectures developed in Section 3.3 are adapted to the partially observable multi-system identification problem. A real-world experiment, whose goal is to model NO_x emissions of Siemens gas turbines, is conducted employing the multi-task learning paradigm to transfer information from the auxiliary systems to the target system (Section 5.4). Therefore, multiple variants of recurrent neural networks are proposed and empirically evaluated.

The subsequent sections are based on the following publication as part of the doctoral research:

- Spieckermann, S., Udluft, S., and Runkler, T. Data-efficient temporal regression with multi-task recurrent neural networks. In *Advances in Neural Information Processing Systems (NIPS), Second Workshop on Transfer and Multi-Task Learning: Theory meets Practice*, 2014.

5.1 Partially Observable System Identification

5.1.1 Introduction

Partially observable system identification is the process of obtaining a model of a dynamical system using experimental data where the state of the system cannot be fully observed by the available measuring devices, e.g. sensors. By aggregating a sequence of observations, it may be possible to estimate the state of the system. Most real-world systems are partially observable. Consider a complex technical system such as a gas turbine equipped with sensors which record various measurements within the system, e.g. the temperature and pressure after the compressor before the combustion chamber. Despite the great number of installed sensors the state of the turbine is not fully observed at a single moment in time. To overcome partial observability, the observable quantities are aggregated over time such that the state of the system can be approximated.

5.1.2 Formal Problem Definition

A system, observed in fixed time intervals τ, is defined by the tuple (S, A, f) with a state space S, an action space A, and an unknown state transition function $f\colon S \times A \to S$ describing the temporal evolution of the state. Further, let $S' \subset S$ be a subspace of the state space and $g_S\colon S \to S'$ be an observation function which maps S to S'. Similarly, let $g_A\colon A \to A'$ define an observation function that maps the action space to a subspace. It is assumed that only S' and A' can be observed.

Let D be a set of observations $(x_{[t-d+1]}, ..., x_{[t]}, y_{[t]}) \in D$ with $x_{[\cdot]} \in X \subset S' \times A'$, $y_{[\cdot]} \in Y$, $Y \subset S'$, $X \cap Y = \emptyset$. Further, let D denote a data set of size $|D|$ drawn from a probability distribution $\mathcal{D}$.

Let $H \subseteq \{h \,|\, h\colon X^d \to Y\}$, $d \in \mathbb{N}$, denote a hypothesis space, i.e. a set of functions that are assumed to approximate the mapping from a sequence of state and action observations to a disjoint target state observation. Further, let $\mathcal{L}\colon Y \times Y \to \mathbb{R}$ denote an error measure between a predicted target $\hat{y}$ and the ground truth y. The optimal hypothesis h^* minimizes the expected error $\varepsilon(h) := \mathrm{E}_{(x_{[t-d+1]},...,x_{[t]},y_{[t]})\sim\mathcal{D}}[\mathcal{L}(h(x_{[t-d+1]},...,x_{[t]},y_{[t]})]$ where E denotes the expectation operator, hence, $h^* = \arg\min_{h\in H} \varepsilon(h)$. Since $\mathcal{D}$ is generally unknown, an approximately optimal hypothesis is determined by minimizing the empirical error $\hat{\varepsilon}_D(h) := \frac{1}{|D|}\sum_{(x_{[t-d+1]},...,x_{[t]},y_{[t]})\in D} \mathcal{L}(h(x_{[t-d+1]},...,x_{[t]},y_{[t]})$ induced by a hypothesis h on a data set D, hence, $\hat{h} = \arg\min_{h\in H} \hat{\varepsilon}_D(h)$.

5.2 Partially Observable System Identification with Recurrent Neural Networks

Partially observable sequences are often modeled using hidden Markov models (see Section 2.5). Given a sequence of observations $(x_{[1]},...,x_{[T]})$ the hidden state transition probabilities and emission parameters are learned such that the probability of an observed sequence given a corresponding hidden state sequence is maximized. Thus, learning the parameters of a hidden Markov model may be considered an unsupervised learning problem. However, the problem class investigated in this chapter differs from unsupervised sequence learning. Instead of learning a model of probable sequences, the relationship between a target variable and a sequence of disjoint environmental and control observations shall be learned. The model may be viewed as a composite model consisting of a state estimation sub-model, which infers a hidden state from the sequence of input observations, and a regression sub-model, which learns the mapping from the hidden state to the target variable. While it may be possible to stack a hidden Markov model for the state estimation and, e.g., a linear regression model, this approach appears unnatural and inefficient since the state estimation is likely to include information that is irrelevant to the regression task. In contrast, a model that learns the input-output mapping directly likely aggregates only relevant information from the input sequence in order to optimally predict the target variable.

Recurrent neural networks are an appropriate choice to perform state estimation (Schäfer & Udluft, 2005; Yadaiah & Sowmya, 2006) with a supervised target. In order to model a state component of a partially observable dynamical system as a function of other observed state and action variables, a recurrent neural network may be defined which processes a sequence of state and action observations $(x_{[t-d+1]}, ..., x_{[t]})$ yielding the predicted target state variable $\hat{y}_{[t]}$. Instead of predicting only a single step, a technique called *overshooting*, i.e. predicting multiple steps, has shown improved results (Zimmermann & Neuneier, 2001; Zimmermann et al., 2007). The network is defined by the following equations.

$$h_{[-d]} = 0 \tag{5.1a}$$
$$h_{[t]} = \phi_h(W_{hh}h_{[t-1]} + W_{hx}x_{[t]} + b_h) \tag{5.1b}$$
$$\forall t \geq 1: \ \hat{y}_{[t]} = \phi_y(W_{yh}h_{[t]} + b_y) \tag{5.1c}$$

The sequence of state and action observations is mapped to the corresponding hidden state sequence by a linear transformation followed by the nonlinear function $\phi_h(\cdot)$ which is typically chosen as $\tanh(\cdot)$. This allows the network to learn the extraction of relevant information from different time steps which is necessary to perform the prediction for $t \geq 1$. Depending on the distribution of $y_{[T]}|x_{[1]}, ..., x_{[T]}$ a matching activation function $\phi_y(\cdot)$ is chosen. Figure 4.1

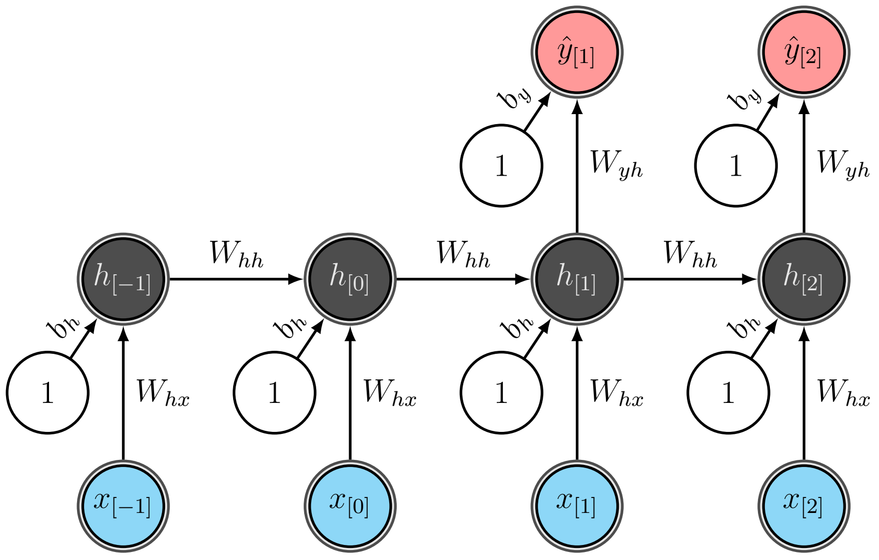

Figure 5.1: Recurrent neural network for partially observable system identification.

depicts a graphical representation of the RNN architecture.

5.3 Partially Observable Multi-System Identification with Recurrent Neural Networks

5.3.1 Naïve RNN

The most naïve approach to exploit information from multiple dynamical systems and share it with another one is to concatenate the data of all systems and learn a joint model. This way, the model is forced to generalize over the different properties of the systems. However, since the training examples of the systems are not distinguished, the model can only learn the average task which may be vastly suboptimal for rather different systems.

The following subsections discuss two recurrent neural architectures that are able to distinguish the systems through an integer identifier. In both models, the hidden state $h_{[t]}$ accumulates relevant information from past time steps into an aggregated representation that contains information relevant to the given learning task.

5.3.2 RNN+ID

One way to incorporate information that allows the model to distinguish between the systems is to tag each training example with an identifier $i \in I$, which corresponds to the system that generated the data. This tag may be provided to the model at each time step as an extra input encoded as the i-th Euclidean standard basis vector e_i with $\dim(e_i) = |I|$. The equations of the RNN+ID architecture are obtained by substituting (5.1b) with (5.2).

$$h_{[t]} = \phi_h(W_{hh}h_{[t-1]} + W_{hx}x_{[t]} + W_{hi}e_i + b_h) \tag{5.2}$$

Figure 5.2 depicts a graphical representation of the RNN+ID architecture. In fact, computing $W_{hi}e_i$ means selecting the i-th column of W_{hi} so the system identifier introduces a separate hidden layer bias for each system. The cross-system bias b_h and the specific biases accessed through $W_{hi}e_i$ can be absorbed into a new system-specific bias $\widetilde{W}_{hi}e_i = b_h + W_{hi}e_i$. Thus, (5.2) can be rewritten as

$$h_{[t]} = \phi_h(W_{hh}h_{[t-1]} + W_{hx}x_{[t]} + \widetilde{W}_{hi}e_i). \tag{5.3}$$

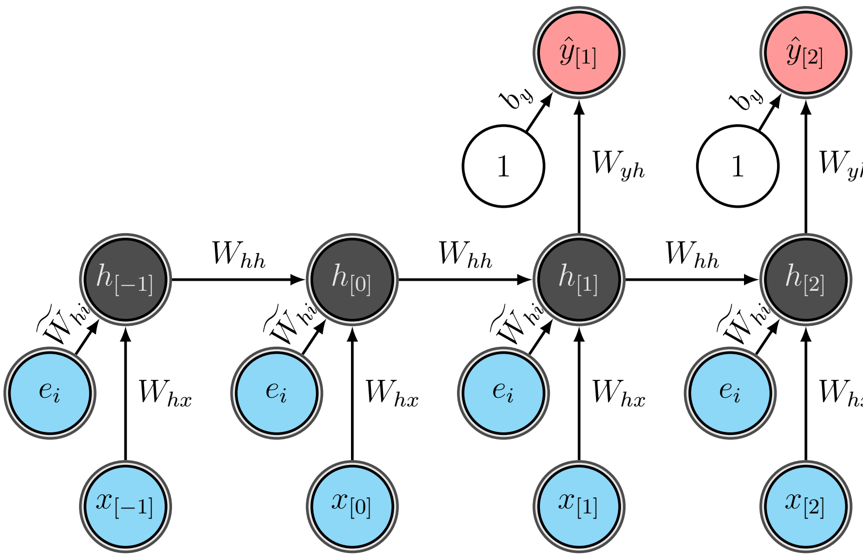

Figure 5.2: RNN+ID architecture for partially observable multi-system identification.

5.3.3 FTRNN

Similar to the FTRNN model proposed in Section 4.3.3 which learns the state transition function of a fully observable dynamical system using auxiliary data from (a) related system(s), the factored tensor weights can be used to extract system-specific features from the sequence of observations of multiple partially observable systems in a data-efficient manner. More specifically, in order to realize a system-specific memory mechanism, the memory transition matrix W_{hh} should be conditioned on the system $i \in I$. Naively, a different matrix could be learned for each system resulting in a third-order tensor $W_{hhi} \in \mathbb{R}^{n_h \times n_h \times |I|}$. Thus, the frontal slices of the tensor represent the memory transition matrices for each system. However, as argued in Section 3.3.3 learning parameters of the full tensor is suboptimal given only limited amounts of data from the target system. Instead, a factored representation of the tensor is learned which consists of cross-system and system-specific parameters. Thus, the expanded linear transformation of each system shares information across all systems yielding a more data-efficient approach to the problem. The equations of the FTRNN architecture are obtained by substituting (5.1b) with (5.4).

$$h_{[t]} = \phi_h(W_{hf}\,\mathrm{diag}(W_{fi}e_i)W_{fh}h_{[t-1]} + W_{hx}x_{[t]} + b_h) \tag{5.4}$$

Figure 5.3 depicts a graphical representation of the FTRNN architecture.

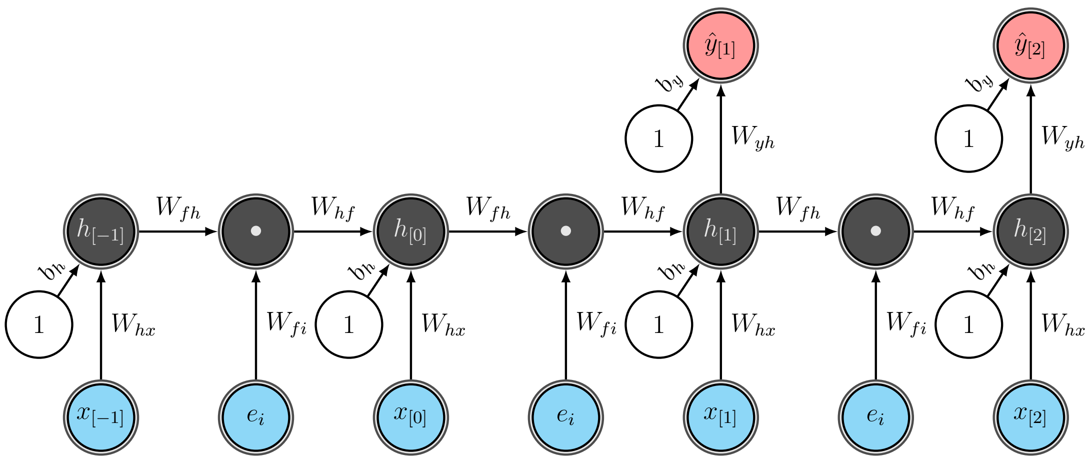

Figure 5.3: FTRNN for partially observable multi-system identification. The node having the •-symbol in its center is a "multiplication node", i.e. the input vectors of the node are multiplied component-wise. In contrast, the standard nodes imply the summation of all input vectors.

5.4 The Partially Observable Multi-Task Learning Problem

The partially observable multi-task learning problem addresses the task of learning a regression function with temporal dependencies of a little observed partially observable dynamical system by utilizing data from multiple well-observed similar systems. In order to achieve this goal, the data of all systems are used to learn a joint model thereof such that information is shared among the systems. Typical applications of this scenario are situations in which a new instance is deployed and observed only for a short time until the model, e.g. a soft-sensor, shall be operational. In case multiple other systems with similar properties, e.g. systems of the same family, have been operated sufficiently long, the information can be utilized as prior knowledge about general structural commonalities among the systems. Then, the few data from the target system are expected to suffice in order to learn its peculiarities.

5.4.1 Formal Problem Definition

Let $I := \{1, 2, ...\}$ denote a set of identifiers for partially observable deterministic systems that show similar dynamics. A system, observed in fixed time intervals τ, is defined by the tuple (S, A, f_i), $i \in I$, with a state space S, an action space A, and an unknown state transition function $f_i \colon S \times A \to S$ describing the temporal evolution of the state. Further, let $S' \subset S$ be a subspace of the state space and $g_S \colon S \to S'$ be an observation function which maps S to S'. Similarly, let $g_A \colon A \to A'$ define an observation function that maps the action space to a subspace. It is assumed that only S' and A' can be observed.

Let D_i be a set of observations $(i, x_{[t-d+1]}, ..., x_{[t]}, y_{[t]}) \in D_i$ of the i-th system with $x_{[\cdot]} \in X \subset S' \times A'$, $y_{[\cdot]} \in Y$, $Y \subset S'$, $X \cap Y = \emptyset$. Further, let $D = \bigcup_{i \in I} D_i$ denote a data set of size $|D|$ drawn from a probability distribution $\mathcal{D}$.

Let $H \subseteq \{h \,|\, h \colon X^d \to Y\}$, $d \in \mathbb{N}$, denote a hypothesis space, i.e. a set of functions that are assumed to approximate the mapping from a sequence of state and action observations to a disjoint target observation. Further, let $\mathcal{L} \colon Y \times Y \to \mathbb{R}$ denote an error measure between a predicted target $\hat{y}$ and the ground truth y. The optimal hypothesis h_i^* minimizes the conditional expected error $\varepsilon_i(h) := \mathrm{E}_{(j, x_{[t-d+1]}, ..., x_{[t]}, y_{[t]}) \sim \mathcal{D}}[\mathcal{L}(h(x_{[t-d+1]}, ..., x_{[t]}, y_{[t]}) \,|\, j = i]$ where E denotes the expectation operator, hence, $h_i^* = \arg\min_{h_i \in H} \varepsilon_i(h)$. Since $\mathcal{D}$ is generally unknown, an approximately optimal hypothesis is determined by minimizing the empirical error $\hat{\varepsilon}_D(h) := \frac{1}{|D|} \sum_{(\cdot, x_{[t-d+1]}, ..., x_{[t]}, y_{[t]}) \in D} \mathcal{L}(h(x_{[t-d+1]}, ..., x_{[t]}, y_{[t]})$ induced by a hypothesis h on a data set D, hence, $\hat{h}_i = \arg\min_{h \in H} \hat{\varepsilon}_{D_i}(h)$.

Given sufficient data $D_{|I|}$, it is expected that $|\varepsilon_{|I|}(\hat{h}_{|I|}) - \varepsilon_{|I|}(h^*_{|I|})| \leq \epsilon$ for some small positive ϵ. In contrast, assuming the amount of data $D_{|I|}$ is insufficient, $|\varepsilon_{|I|}(\hat{h}_{|I|}) - \varepsilon_{|I|}(h^*_{|I|})| \gg \epsilon$ and $\hat{h}_{|I|}$ may be useless. The problem addressed in this section is to develop and assess methods that yield a better hypothesis of an insufficiently observed system through multi-task learning in order to utilize auxiliary information from $\bigcup_{i \in I \setminus \{|I|\}} D_i$ as prior knowledge of the transition function $f_{|I|}$.

Therefore, the hypothesis space and the empirical error are redefined as follows. Let $H' \subseteq \{h \,|\, h \colon I \times X^d \to Y\}$ denote an extended hypothesis space, which includes the system identifier into the product space of arguments and thus jointly approximates the functions of each system. Further, let $\hat{\varepsilon}'_D(h) := \frac{1}{|D|} \sum_{(i, x_{[t-d+1]}, ..., x_{[t]}, y_{[t]}) \in D} w_i \mathcal{L}(h(i, x_{[t-d+1]}, ..., x_{[t]}), y_{[t]})$ denote the empirical error of a hypothesis $h \in H'$ with the system-specific error weight w_i. If the the empirically optimal hypothesis $\hat{h}' = \arg\min_{h \in H'} \hat{\varepsilon}'_D(h)$ $(D = \bigcup_{i \in I} D_i)$ yields a smaller expected error than $\hat{h}_{|I|}$, i.e. $\varepsilon_{|I|}(\hat{h}'_{|I|}) < \varepsilon_{|I|}(\hat{h}_{|I|})$ with $\hat{h}'_i(x_{[t-d+1]}, ..., x_{[t]}) := \hat{h}'(i, x_{[t-d+1]}, ..., x_{[t]},)$, information from the well observed system was successfully utilized in the hypothesis search to find a better hypothesis of $f_{|I|}$ despite few data.

5.4.2 Experiments

The utility of the models presented in Section 5.3 was evaluated on real-world gas turbine data comprising various hardware configurations. In particular, various burners had been installed and tested over the course of several weeks during which sensor data were being collected. The goal was to obtain a model of the NO_x emissions given ambient conditions, e.g. temperature, pressure, humidity, and control parameters, e.g. angle of the inlet guide vane, position of fuel valves, in total 23 values per time step. As a result of the different configurations, the NO_x production changed. Despite only relatively few samples of one of the configurations an accurate NO_x model of this instance was required.

Six learning tasks $I = \{1, ..., 6\}$, each defining the above described modeling task on data from turbines with different hardware configurations, were available. Out of the six tasks, five source tasks $\{1, ..., 5\}$ were selected which served as prior knowledge for the target task labeled $\{6\}$. The examples used to train and evaluate the models were generated by extracting T-step windows of the sequences of observations. The data sets were decorrelated using the block validation method discussed in Section 2.3.3. The source tasks' data comprised 6072, 7126, 5448, 8335, and 1361 training examples, and there were 3182 examples available of the target task $\{6\}$. In addition, the training examples of the target task were upsampled to match the average number of samples of the source tasks. In order to evaluate the model error a test set with 8895 examples was set aside.

The first step was to gradually gain an understanding of the nature and difficulty of the task. Therefore, a simple L_2-regularized linear regression model, which learned the mapping $X \to Y$, a multi-step L_2-regularized linear regression $X^d \to Y$ mapping a sequence of inputs to the target variable, and a linear RNN model as described in Section 5.2 with $n_h \in \{5, 8, 10, 20\}$ and $d = T = 5$ were compared. An ensemble of 10 members with randomly initialized parameters was formed whose predictions were averaged. Figure 5.4 compares the results of these models using the mean squared error per time step of the zero mean unit variance NO_x targets according to the training set standardization. The

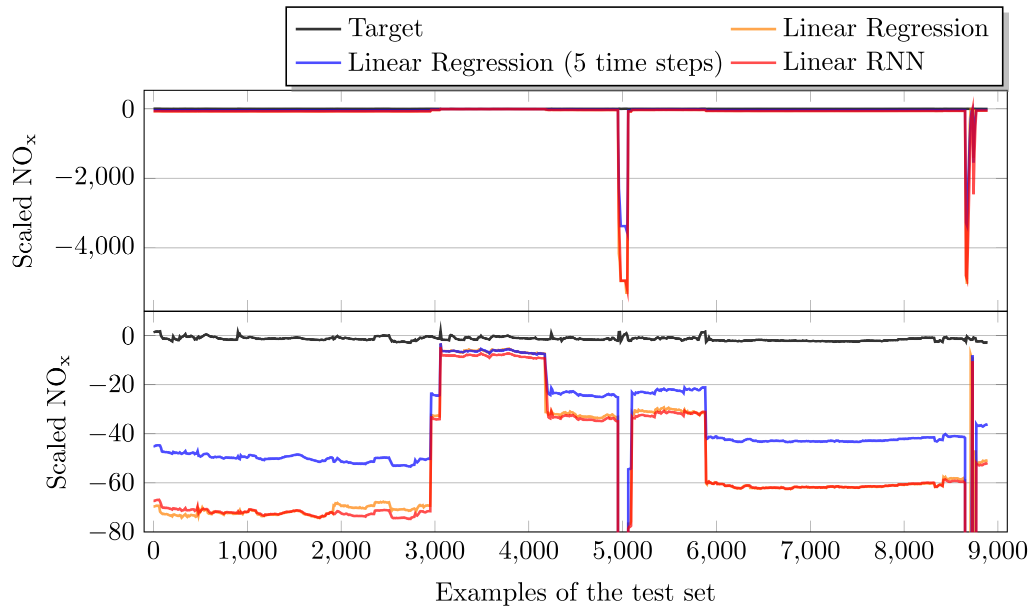

Figure 5.4: Comparison of the linear model performances in modeling the NO_x emissions of a target gas turbine without knowledge transfer from other related turbines.

plot shows that none of the linear models was able to accurately predict the NO_x emissions. Among these models, the linear regression which took input observations from five past subsequent time steps into account, performed best in relative terms but poorly in absolute terms nevertheless. This result suggested that (i) the linear hypothesis was invalid and (ii) there was a temporal dependency between the target observation and the inputs, which is expected in this domain due to delayed effects in the turbine dynamics.

To improve performance, nonlinear RNN models learned only from the target task data as well as multi-task models, i.e. the Naïve RNN, RNN+ID and FTRNN, were compared. The models were configured as follows: $n_{f_h} = n_h \in \{5, 8, 10, 20\}$, $T = 10$, $d = 5$. Ensembles of 10 members with randomly initialized parameters were formed whose predictions were averaged. Figure 5.5 compares the results of the explored models using the mean squared error per time step of the zero mean unit variance NO_x targets according to the training set standardization. As shown in Figure 5.5a the FTRNN performed best across the range of considered hidden layer sizes. The RNN+ID yielded a comparable but consistently larger error. Compared to the RNN trained only on the target task data, the two models yielded an improvement on the order of a factor 10. The Naïve RNN, which was the simplest multi-task learning model in the comparison, suffered from the auxiliary learning tasks. In order to better understand the implications of these results the prediction quality of the models is depicted in Figure 5.5b by comparing their predicted (rescaled) NO_x values with the ground truth. Although the target task RNN outperformed the Naïve RNN in terms of the MSE it can be observed that it was in fact unable to learn the input-output relationship but rather predicted a nearly constant value on the test set. The Naïve RNN appeared to have captured some of the structure of the input-output relationship, but could not adjust properly to each individual task. In contrast, the RNN+ID and FTRNN could accurately predict the NO_x emissions despite only few data of the target task.

5.4.3 Discussion

This section demonstrated the utility of multi-task learning in the context of real-world gas turbine NO_x emission modeling. In a first set of experiments gas turbine NO_x emissions were modeled by simple linear models in order to better understand the difficulty of the task. As it turned out these models were unsuccessful in inferring the relationship between the observable sensor readings and the NO_x emissions from the available data of the target gas turbine. However, the results indicated that there were temporal dependencies between the NO_x emissions and the input observations likely due to delayed effects in the turbine dynamics which was a hypothesis consistent with a domain understanding of the problem at hand. A second set of experiments showed that a recurrent neural network trained on the target turbine data alone achieved better but still rather poor predictive performance, too, due to insufficient data. However, the model was able to predict a small region in the test data comparatively accurately while the remaining regions appeared to be modeled as an average of the observed NO_x measurements. In order to augment the target turbine data, auxiliary data from multiple related source turbines were utilized by three vari-

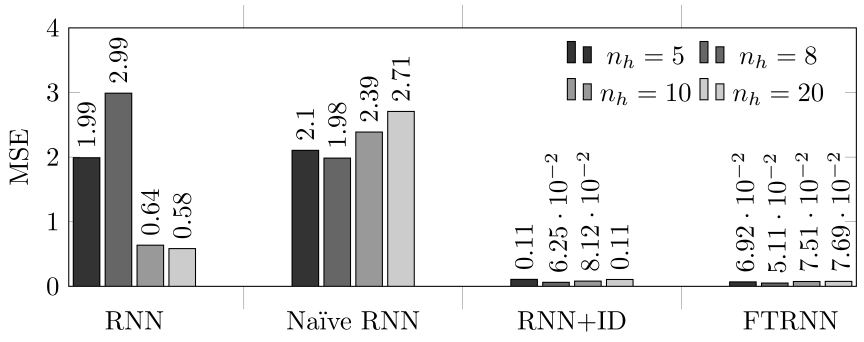

(a) Comparison of the model errors for different recurrent neural network architectures and different hidden layer sizes. The plot shows the MSE of the first NO_x prediction using the standardized values. A column represents a particular size of the hidden layer, i.e. the number of hidden neurons, in the corresponding recurrent neural network architecture.

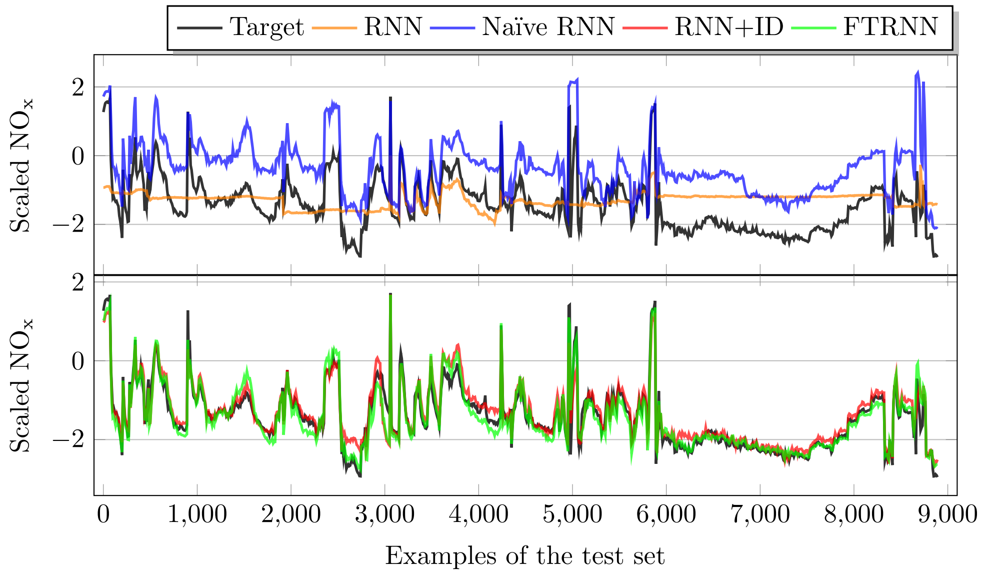

(b) Comparison of the model predictions for different recurrent neural network architectures using the optimal hidden layer sizes. The plots show the predicted standardized NO_x emission values and the ground truth based on the test data set. The x-axis indicates the row number of the test example. The plot is split into two subplots to better distinguish the error curves.

Figure 5.5: Comparison of the nonlinear model performances in modeling the NO_x emissions of a target gas turbine with and without knowledge transfer from other related turbines.

ants of recurrent neural network architectures designed to shared information among all systems. Among them was the novel Factored Tensor Recurrent Neural Network which encodes cross-system and system-specific information into a factored third-order tensor. As a result, training a simple RNN (i.e. the Naïve RNN) on the concatenated source and target system data turned out unsuccessful. The RNN+ID, which received a one-hot encoded task identifier as an additional input, yielded a significantly more accurate NO_x model and, thus, a significant improvement over simpler approaches. The FTRNN consistently outperformed all other models.

Multi-task learning is a promising learning paradigm to obtain an accurate model of a NO_x sensor when only few data of a particular target task are available. Prior knowledge about the relationship between environmental sensor values and NO_x emissions could be incorporated successfully by means of the Factored Tensor Recurrent Neural Network in the conducted experiments. The improvement from a model learned only on the target task data to a multi-task model was significant.

CHAPTER 6

Conclusions & Future Work

6.1 Conclusions

In this thesis, the problem of data-driven fully and partially observable system identification given only few target system data was introduced, motivated by real-world industrial use cases, and formally defined. Different approaches to obtain an accurate model of the little observed task of interest were developed and benchmarked. Knowledge transfer among similar dynamical systems was explored under three learning paradigms: dual-task learning, multi-task learning, and transfer learning. In particular, a novel recurrent neural network architecture—the Factored Tensor Recurrent Neural Network—was proposed. This network architecture utilizes prior knowledge from similar systems by encoding system-specific and cross-system information within a joint model using factored third-order tensors according to the *Parallel Factor Analysis* factorization scheme. Therein, system-specific information is encoded in the frontal diagonal slices of the third-order core tensor. Thus, only few parameters per system need to be learned compared to the number of cross-system parameters which are encoded into two full matrices. Therefore, training the model is highly data-efficient with respect to learning the peculiarities of each individual system. The architecture is theoretically motivated and inspired by a mathematically similar formulation previously used in a natural language modeling context. In addition, a novel regularization technique was proposed for the Factored Tensor Recurrent Neural Network when used in the dual-task learning setting where plenty of data from a source system and only few data from a target system are available. The regularization penalizes diverging system-specific parameters asymmetrically by tying the parameters of the target system to those of the source system but not vice versa. Thus, only the target system parameters are encouraged to remain close to the reliably learned source system parameters, but biased and/or unreliable information from the target system does not affect the parameters of the source system sub-model. Experiments were conducted on two synthetic simulations and real-world gas turbine data.

In all experiments, a naïve model of the respective target task, which was merely learned from few examples of that task, was unable to generalize well to a representative set of unseen examples. Augmenting the training examples of the target task with auxiliary data from one or multiple related task(s) could improve the unmodified model in most cases, but the resulting performance was insufficient nevertheless. This observation is explained by the fact that additional data, although originating from different but related sources, may help in principle, but the model was not aware that the examples had not been generated by the same task. Providing the model with task-discriminating information was the key to enabling effective and data-efficient knowledge transfer among related tasks. The obvious approach, in which a task identifier is encoded as a "one-hot" vector and fed to the model at each time step, requires no particular knowledge concerning the nature of the tasks' similarities and dissimilarities. However, this knowledge was available in the conducted experiments and it is likely available, at least in part, in real-world problems. Incorporating it into the model according to the proposed Factored Tensor Recurrent Neural Network architecture decreased the model error by more than an order of magnitude in some of the conducted experiments. The Factored Tensor Recurrent Neural Network consistently achieved lower model errors in all experiments.

Although significantly more empirical evidence would be required to support a general superiority of the Factored Tensor Recurrent Neural Network across a broad spectrum of problems and applications, this thesis laid out the foundation of promising research direction to effectively utilize data from related dynamical systems as prior knowledge of the system of interest. While the Factored Tensor Recurrent Neural Network was motivated and developed in the context of system identification tasks, it is in fact a general model suitable for knowledge transfer among related sequence learning tasks.

6.2 Future Work

An interesting continuation of this work may be found in the reinforcement learning domain. Reinforcement learning has been successfully applied in real-world industrial use cases (e.g. Schäfer et al., 2007a) which are, at the same time, likely subject to limited data availability. In model-based reinforcement learning, models of the state transition and reward functions need to be learned before an optimal policy can be obtained. These models may be difficult to learn given only few data from the target system. However, when data from similar systems is available, it is likely possible to learn a better model using the methods proposed in this thesis. In particular, it would be interesting to extend the Recurrent Control Neural Network (Schäfer et al., 2007b) by the factored tensor components to enable parameter transfer among multiple related systems in the model as well as policy learning phases. Thus, not only the state transition submodel but also the policy submodel might be able to benefit from the auxiliary information available from related systems. In model-free reinforcement learning, learning models of the state transition and reward functions is bypassed. For instance, a neural network based approach to this problem is the Policy Gradient Neural Rewards Regression (Schneegaß et al., 2007) which may be extended by factored tensor components in order to combine information from multiple related systems. Investigations along these lines would be interesting and relevant both academically and with regard to practical application. Finally, it would be interesting to conduct studies of the FTRNN model in the context of other sequence learning problems in order to assess its ability as a general approach to RNN-based multi-task and transfer learning through parameter transfer.

Bibliography

Ajakan, H., Germain, P., Larochelle, H., Laviolette, F., and Marchand, M. Domain-adversarial neural networks. In *Advances in Neural Information Processing Systems (NIPS), Second Workshop on Transfer and Multi-Task Learning: Theory meets Practice*, 2014.

Andersen, A. H. and Rayens, W. S. Structure-seeking multilinear methods for the analysis of fMRI data. *NeuroImage*, 22(2):728–739, 2004.

Andersen, C. M. and Bro, R. Practical aspects of PARAFAC modeling of fluorescence excitation-emission data. *Journal of Chemometrics*, 17(4):200–215, 2003.

Appellof, C. J. and Davidson, E. R. Strategies for analyzing data from video fluorometric monitoring of liquid chromatographic effluents. *Analytical Chemistry*, 53(13):2053–2056, 1981.

Bailer-Jones, C. A. L., MacKay, D. J. C., and Withers, P. J. A recurrent neural network for modelling dynamical systems. *Network: Computation in Neural Systems*, 9(4):531–547, 1998.

Barto, A. G., Sutton, R. S., and Anderson, C. W. Neuronlike adaptive elements that can solve difficult learning control problems. *IEEE Transactions on Systems, Man and Cybernetics*, (5):834–846, 1983.

Bastien, F., Lamblin, P., Pascanu, R., Bergstra, J., Goodfellow, I. J., Bergeron, A., Bouchard, N., and Bengio, Y. Theano: new features and speed improvements. In *Advances in Neural Information Processing Systems (NIPS), Workshop on Deep Learning and Unsupervised Feature Learning*, 2012.

Bayer, J., Osendorfer, C., Korhammer, D., Chen, N., Urban, S., and van der Smagt, P. On fast dropout and its applicability to recurrent networks. In *Proceedings of the International Conference on Learning Representations (ICLR)*, 2014.

Bengio, Y. Deep learning of representations for unsupervised and transfer learning. *Journal of Machine Learning Research (JMLR) – Proceedings Track*, 27: 17–36, 2012.

Bengio, Y., Simard, P., and Frasconi, P. Learning long-term dependencies with gradient descent is difficult. *IEEE Transactions on Neural Networks*, 5(2): 157–166, 1994.

Bengio, Y., Lamblin, P., Popovici, D., and Larochelle, H. Greedy layer-wise training of deep networks. *Advances in Neural Information Processing Systems*, 19:153, 2007.

Bergstra, J., Breuleux, O., Bastien, F., Lamblin, P., Pascanu, R., Desjardins, G., Turian, J., Warde-Farley, D., and Bengio, Y. Theano: a CPU and GPU math expression compiler. In *Proceedings of the Python for Scientific Computing Conference (SciPy)*, 2010. Oral Presentation.

Breiman, L. Bagging predictors. *Machine learning*, 24(2):123–140, 1996.

Carroll, J. D. and Chang, J.-J. Analysis of individual differences in multidimensional scaling via an n-way generalization of "eckart-young" decomposition. *Psychometrika*, 35(3):283–319, 1970.

Caruana, R. Multitask learning: A knowledge-based source of inductive bias. In *Proceedings of the 10th International Conference on Machine Learning (ICML)*, pp. 41–48, 1993.

Caruana, R. Multitask learning. *Machine Learning*, 28(1):41–75, 1997.

Cattell, R. B. "parallel proportional profiles" and other principles for determining the choice of factors by rotation. *Psychometrika*, 9(4):267–283, 1944.

Cybenko, G. Approximation by superpositions of a sigmoidal function. *Mathematics of Control, Signals and Systems*, 2(4):303–314, 1989.

De Lathauwer, L. and Castaing, J. Tensor-based techniques for the blind separation of DS-CDMA signals. *IEEE Transactions on Signal Processing*, 87(2): 322–336, 2007.

Düll, S., Udluft, S., and Sterzing, V. Solving partially observable reinforcement learning problems with recurrent neural networks. In *Neural Networks: Tricks of the Trade*, pp. 709–733. Springer, 2012.

Elman, J. L. Finding structure in time. *Cognitive Science*, 14(2):179–211, 1990.

Florian, R. V. Correct equations for the dynamics of the cart-pole system. *Center for Cognitive and Neural Studies (Coneural), Romania*, 2007.

Forssell, U. and Lindskog, P. Combining semi-physical and neural network modeling: An example of its usefulness. In *Submitted to the 11th IFAC Symposium on System Identification (SYSID'97) to be held in Fukuoka, Japan*, 1997.

Girosi, F., Jones, M., and Poggio, T. Regularization theory and neural networks architectures. *Neural Computation*, 7(2):219–269, 1995.

Glorot, X., Bordes, A., and Bengio, Y. Domain adaptation for large-scale sentiment classification: A deep learning approach. In *Proceedings of the 28th International Conference on Machine Learning (ICML)*, pp. 513–520, 2011.

Golub, G. H. and van Loan, C. F. *Matrix Computations*, volume 1. Johns Hopkins University Press, 1996.

Harshman, R. A. Foundations of the PARAFAC procedure: Models and conditions for an "explanatory" multi-modal factor analysis. 1970.

Harshman, R. A. and Lundy, M. E. PARAFAC: Parallel factor analysis. *Computational Statistics & Data Analysis*, 18(1):39–72, 1994.

Haykin, S. *Neural Networks: A Comprehensive Foundation.* Prentice Hall PTR, Upper Saddle River, NJ, USA, 2 edition, 1998.

Hinton, G. E. and Salakhutdinov, R. R. Reducing the dimensionality of data with neural networks. *Science*, 313(5786):504–507, 2006.

Hinton, G. E., Srivastava, N., Krizhevsky, A., Sutskever, I., and Salakhutdinov, R. R. Improving neural networks by preventing co-adaptation of feature detectors. *arXiv preprint arXiv:1207.0580*, 2012.

Hitchcock, F. L. The expression of a tensor or a polyadic as a sum of products. *Journal of Mathematics and Physics*, 6:164–189, 1927.

Hochreiter, S. Untersuchungen zu dynamischen neuronalen netzen. Master's thesis, Technical University of Munich – Department of Informatics, 1991.

Hochreiter, S., Bengio, Y., Frasconi, P., and Schmidhuber, J. Gradient flow in recurrent nets: The difficulty of learning long-term dependencies. In Kremer and Kolen (eds.), *A Field Guide to Dynamical Recurrent Neural Networks*. IEEE Press, 2001.

Hornik, K. Approximation capabilities of multilayer feedforward networks. *Neural Networks*, 4(2):251–257, 1991.

Hornik, K., Stinchcombe, M., and White, H. Multilayer feedforward networks are universal approximators. *Neural networks*, 2(5):359–366, 1989.

İrsoy, O. and Cardie, C. Modeling compositionality with multiplicative recurrent neural networks. In *Proceedings of the International Conference on Learning Representations*, 2015. Under review.

Jacobs, R. A., Jordan, M. I., Nowlan, S. J., and Hinton, G. E. Adaptive mixtures of local experts. *Neural Computation*, 3(1):79–87, 1991.

Jaeger, H. and Haas, H. Harnessing nonlinearity: Predicting chaotic systems and saving energy in wireless communication. *Science*, 304(5667):78–80, 2004.

JáJá, J. Optimal evaluation of pairs of bilinear forms. *SIAM Journal on Computing*, 8(3):443–462, 1979.

Jordan, M. I. and Jacobs, R. A. Hierarchical mixtures of experts and the EM algorithm. *Neural Computation*, 6(2):181–214, 1994.

Kohavi, R. and Provost, F. Glossary of terms. *Machine Learning*, 30(2-3): 271–274, 1998.

Kolda, T. G. and Bader, B. W. Tensor decompositions and applications. *SIAM Review*, 51(3):455–500, 2009.

Koren, Y. The bellkor solution to the netflix grand prize. *Netflix Prize Documentation*, 2009.

Kröse, B. and van der Smagt, P. *An Introduction to Neural Networks*. University of Amsterdam, Amsterdam, The Netherlands, 1994.

Kruskal, J. B. Three-way arrays: Rank and uniqueness of trilinear decompositions, with application to arithmetic complexity and statistics. *Linear Algebra and Its Applications*, 18(2):95–138, 1977.

Martens, J. Deep learning via Hessian-Free optimization. In *Proceedings of the 27th International Conference on Machine Learning (ICML)*, pp. 735–742, 2010.

Martens, J. and Sutskever, I. Learning recurrent neural networks with Hessian-Free optimization. In *Proceedings of the 28th International Conference on Machine Learning (ICML)*, pp. 1033–1040, 2011.

Martens, J. and Sutskever, I. Training deep and recurrent networks with Hessian-Free optimization. In *Neural Networks: Tricks of the Trade*, pp. 479–535. Springer, 2012.

Martınez-Montes, E., Valdés-Sosa, P. A., Miwakeichi, F., Goldman, R. I., and Cohen, M. S. Concurrent EEG/fMRI analysis by multiway partial least squares. *NeuroImage*, 22(3):1023–1034, 2004.

Michie, D. and Chambers, R. A. Boxes: An experiment in adaptive control. *Machine Intelligence*, 2(2):137–152, 1968a.

Michie, D. and Chambers, R. A. Boxes as a model of pattern formation. In Waddington, C. (ed.), *Towards a Theoretical Biology*, volume 1, pp. 206–215. Edinburgh: Edinburgh University Press, 1968b.

Mikolov, T., Karafiát, M., Burget, L., Cernockỳ, J., and Khudanpur, S. Recurrent neural network based language model. In *Proceedings of the 11th Annual Conference of the International Speech Communication Association (INTERSPEECH)*, pp. 1045–1048, 2010.

Minsky, M. L. and Papert, S. *Perceptrons: An Introduction to Computational Geometry.* MIT Press, 2 edition, 1988.

Mitchell, B. C. and Burdick, D. S. Slowly converging PARAFAC sequences: Swamps and two-factor degeneracies. *Journal of Chemometrics*, 8(2):155–168, 1994.

Mitchell, T. M. *Machine Learning.* McGraw-Hill, Inc., New York, NY, USA, 1 edition, 1997. ISBN 0070428077, 9780070428072.

Mitchell, T. M. The need for biases in learning generalizations. In Shavlik, J. W. and Dietterich, T. G. (eds.), *Readings in Machine Learning*, pp. 184–191. Morgan Kauffman, 1980.

Mocks, J. Topographic components model for event-related potentials and some biophysical considerations. *IEEE Transactions on Biomedical Engineering*, 35 (6):482–484, 1988.

Neuneier, R. and Zimmermann, H.-G. How to train neural networks. In *Neural Networks: Tricks of the Trade, This Book is an Outgrowth of a 1996 NIPS Workshop*, pp. 373–423. Springer, 1998.

Nocedal, J. and Wright, S. J. *Numerical Optimization.* Springer, 2 edition, 2006. ISBN 978-0-387-30303-1.

Pan, S. J. and Yang, Q. A survey on transfer learning. *IEEE Transactions on Knowledge and Data Engineering*, 22(10):1345–1359, 2010.

Pearlmutter, B. A. Fast exact multiplication by the hessian. *Neural Computation*, 6(1):147–160, 1994.

Piotte, M. and Chabbert, M. The pragmatic theory solution to the netflix grand prize. *Netflix Prize Documentation*, 2009.

Rabiner, L. A tutorial on hidden Markov models and selected applications in speech recognition. *Proceedings of the IEEE*, 77(2):257–286, 1989.

Rehkugler, H. and Zimmermann, H. G. *Neuronale Netze in der Ökonomie: Grundlagen und finanzwirtschaftliche Anwendungen.* Verlag Vahlen, München, 1994.

Rosenblatt, F. The perceptron: A probabilistic model for information storage and organization in the brain. *Psychological Review*, 65(6):386–408, 1958.

Rumelhart, D. E. Learning representations by back-propagating errors. *Nature*, 323(9):533–536, 1986.

Rumelhart, D. E., Hinton, G. E., and Williams, R. J. Learning representations by back-propagating errors. *Cognitive Modeling*, 1988.

Schäfer, A. M. and Udluft, S. Solving partially observable reinforcement learning problems with recurrent neural networks. In *Proceedings of the European Conference on Machine Learning (ECML), Workshop on Reinforcement Learning in Non-Stationary Environments*, pp. 71–81, 2005.

Schäfer, A. M. and Zimmermann, H.-G. Recurrent neural networks are universal approximators. In *Proceedings of the 16th International Conference on Artificial Neural Networks (ICANN)*, pp. 632–640. Springer, 2006.

Schäfer, A. M. and Zimmermann, H.-G. Recurrent neural networks are universal approximators. *International Journal of Neural Systems*, 17(4):253–263, 2007.

Schäfer, A. M., Schneegaß, D., Sterzing, V., and Udluft, S. A neural reinforcement learning approach to gas turbine control. In *Proceedings of the International Joint Conference on Neural Networks (IJCNN)*, pp. 1691–1696, 2007a.

Schäfer, A. M., Udluft, S., and Zimmermann, H.-G. The recurrent control neural network. In *Proceedings of the 15th European Symposium on Artificial Neural Networks, Computational Intelligence and Machine Learning (ESANN)*, pp. 319–324, 2007b.

Schneegaß, D., Udluft, S., and Martinetz, T. Improving optimality of neural rewards regression for data-efficient batch near-optimal policy identification. In *Proceedings of the 17th International Conference on Artificial Neural Networks (ICANN)*, pp. 109–118. Springer, 2007.

Sidiropoulos, N. D. and Budampati, R. S. Khatri-rao space-time codes. *IEEE Transactions on Signal Processing*, 50(10):2396–2407, 2002.

Sidiropoulos, N. D., Bro, R., and Giannakis, G. B. Parallel factor analysis in sensor array processing. *IEEE Transactions on Signal Processing*, 48(8): 2377–2388, 2000a.

Sidiropoulos, N. D., Giannakis, G. B., and Bro, R. Blind PARAFAC receivers for DS-CDMA systems. *IEEE Transactions on Signal Processing*, 48(3):810–823, 2000b.

Siegelmann, H. T. and Sontag, E. D. Turing computability with neural nets. *Applied Mathematics Letters*, 4(6):77–80, 1991.

Socher, R. *Recursive Deep Learning for Natural Language Processing and Computer Vision*. PhD thesis, Stanford University, 2014.

Socher, R., Chen, D., Manning, C. D., and Ng, A. Y. Reasoning with neural tensor networks for knowledge base completion. In *Advances in Neural Information Processing Systems (NIPS)*, pp. 926–934, 2013a.

Socher, R., Perelygin, A., Wu, J. Y., Chuang, J., Manning, C. D., Ng, A. Y., and Potts, C. Recursive deep models for semantic compositionality over a sentiment treebank. In *Proceedings of the Conference on Empirical Methods in Natural Language Processing (EMNLP)*, pp. 1631–1642, 2013b.

Spieckermann, S., Düll, S., Udluft, S., Hentschel, A., and Runkler, T. Exploiting similarity in system identification tasks with recurrent neural networks. In *Proceedings of the 22nd European Symposium on Artificial Neural Networks, Computational Intelligence and Machine Learning (ESANN)*, 2014a.

Spieckermann, S., Düll, S., Udluft, S., and Runkler, T. Multi-system identification for efficient knowledge transfer with factored tensor recurrent neural networks. In *Proceedings of the European Conference on Machine Learning (ECML), Workshop on Generalization and Reuse of Machine Learning Models over Multiple Contexts*, 2014b.

Spieckermann, S., Düll, S., Udluft, S., and Runkler, T. Regularized recurrent neural networks for data efficient dual-task learning. In *Proceedings of the 24th International Conference on Artificial Neural Networks (ICANN)*, 2014c.

Spieckermann, S., Udluft, S., and Runkler, T. Data-efficient temporal regression with multi-task recurrent neural networks. In *Advances in Neural Information Processing Systems (NIPS), Second Workshop on Transfer and Multi-Task Learning: Theory meets Practice*, 2014d.

Spieckermann, S., Düll, S., Udluft, S., Hentschel, A., and Runkler, T. Exploiting similarity in system identification tasks with recurrent neural networks. *Neurocomputing*, (Special Issue ESANN 2014), 2015. Extended version. Invited paper.

Srivastava, N., Hinton, G. E., Krizhevsky, A., Sutskever, I., and Salakhutdinov, R. R. Dropout: A simple way to prevent neural networks from overfitting. *The Journal of Machine Learning Research (JMLR)*, 15(1):1929–1958, 2014.

Stamp, M. A revealing introduction to hidden Markov models, 2004. `http://citeseerx.ist.psu.edu/viewdoc/download?doi=10.1.1.296.4205&rep=rep1&type=pdf`.

Sutskever, I., Martens, J., and Hinton, G. E. Generating text with recurrent neural networks. In *Proceedings of the 28th International Conference on Machine Learning (ICML)*, pp. 1017–1024, 2011.

Sutskever, I., Martens, J., Dahl, G., and Hinton, G. On the importance of initialization and momentum in deep learning. In *Proceedings of the 30th International Conference on Machine Learning (ICML)*, pp. 1139–1147, 2013.

Sutton, R. S. and Barto, A. G. *Reinforcement Learning: An Introduction*, volume 1. Cambridge University Press, Cambridge, MA, USA, 1998.

Taigman, Y., Yang, M., Ranzato, M., and Wolf, L. DeepFace: Closing the gap to human-level performance in face verification. In *IEEE Conference on Computer Vision and Pattern Recognition (CVPR)*, pp. 1701–1708. IEEE Press, 2014.

Taylor, G. W. and Hinton, G. E. Factored conditional restricted Boltzmann machines for modeling motion style. In *Proceedings of the 26th International Conference on Machine Learning (ICML)*, pp. 1025–1032, 2009.

Taylor, M. E. and Stone, P. Transfer learning for reinforcement learning domains: A survey. *Journal of Machine Learning Research (JMLR)*, 10:1633–1685, 2009.

Ten Berge, J. M. Kruskal's polynomial for $2 \times 2 \times 2$ arrays and a generalization to $2 \times n \times n$ arrays. *Psychometrika*, 56(4):631–636, 1991.

Thrun, S. Is learning the n-th thing any easier than learning the first? *Advances in Neural Information Processing Systems (NIPS)*, pp. 640–646, 1996.

Torrey, L. and Shavlik, J. Transfer learning. In Olivas, E. S., Guerrero, J. D. M., Sober, M. M., Benedito, J. R. M., and López, A. J. S. (eds.), *Handbook of Research on Machine Learning Applications and Trends: Algorithms, Methods, and Techniques*, volume 1, pp. 242–264. IGI Global, 2009.

Töscher, A., Jahrer, M., and Bell, R. M. The bigchaos solution to the netflix grand prize. *Netflix Prize Documentation*, 2009.

Wolpert, D. H. Stacked generalization. *Neural Networks*, 5(2):241–259, 1992.

Yadaiah, N. and Sowmya, G. Neural network based state estimation of dynamical systems. In *International Joint Conference on Neural Networks (IJCNN)*, pp. 1042–1049. IEEE, 2006.

Yao, Y., Rosasco, L., and Caponnetto, A. On early stopping in gradient descent learning. *Constructive Approximation*, 26(2):289–315, 2007.

Yu, D., Deng, L., and Seide, F. Large vocabulary speech recognition using deep tensor neural networks. In *Proceedings of the 13th Annual Conference of the International Speech Communication Association (INTERSPEECH)*, 2012.

Yu, D., Deng, L., and Seide, F. The deep tensor neural network with applications to large vocabulary speech recognition. *IEEE Transactions on Audio, Speech, and Language Processing*, 21(2):388–396, 2013.

Zimmermann, H.-G. and Neuneier, R. Neural network architectures for the modeling of dynamical systems. In Kolen, J. F. and Kremer, S. C. (eds.), *A Field Guide to Dynamical Recurrent Networks*, pp. 311–350. IEEE Press, 2001.

Zimmermann, H.-G., Grothmann, R., Schäfer, A. M., and Tietz, C. Modeling large dynamical systems with dynamical consistent neural networks. In Haykin, S., Principe, J. C., Sejnowski, T. J., and Mcwhirter, J. (eds.), *New Directions in Statistical Signal Processing: From Systems to Brains*, chapter 8, pp. 203–241. MIT Press, 2007.